Strengthening monumental timber floors with a reversible intervention to accommodate acoustic measures

J.A.A. Brand

Technische Universiteit Delft

TU Delft

Strengthening monumental timber floors with a reversible intervention to accommodate acoustic measures

by

J.A.A. Brand

to obtain the degree of Master of Science
at the Delft University of Technology.
to be defended publicly on Friday March 11, 2022 at 04:00 PM.

In cooperation with:

abt

Student number:	4370988	
Project duration:	February, 2021 – March, 2022	
Thesis committee:	Dr. ir. G. J. P. Ravenshorst,	TU Delft (Chairman)
	Ir. S. Pasterkamp,	TU Delft
	Ir. C. J. Janssen,	TU Delft
	Ing. W. H. Klaverveld RC,	ABT

An electronic version of this thesis is available at http://repository.tudelft.nl/.

TU Delft

“To engineers who, rather than blindly following the codes of practice, seek to apply the laws of nature.”

T.Y. Lin, 1955

Abstract

For centuries timber has been the most commonly used material for constructions. All over the world examples of timber structures that date back from a few centuries are still standing today. The Netherlands feature about 60,000 national monuments with internally timber structures. These timber structures often need strengthening due to increasing loads that are applied. The strengthening techniques are narrowed down to a few options whenever historical ceiling designs, such as ceiling paintings, plaster works or timber beams need to remain intact.

Timber floors encounter two major challenges: low stiffness which leads to limited load-bearing capacity and low surface mass which leads to poor acoustic sound insulation. This research seeks to provide structural engineers to make a factual choice in an early design stage for using a reversible strengthening technique on a monumental timber floor preserving original appearance. This strengthening technique is verified for strength, stiffness and acoustics, both airborne and structure-borne sound transmission. To this end, the following research question was formulated: "What is the influence on the strength, stiffness and acoustic properties of monumental timber floors by strengthening them with multiple layers of plates fastened on top of the existing floor?"

To answer the research question, a case study was performed on two monumental floors of the Prinsenhof Museum in Delft. These floors were investigated for their current strength, stiffness and acoustic properties. Then, equations were derived which considered the separate timber plates in the reinforcement technique as an equivalent layer. This equivalent layer is used to determine the effective stiffness for mechanically connected girders by the γ-method. These equations were validated using software for 2D frameworks. Subsequently, a parameter study was used to determine the influence of the parameters on the strength, stiffness and acoustic properties. Finally, by applying the reinforcement technique to the case study based on the results of the parameter study, the strengthening technique was assessed more in detail by taking into account the influence of the non-cooperating intermediate layer.

The results of the parameter study and the case study demonstrated that the strengthening technique increase the strength and stiffness of the floor considerably. However, by increasing the stiffness, the connections between the additional timber plates and the reinforced component becomes governing. Furthermore, the increase in stiffness does not significantly improve the acoustic sound insulation, as this is mainly governed by the surface mass of the timber floor.

It is therefore concluded that strengthening of monumental timber floors, by means of several layers of separate timber plates fastened on top of the floor, is an effective way to achieve the desired strength and stiffness. Thick plates, small spacing between fasteners and inclined fasteners are a requirement to achieve higher strength and stiffness. However, additional measures must be taken to meet the sound transmission requirements. For the original perseverance of the monumental timber floor and reversibility, these measures would be dry floating floors. A significant fact is that dry floating floors only add mass and do not increase stiffness, which lowers the maximum allowable load on the floor.

A major limitation of this thesis is the consideration of the non-cooperating intermediate layer between the additional timber layers and the reinforced component. This intermediate layer results in multiple shear planes between the reinforced component and the additional timber plates. This thesis suggested to use a factor, determined from Roensmaens et al. (2020) research, to convert the multiple shear planes into a single shear plane. It is therefore important that further research investigates the influence of these multiple shear planes that do not contribute to the bending stiffness of the reinforced component.

Preface

In front of you is my thesis ”Strengthening monumental timber floors with a reversible intervention to accommodate acoustic measures”, and it marks the end of my time as a student at Delft University of Technology. Following my bachelor’s degree in Civil Engineering, I pursued a master’s degree in Structural Engineering with a focus on steel and timber structures. It has been a personal challenge for me to write my thesis. Working in a team with short deadlines works best for me which is practically the polar opposite of writing a master thesis. The unusual times surrounding the outbreak of the COVID-19 pandemic as well as several lock-downs did not make matters any easier. Nevertheless, I can honestly state that I am satisfied with the end result.

First and foremost, I want to express my gratitude to the members of my graduation committee: Geert Ravenshorst, Sander Pasterkamp, Christien Janssen and Willem Klaverveld. For their guidance, assistance and suggestions during the whole research period. I was very pleased with all the insightful feedback I got after each meeting. It helped me a lot in improving my report during my graduation period. I would like to express my gratitude to Geert Ravenshorst for is broad knowledge, as well as his passion and enthusiasm which inspired me towards timber structures. Your suggestion to create an equivalent layer served as the foundation for my methods. Your remarks and critical analysis on my methods were an eye-opener. I appreciate Sander Pasterkamp’s efforts in helping to develop the implementation of the equivalent layer and addressing the flaws in my MatrixFrame models. I would like to express my gratitude to Christien Jansen for sharing her expertise regarding the acoustic calculations and providing feedback on my report.

Second, I would like to express my deep appreciation to my supervisors and all of my ABT colleagues who helped me along the journey, especially during this pandemic. I am grateful for the inspiring and engaging work atmosphere as well as the chance to undertake this study on their behalf. I had a wonderful time and learned a lot thanks to the excellent facilities provided throughout my research period. Willem Klaverveld, Earnest Alderliesten, Okke Willebrands and Alfons Hartman deserve special mention. Willem, thank you for introducing me to the challenges that occur in monumental timber constructions and for providing practical insights. Thank you, Earnest, for always being there to assist me when I got stuck. All of our discussions were beneficial in terms of improving and rethinking my arguments. Okke, thank you for sharing your knowledge on timber structures and connections. Thank you, Alfons, for all your insights on acoustics. To all my colleagues, thank you for all of your guidance and support during my thesis. I hope to stay in contact, regardless what my career will entail.

Furthermore, I want to thank my friends and roommates for the great times we shared in Delft, as well as the invaluable lessons they taught me that I will carry with me for the rest of my life. My thesis was written most of the time in their presence. They were very supportive and had genuine interest in how I was progressing. Moreover, I want to thank them especially for all the times they did not ask about my thesis and took my mind off it. I am fortunate to have my girlfriend, Lisanne, who was always there to talk to me, to inspire me and to make me laugh.

Last but not least, my parents. I want to thank you for enabling me to study in Delft and for giving me the courage to make the decisions I did throughout my studies. Your unconditional confidence allowed me to grow into the person I am today. You both supported me in your own way. Dad, thank you for your passion in constructions. You inspired me to study Civil Engineering in Delft. Mom, I owe you for the many evening and weekend hours you spent on reading the drafts and provide me with lots of comments.

J.A.A. Brand
Delft, March 2022

Contents

Nomenclature

a	length of plate (a<b)	m
a_i	distance to center of gravity	m
A	area	m^2
A_a	amount of sound-absorbing material	m^2
$A_{receive}$	volume of the receiving room	m^3
b	width of plate (a<b)	m
B	bending stiffness	Nm^2
B_x	bending stiffness in x-direction	Nm^2
B_y	bending stiffness in y-direction	Nm^2
c	wave velocity	m/s
c_0	speed of air	m/s
c_b	bending wave velocity	m/s
C	joint constant	-
d	diameter fastener	mm
E	modulus of elasticity	N/m^2
EA_{plate}	axial stiffness of a plate	N
$(EI)_L$	bending stiffness element	Nm^2/m
EI_{eff}	effective bending stiffness	Nm^2
f	frequency	Hz
f_c	coincidence frequency	Hz
f_n	natural frequency	Hz
F	reference force	N
I	moment of inertia	m^4
k	wave number	m^{-1}
K	stiffness coefficient	N/m^2
$K_{fastener}$	stiffness of the fastener	N/mm
K_{plate}	stiffness of the plate	N/mm
$K_{ser,\perp}$	perpendicular slip modulus	N/mm
$K_{ser,\parallel}$	axial slip modulus	N/mm
K_{ser}	inclined slip modulus	N/mm
l	length element	m
L	length of one plate	mm
ΔL	elongation plate (length)	m
ΔL_{eq}	elongation equivalent layer (length)	m
L_F	sound level of force on the floor	dB
L_n	sound level in receiving room due to impact sound	dB
$L_{p,i}$	sound level of source i	dB
$L_{p,receive}$	sound level in the receiving room	dB
$L_{p,send}$	sound level in the emitting room	dB
$L_{p,total}$	total sound level in the room	dB
L_w	penetration length in timber element	mm
$\Delta L_{total,np,plates}$	elongation of the segment with n_p amount of plates	mm

m'	mass per unit area	kg/m^2
n_{fpp}	number of fasteners on 1/n_p of the segment	-
n_p	number of plates	-
n_y	number of fasteners in width direction	-
R	direct sound transmission loss	dB
R_d	sound reduction for direct sound transmission	dB
R_f	sound reduction for flanking sound transmission	dB
R_{random}	direct sound transmission loss of random incidence	dB
R_{Total}	total sound transmission reduction	dB
$Re(Y)$	driving-point mobility	m/Ns
S	area of the separating element	m^2
T	reverberation time	s
T_s	reverberation time of the room	s
u	deformation fastener	m
V	volume of the room (L x W x H)	m^3
$Y_{orthotropic,plate}$	driving-point mobility orthotropic plate	m/Ns
$Y_{thin,plate}$	driving-point mobility thin plate	m/Ns
α	angle of the fastener	°
η_{tot}	internal damping	-
η_{int}	initial damping ≈ 0.01	-
γ	joint efficiency coefficient	-
λ	wavelength	m
μ	friction between timber elements	-
ω	angular frequency	Hz
ρ	density	kg/m^3
ρ_0	density of air	kg/m^3
ρ_{mean}	mean density	kg/m^3
σ	sound radiation factor	-
σ_f	radiation factor for forced vibrations	-

1

Introduction

This chapter presents at first some background information about the problem. Subsequently, the problem analysis and the objective of the thesis are explained. At last the outline of the report is given.

1.1. Background

One of the basic human needs is protection and shelter against the weather. For centuries timber has been the most commonly used building material in the world. Therefore, timber is often found in monumental floors, see Figure 1.1. All over the world, examples of timber structures dating back from a few centuries are still standing today (Kouroussis et al., 2017). The fact is, the majority of these timber structures have surpassed their useful service life, but nearly all still perform structurally well.

Meanwhile, structural regulations and standards for comfort with regard to acoustics have increased over the past decades. As a consequence of their light weight, timber floors often have acoustical issues, particularly at low frequencies. Martins et al. (2015) suggested that changes in structural parameters are needed, to improve acoustical as well as structural performances.

The timber supporting structures, as mentioned above, are often found in monumental constructions. Heritage takes an important place in our modern societies and its preservation is therefore our societies' duty. Preservation of historical constructions is not only a cultural requirement but also an economical need caused by increasing tourism and leisure industries (Arêde and Varum, 2008, Cointe et al., 2007). According to de Vries (2020) from the Central Government Real Estate Agency, the Netherlands feature about 60,000 national monuments, mostly of traditional design. Many of them have masonry walls and internally timber structures. These timber structures are roughly divided into three categories: foundations, floor structures and roof structures. To strengthen timber structures, a number of technical options are possible. These technical possibilities, however, are narrowed down to a few options whenever historical ceiling designs, such as ceiling paintings, plaster works or timber beams need to remain intact.

Figure 1.1: Monumental timber floor in Prinsenhof in Delft [Figure from ABT]

1.2. Problem analysis

External loads must be adopted and transferred to the ground, as well as the equivalent internal loads such as the normal force, shear force and moment. As a result, the structure is subjected to loads and deformations that must not exceed the design strength and deformation limitations (Franke et al., 2015).

In practice, timber load-bearing structures within monumental buildings often need strengthening due to an increase in applied loads. These increased loads are often the result of a change of use, such as private use to public or commercial use.

Almost all substantial historical buildings of large extend need air handling units to create a healthy indoor climate and keep humidity levels constant. The latter could be a significant issue for timber constructions as a higher humidity could cause higher risk of biodegradability by fungus or insects. These air handling units are usually installed in the attic to diminish the length of air ducts. These modern units usually surpass the load-bearing capacity of the timber floor. In addition, they introduce airborne and structure-borne sound issues, see Figure 1.2. To overcome this problem, ABT (a Dutch advising company for structural engineering and design) has the wish to do research on a reversible strengthening techniques on monumental timber floors regarding their structural as well as their acoustic properties.

Another drawback of timber floor structures is related to the propagation of impact sounds induced by human activities, see Figure 1.2. Research from Ljunggren et al. (2014) showed that impact sounds are a common complaint of inhabitants in timber structures, because it is more difficult to reduce than airborne sounds. A reason for that is the significantly higher amount of energy produced per square meter. Caniato et al. (2017) states that floating floor solutions are nowadays one of the best solutions to reduce impact sounds in heavy-weight buildings. These floating floors consist of a heavy bare floor, a resilient layer and a heavy upper slab. However, since monumental timber floors are often already at their maximum load-bearing capacity, they cannot support this additional weight of the floating floor.

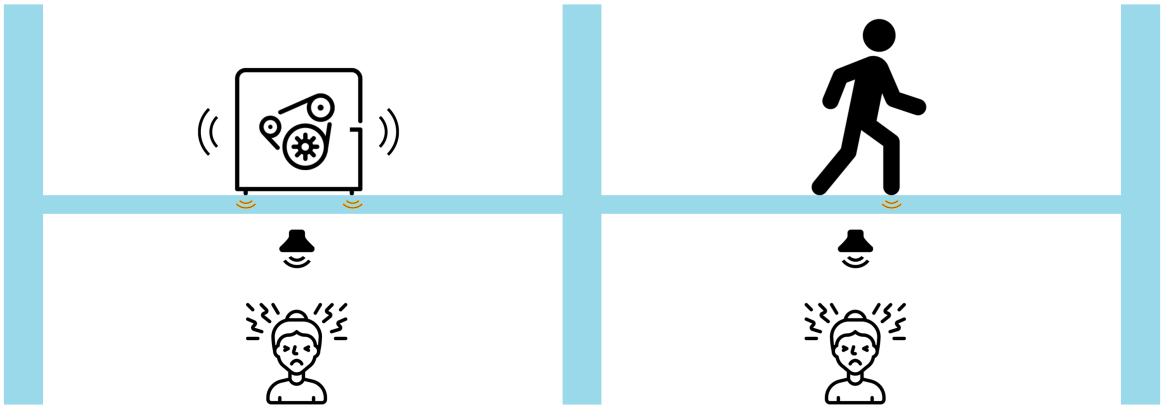

Figure 1.2: Transmitted sounds due to equipment (LEFT) and human activity (RIGHT)

1.3. Objective

The aim of this research is to offer structural engineers, who are not specialized in acoustics, to make a factual choice in an early design stage for using a reversible strengthening technique on a monumental timber floor preserving its original appearance. This strengthening technique is verified for strength, stiffness and acoustics, both airborne and structure-borne sound transmission.

1.3.1. Research question

The answer to the next question will contribute to solving the above-mentioned problem:

"What is the influence on the strength, stiffness and acoustic properties of monumental timber floors by strengthening them with multiple layers of plates fastened on top of the existing floor?"

1.3.2. Sub-questions

In order to simplify the process of answering the research question, multiple sub-questions are defined. To define these questions, a global view of the elements is required. At first, a deeper knowledge of properties which are associated with structural and acoustic problems on timber floor needs to be gained. This is accomplished by a literature review and the set-up of a case study for a monumental timber floor. Second, the calculation method for the new strengthening technique is created and validated. Subsequently, the influence of the configuration parameters is determined. Finally, the strengthening technique is applied on the case study of a monumental timber floor with the use of the gained information from the parameter study. The sub-questions are formulated according to the explained process:

1. ”What are the key parameters for structural assessment of monumental timber floors and how do they influence the structural assessment?”

2. ”What are the important parameters for sound transmission through monumental timber floors and how do they influence the sound insulation?”

3. ”How can multiple layers of separate timber plates which are fastened on top of the existing beam, be incorporated into the stiffness calculations and how can this be validated?”

4. ”What are the key parameter that influence the strengthening configuration and how do they influence the strength, stiffness and sound transmission properties of monumental timber floors?”

5. ”Which aspects should be taken into account when the strengthening technique is applied to an existing monumental timber floor?”

1.3.3. Scope

The scope of this thesis is limited, in order to complete this research within the given time frame. The limitations that are set:

- When strengthening timber structures, the current state of the timber and grade needs to be assessed. Normally this is done through non-destructive testing. In addition, due to mechanical and biological degradation, the cross section and/or characteristics of the material of the members in existing timber constructions might be diminished. Both forms of damage have an impact on the load-bearing capability and serviceability of individual parts or the entire structure. Damage or failure must be recognized and appraised for the timber structure’s resilience and serviceability throughout the evaluation process. For this thesis the assessment of the grade and degradation of the existing timber structure is out of scope. The required parameters are assumed to be known;

- For the verification of the equivalent layer, only a beam on two hinged supports is assumed. Clamping and multiple supports are not considered.

- Airborne and structure-borne sounds are transmitted directly and indirectly. For this thesis the flanking (indirect) transmission of sound is excluded because it is assumed that the masonry walls have enough mass to dissipate the sound. In addition sound leaks are also excluded;

- The vibrations of machines, which can result in sounds due to vibrations of the floor, are excluded in this thesis. As these can be mounted on dampers that absorb most of the vibrations.

1.4. Methodology

Chapter 1 - Introduction

In the first chapter, a general introduction of the thesis is presented. The relevance is portrayed by the problem analysis and objective, followed by the research question.

Chapter 2 - Monumental timber floors
The first part of the theoretical background aims to analyse the different types of monumental timber floors, examines the techniques to strengthen them and investigates all components required for reinforcements. In addition, the key structural parameters that influence the strength and stiffness will be determined, by means of a preliminary case study on a monumental timber floor in the Prinsenhof Museum.

Chapter 3 - Acoustic transmission
The second part of the theoretical background aims to analyse methods to assess the acoustic properties and performances of structures. Acoustic transmissions can be divided into airborne and structure-borne sounds and this chapter aims to determine how to calculate these sound transmissions by simple equations. In addition, the important acoustic parameters which influence airborne and structure-borne sound transmission will be determined by a case study.

Chapter 4 - Equivalent layer
The first part of the methodological framework aims to derive equations for an equivalent layer consisting of multiple layers of separate timber plates.

Chapter 5 - Verification model
The second part of the methodological framework validates these equations on stiffness and stresses by the use of 2D framework software.

Chapter 6 - Parameter study
The parameter study describes the influence of the configuration parameters of the strengthening technique on strength, stiffness and acoustic properties.

Chapter 7 - Case study
A case study of the monumental timber floor structure of the Prinsenhof Museum in Delft ensures that the strengthening technique which is applied, is verified for practical use.

Chapter 8 - Discussion
In chapter 8, the results of the parameter study and case study are clarified, discussed and related to the theoretical background. Furthermore, the limitations and implications of the results are discussed.

Chapter 9 - Conclusion and recommendations
The findings obtained in the different parts of the research lead to the answer of the research question. Finally, recommendations for further research are given.

I

Theoretical background

2

Monumental timber floors

Timber is a natural material consisting of cells with orthotropic strength properties due to its straw-like structure. It is strong and stiff when loaded parallel to the grain, but relatively weak when loaded perpendicular to the grain. Figure 2.1 illustrates that for Azobe (D70) the tensile strength in the tangential direction is only 1.4% of its longitudinal direction (Drs. W.F. Gard, 2018).

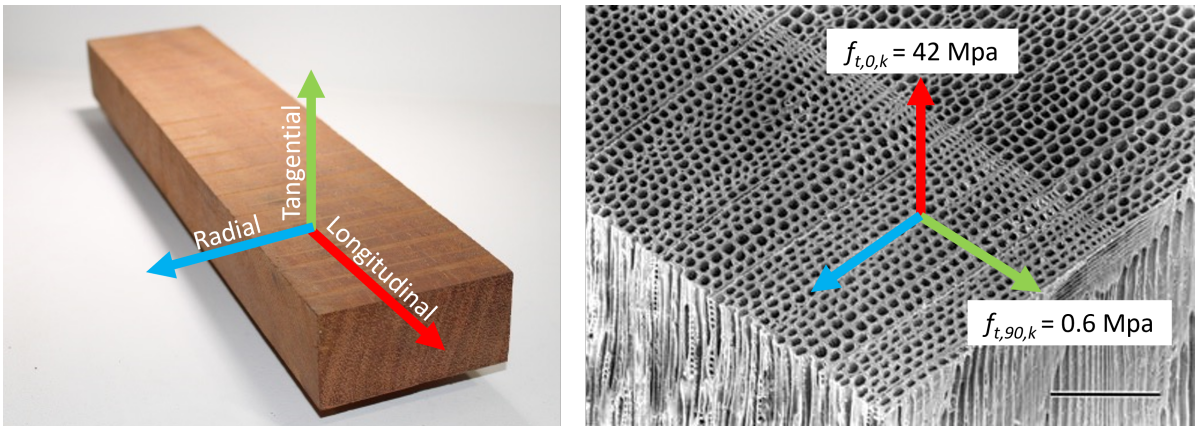

Figure 2.1: Orthotropic material properties of timber (Azobe D70) (Drs. W.F. Gard, 2018, slide 7)

2.1. Timber products

These non-homogeneous properties are a result of the growth process of trees. During this growth, knots or other growth-related features will occur which have influence on its strength. This explains the variation of strength within a single member. Therefore timber products are produced with wood parts with insignificant flaws in order to minimize the variation in material characteristics. Table 2.1 shows six wood products and their components. Each consecutive product consist of smaller components then the previous. Smaller components reduce variation of material properties within a single member.

Timber product	Components
Sawn timber	Timber beams, planks and boards
Cross laminated timber	Boards
Laminated veneer lumber	Veneer
Plywood	Veneer or sawn timber
Particleboard	Particles (chips)
Fibreboard	Fibres

Table 2.1: Timber products and their components (Joachim Blaß and Sandhaas, 2017, p. 99)

2.1.1. Sawn timber

A tree in its natural form has limited structural use. Therefore timber is converted to a structural shape that meets the construction needs. Sawn timber is the most common structural timber material and is also the main component of glued laminated timber (glulam). Sawn timber is produced by sawing logs in longitudinal direction and the main products are boards, planks and square timber beams. Square timber beams are often cut by the free-of-heart method shown as the right picture in Figure 2.2, as it reduces the shrinkage cracks (Joachim Blaß and Sandhaas, 2017).

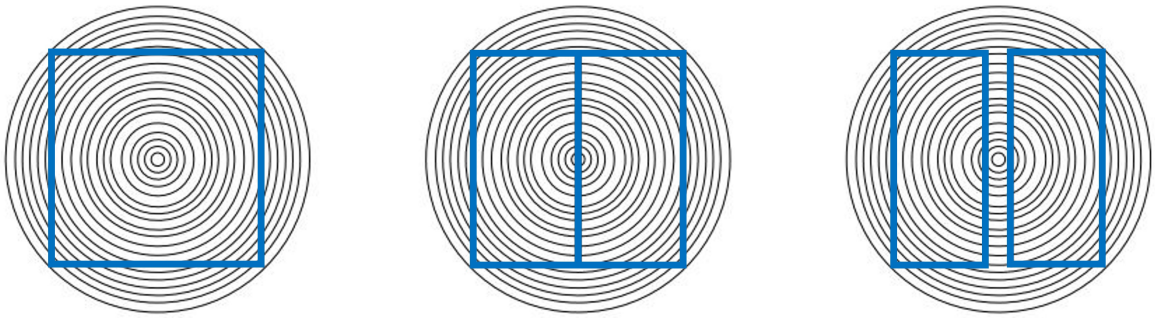

Figure 2.2: Different cutting types for square timber. Left: Single-stem cut. Middle: Dual-stem split-heart cut. Right: Dual-stem free-of-heart cut (Joachim Blaß and Sandhaas, 2017, p. 100)

Timber grading

Timber logs are produced from a wide range of trees and their properties depend on their type, genetic material and environmental conditions. The mechanical properties of sawn timber can have a big dispersion. This dispersion not only differs per tree, but also within the same stem. Since the use of timber as a structural member depends on their strength characteristic, using ungraded timber would make it impossible to benefit from the high strength of the main part of the log. Hence for structural, but also for economical reasons, timber pieces are graded into different strength classes.

Traditionally timber is graded by means of visual assessment (as mentioned in NEN-EN 14081-1 (2016)). Nowadays more innovative techniques are developed to grade the timber mechanically (as mentioned in NEN-EN 14081-1 (2016)). Both methods use the main characteristics of the timber members to connect them to a certain strength grade (as mentioned in NEN-EN 384 (2018)).

Timber has several characteristics that are important for the quality and grade. There are a few other natural characteristics, such as reaction wood, juvenile wood and fungal decay, but these effects don't matter in grading the timber. Linville et al. (2012) described the main characteristics:

- Specific gravity (density) is used to indicate the strength and stiffness of timber which is free of strength-reducing characteristics. The strength and stiffness will increase when the specific gravity is higher.

- Knots are formed by branches. Branches grow in the perpendicular direction of the tree trunk. Since branches disrupt the longitudinal direction of the grain, knots are considered as strength-reducing characteristics. The magnitude of its strength-reducing effect depends on shape, size, frequency and location in the member.

- Slope of grain is the direction of the longitudinal fibres compared to the longitudinal axis of the structural component. It is often favored to have both parallel to each other, because timber is an orthotropic material. Grain deviation severely decrease the strength properties.

- Modulus of elasticity (MoE) is used to determine the stiffness of timber and has a correlation with the above-mentioned characteristics. High MoE implies high specific gravity and strength and low slope of grain.

Mechanical properties
In order to standardize characteristic values of timber in calculations, timber is graded in 26 strength classes. Each class contains different species with similar strength properties. These characteristics are described in Table 1 to 3 of the additional standard NEN-EN-ISO 338 (2016)

These 26 strength classes are based on edgewise bending tests and divided in 12 classes for softwoods (C14 - C50) and 14 for hardwoods (D18 - D80). The letters C and D refer respectively to coniferous species (softwood) and deciduous species (hardwood). The numbers refer to the 5-percentile characteristic bending strength in N/mm^2.

When structural timber members of a monumental buildings need to be recalculated, it is common use to take the standard quality for softwoods which is C18, respectively D18 for hardwoods. This in order to reduce time and costs.

2.1.2. Wood-based panels

Wood-based panels are composed of wood that is broken down into sawn timber, veneers, particles, wood shavings or fibres and then reassembled with the use of appropriate adhesives. The most common forms of panels are panels made out of solid wood, veneer-based, chip-based or fibreboards see Figure 2.3. The benefits of these plate-shaped materials over sawn timber include approximated isotropy in plane and minimal property variation.

Figure 2.3: Examples of wood-based panels (Top: solid wood panel, LVL and plywood. Bottom: OSB and particleboard) (Joachim Blaß and Sandhaas, 2017, p. 121-128)

Solid-wood panels
Solid-wood panels are boards made up of three or five bonded softwood or veneer layers, with grain directions running at right angles between consecutive layers. They are basically cross laminated timber elements (CLT). However, they have thin layers and are not used as independent structural elements. They are only considered to be load-bearing when used as sheathing.

Veneer-based panels
Veneer-based panels are produced by thin sheet layers which are glued. This section discusses two types of veneer-based panels:

Laminated veneer lumber (LVL) has its layers fibre direction either parallel to the longitudinal direction of the panel or slightly (up to 25%) perpendicular to that direction. It is often used as load-bearing sheathing or like glue-laminated timber as a beam.

Plywood has its layers run at right angles between consecutive layers and comprises of at least three plies that are glued one to another. It is commonly used as a sheathing material in diaphragms that are either horizontal (floors) or vertical (walls). The stiffness of a plywood panel is like a CLT-panel dictated by layers with the grain running parallel to the stress direction.

Chip-based panels
Chip-based panels are produced from small timber chips. Oriented Strand Boards (OSB) is a chip-based panel made of (multiple layers) longitudinal strands that run parallel to the board. The middle-layered strands should be in random direction while the top-layered should run parallel to the board direction, giving OSB distinct longitudinal and perpendicular characteristics.

In addition to OSB there are particleboards. They are formed by smaller wood chips which are pressed together with adhesive. Particleboards consist of many layers, but their loose connection of particles in the middle layer reduces tensile strength when loaded out of plane. The boards are primarily used for structural floor and roof decking, as well as structural wall sheathing.

Fibreboards
The panel with the least variation in material properties are fibreboards. They are quasi-isotropic, implying their in-plane characteristics apply in all directions. They can be produced by a wet process (hardboards) or dry process (MDF, medium-density fibreboards). Fibreboards consist of individual or bundled fibres that contain, depending on the manufacturing technique, different amounts of chemicals and adhesives.

Material properties
The wood-based panels described before have different properties, Table 2.1.2 demonstrates these properties. The first two rows of the table describe the properties of structural plates and the last five rows of non-structural plates.

Type	Density [kg/m^3]	Bending strength [N/mm^2]	Modulus of elasticity [N/mm^2]
CLT	480-500	24	11000
LVL	400-700	34-86	9000-19000
Plywood	400-600	34-43	7000-8600
OSB	500-800	22-35	4400-6300
Particleboard	600-800	15-24	2800-4100
MDF	700-900	36	3600
Hardboard	900-1000	31-56	3100-5500

Table 2.2: Timber properties of two structural and five panel products (The Engineering Toolbox, ndc)

2.2. Traditional timber floors

The Netherlands features about 60,000 national monuments, of which an estimated 50,000 are of traditional design. Most buildings have masonry walls and internally timber structures (de Vries, 2020). Usually traditional timber floors are constructed by timber boards nailed onto timber beams which are simply supported on the masonry walls, see Figure 2.4. Sometimes these floor structures contain secondary elements, like timber joist, which span between the beams to increase the load-bearing capacity of the floor. The type of timber products found in these floors is mainly sawn timber.

Figure 2.4: Different types of monumental timber floor structures (Left) Common timber-beam floor (Middle) Decorated and carved timber-beam floor (Right) Bi-directional timber-beam floor (Corradi et al., 2019)

The walls of most old buildings consist of masonry on which the main timber beams are simply or rigid supported. Arêde and Varum (2008) described that in practice it is often the case that beams are supported on 2/3 or the full thickness of the wall. Under the timber beams at the support, materials like natural slate are placed to prevent moisture degradation. In extend to prevent any biological degradation, the ends of the beams are often painted with oil, lead or tar solution.

Another common support is a beam supported on corbels, see Figure 2.5. These corbels ensure that the span is reduced which results in smaller moments and thus smaller stresses in the floor construction.

Figure 2.5: Example of corbel pieces

A safe assumption to assess the current strength of these timber floors would be that the beams, joists and planks do not cooperate as a system and that they all carry the load as single elements. The floors supported on masonry walls can be schematised as a beam with hinged supports and floors which have corbel pieces as a continuous beam on four supports (see Figure 2.6). Section ”Equation for two and four hinged supports systems” in Appendix A explains more about the load distribution over these systems.

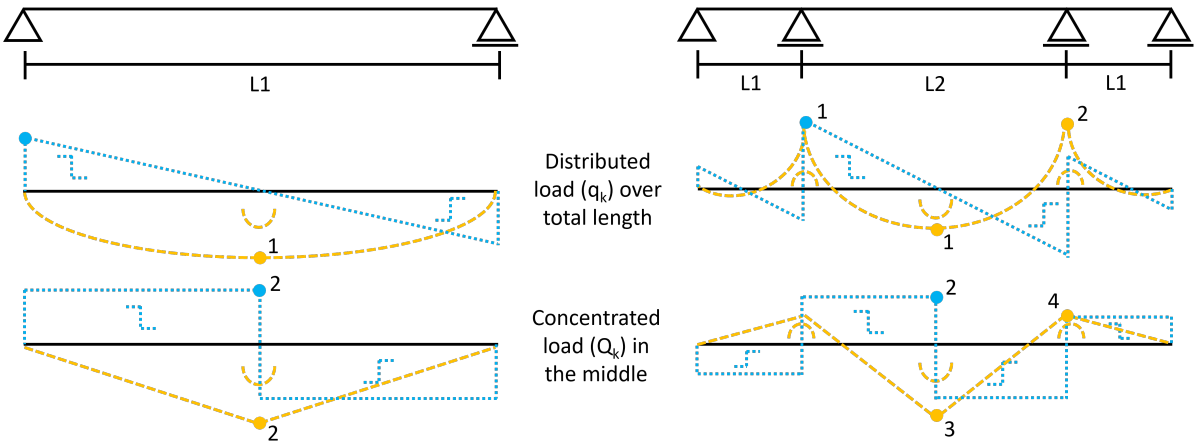

Figure 2.6: Schematization for (Left) a simply supported system and (Right) a continuous system on four supports

2.2.1. Failure types

External loads must be adopted and transferred to the ground, as well as the equivalent interior loads (normal force, shear force and moment). As a result, the structure is subjected to loads and deformations that must not exceed the design strength and deformation limitations. Franke et al. (2015) described in his research the typical types of failure which are: cracks, bending failure, compression failure, tension failure, shear failure and insects and fungi. See Figure 2.7 for the typical types of failure.

Additionally the failure analysis of Frese and Blaß (2011b) and Frese and Blaß (2011a) on timber buildings in Germany offers a summary of important types of failure, with bending failure accounting for 80% of all failures. Bending of a member results in tension and compression stresses being distributed over the cross section depth. These longitudinal tension stresses cause the timber fibres to break, resulting in brittle failure (Franke et al., 2015).

Figure 2.7: Types of failure (F.L.T.R.); cracks (Wikimedia Commons, 2005), bending failure (Franke et al., 2015), shear failure (Schmid et al., 2010) and insects and fungi (Wikimedia Commons, 2020)

2.3. Strengthening of timber floors

Strengthening of structural elements might be necessary due to increased applied loads or degradation of the structural elements. Often the humidity levels are high in masonry walls because of moisture which is infiltrated but cannot be evaporated due to lack of ventilation. These conditions increase the risk of biological decay of the ends of the beams. However, this thesis does not focus on techniques used on timber elements that are subjected to biological decay but only on the reinforcement methods on timber floor structures which are subjected to increased loads.

The addition of elements to strengthen structures (see Figures 2.8, 2.9 and 2.10) is a common technique to increase the load-carrying capacity or to decrease the deflections of a floor (Arêde and Varum, 2008, p. 130-132). An effective way to strengthen timber beams is to nail or screw elements like steel plates or timber boards to the main beam. Another option is bonding elements like FRP bars or plates to the main beam. The additional elements can either be parallel to the main beam (to get an increased moment of inertia) or perpendicular to the main beam (to reduce the span). However, all these options are unfavourable for strengthening monumental timber floors because they often impair the original appearance of the monumental timber ceiling.

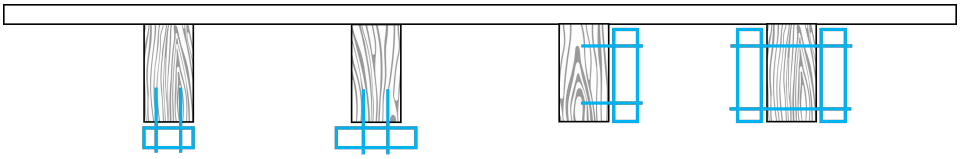

Figure 2.8: Examples of reinforcement techniques of timber floor beams with additional timber elements

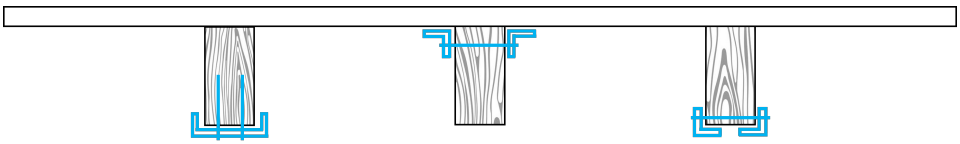

Figure 2.9: Examples of reinforcement techniques of timber floor beams with additional steel elements

Strengthening a monumental timber floor without impairing this monumental appearance can be achieved by creating composite action with the beam and the floor. This is done by adding layers over the existing floor like a concrete slab, timber planks or timber-based panels, see Figure 2.10. These connected layers increase the effective bending stiffness of the floor. The structural behaviour of the resulting timber composite structure is governed by the strength and stiffness of the mechanical fasteners that connect the existing timber beams to the new elements. Timber layers are preferred by the Central Government Real Estate Agency because if they are connected with screws, the reinforcement can also be reversed when needed. This reversibility is also supported by a higher sustainability as materials can be used in a circular way.

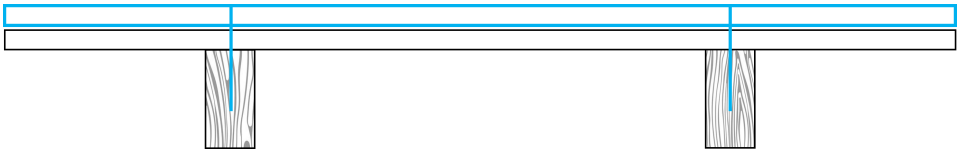

Figure 2.10: Examples of reinforcement techniques of timber floors using CLT or a concrete layer

The most prevalent scenarios and reinforcement strategies have been outlined. Other types of failure, such as tensile and compressive failure parallel to the grain, aren't covered in this article, and are not governing as described in Section 2.2.1. In practice, the choice of reinforcing technique for existing timber beams will be influenced not only by the reinforcement's capacity to offer necessary structural strengthening, but also by aesthetics, the necessity for reversibility, access for maintenance, and available expertise. Because reinforcing elements have different stiffness, thermal expansion, and moisture absorption properties than timber, factors like constrained shrinkage and swelling caused by thermal or moisture changes must be considered, and if necessary, additional thermal or moisture induced stresses should be accounted for in the design (Franke et al., 2015). For these reasons, only strengthening of monumental timber floors by means of additional timber layers on top of the floor will be considered.

2.3.1. Additional timber layers

Strengthening monumental timber floors through additional layers of timber on top of the existing floor is effective at preserving the monumental appearance of the beams and joists. In order to make calculations, three characteristics of these layers are important for strengthening the floor: the type of timber plate, the size and the method of attachment to the existing floor.

Two types of timber plates can be used: structural and non-structural plates. The structural plates (CLT and LVL) are plates that can be used to sustain loads. The non-structural plates (plywood, OSB, particleboard, MDF and hardboard) cannot support floor loads without timber beams. However, when properly connected to the existing structure, non-structural plates will strengthen the existing structure. Table 2.2 from the previous section shows that the structural plates have greater strength and stiffness with a lower density. This is of great importance when strengthening an existing timber floor, since more dead weight reduces the load capacity.

In order to achieve optimal load-carrying capacity with structural plates, these must span from wall to wall. However, it is often not possible to fit those dimensions through existing doors or windows and these plates are often too heavy to lift without machines. A better option is therefore to strengthen monumental timber floors with non-structural plates. As indicated in Table 2.2, plywood offers the best material characteristics. In order to create a uniform layer, several layers of plywood should be stacked, avoiding alignment of seams, see Figure 2.11. This figure illustrates two additional layers (red and green lines) on the existing floor (blue lines), where the seams over the span (not the edges) do not coincide. These layers should be connected with the existing structure to cooperate as one system. This connection could be established either through adhesives or fasteners. Since modifications must be reversible, fasteners are often preferred for strengthening monumental timber floors.

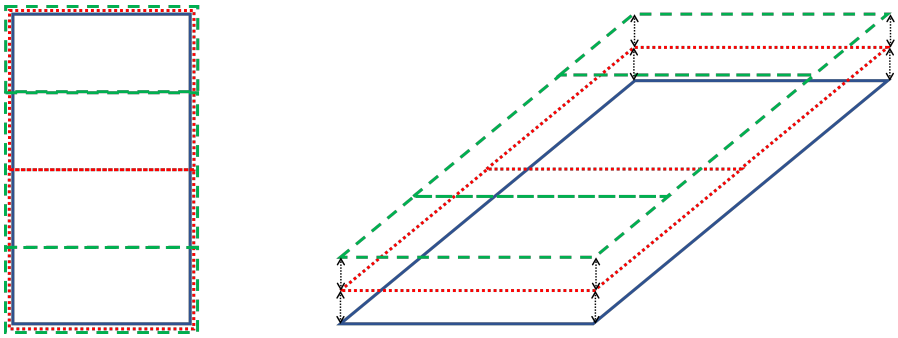

Figure 2.11: Seams of multiple layers should not be aligned

If the additional layers do not overlap, see the upper system in Figure 2.12, some parts of the system will have a lower effective stiffness. This results in a lower load-bearing capacity due to lower internal forces (normal focrce, shear force and moment) at these locations. Furthermore, the effective stiffness of the whole system will be significantly lowered compared to overlapped layers, resulting in larger deflections.

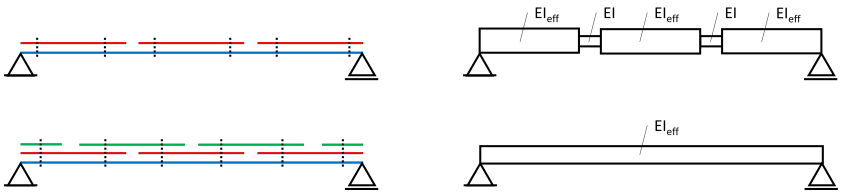

Figure 2.12: Effective stiffness due to multiple layers

2.3.2. Fasteners

As mentioned in the previous paragraph, the mechanical fasteners that connect the new elements to the existing structure often govern the strength and stiffness of the composite system. These connectors can be nails, staples, screws, dowels and threaded rods, see Figure 2.13. These dowel-type fasteners transfer the forces between the members through generating bending and tensile stresses in the fasteners as well as embedment and shear stresses in the timber along the shank.

Self-tapping screws are preferred when strengthening monumental timber floors, as they considerably reduce the preparation time by eliminating the need for pre-drilling and they are the product of choice for a reversible intervention.

Figure 2.13: Examples of different dowel-type fasteners

The grain angle is one of the most important factors which influences the strength and stiffness characteristics timber. The direction of the force has an impact on the behaviour of the joint. As illustrated in Figure 2.14, the strength of the timber reduces as the angle between the timber grain and the loading direction increases, with the same effect for stiffness. Stresses perpendicular to the grain reduce the load-bearing capacity of a joint tremendously and even cause the timber element to split.

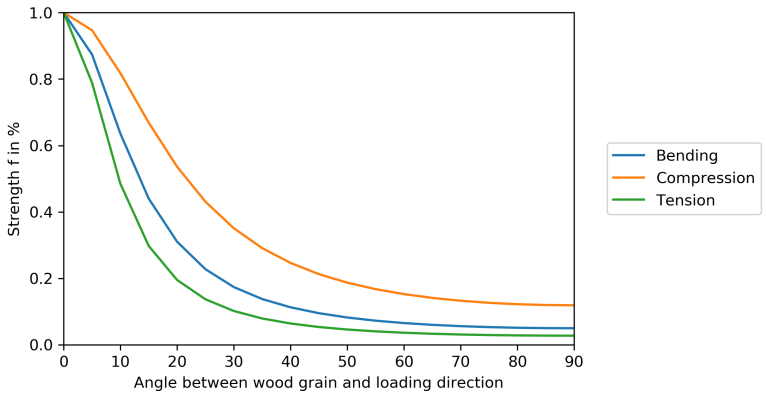

Figure 2.14: Influence of the grain angle (ϕ) on tensile, bending and compression strength (Grade C24) (Schlotzhauer et al., 2018)

Besides the grain angle, the diameter of the fastener also plays a major role (Whale and Smith, 1986). The strength in the timber element around the joint is reduced through the transferred of the fastener. However, there is one exception: the load-bearing capacity of fasteners up to a diameter of 8 millimeters are unaffected by the grain angle.

Slip modulus
When fasteners are placed perpendicular to the load the strength can be calculated by shear alone, by means of Equation 2.1 reported in Table 7.1 of NEN-EN 1995-1-1 (2011).

$$K_{ser,\perp} = \frac{\rho_{mean}^{1.5} \cdot d}{23} \tag{2.1}$$

Where:

$K_{ser,\perp}$	perpendicular slip modulus	N/mm
ρ_{mean}	mean density timber	kg/m^3
d	diameter fastener	mm

The withdrawal capacity is determined by the axial slip modulus of the threaded part anchored by a length L_w into the element. Blaß and Steige (2019) introduced Equation 2.2 to calculate the axial slip modulus. Kevarinmäki (2002) presented Equation 2.3 in order to calculate the axial slip modulus for multiple layered timber elements.

$$K_{ser,\parallel} = 2 \cdot d^{0.6} \cdot L_w^{0.6} \cdot \rho_{mean}^{0.9} \tag{2.2}$$

$$K_{ser,\parallel} = \frac{1}{\frac{1}{K_{ser,\parallel,1}} + \frac{1}{K_{ser,\parallel,2}}} \tag{2.3}$$

Where:

$K_{ser,\parallel}$	axial slip modulus	N/mm
ρ_{mean}	mean density timber	kg/m^3
d	diameter fastener	mm
L_w	penetration length in timber element	mm

Vertical placement has the disadvantage that the relative slip between the two parts is largely resisted by the fastener in bending, resulting in poor slip stiffness. In order to achieve a stiffer connection, fasteners can be placed inclined. The load transfer mechanism now includes not only the fasteners bending capacity and the timber embedment strength, but also the fasteners withdrawal capacity and the friction between the timber parts caused by the geometrical arrangement. Tomasi et al. (2010) presented Equation 2.4 for determining the stiffness of screws placed at an angle. The lateral and axial stiffness of an inclined screw are combined to determine its stiffness.

$$K_{ser} = K_{ser,\perp} \cdot \cos\alpha(\cos\alpha - \mu \sin\alpha) + K_{ser,\parallel} \cdot \sin\alpha(\sin\alpha + \mu \cos\alpha) \tag{2.4}$$

Where:

K_{ser}	inclined slip modulus	N/mm
$K_{ser,\perp}$	perpendicular slip modulus	N/mm
$K_{ser,\parallel}$	axial slip modulus	N/mm
α	angle of the fastener	°
μ	friction between timber elements ≈0.25	-

If the fasteners are X-positioned, the friction component μ between the timber elements disappears and the total slip modulus can be calculated with Equation 2.5 (Tomasi et al., 2010).

$$K_{ser} = K_{ser,\perp} \cdot (\cos\alpha)^2 + K_{ser,\parallel} \cdot (\sin\alpha)^2 \tag{2.5}$$

Inclined fasteners are most effective between 30 and 60 degrees, as they can create more rigid joint compared to vertical-placed fasteners (see Figure 2.15). It is not used to place fasteners at larger angles, because this would be impractical and would afford unusual length.

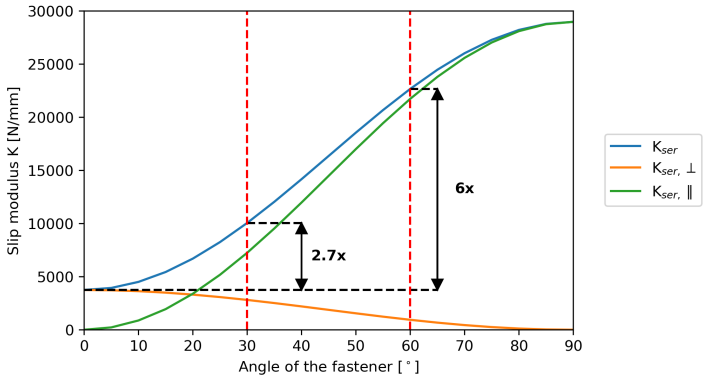

Figure 2.15: Relation of the fastener angle compared to the slip modulus, Equations 2.1, 2.2 and 2.5 (d=10mm; l_w=100mm; ρ_{mean}=400kg/m^3)

Failure mechanism

Dowel-type fasteners can be subjected to two types of loads. The first is shear, when a load is applied perpendicular to the axis of the fastener. The second is withdrawal or pushing in, when a load is applied in the direction of axis of the fastener. A combination of both is also possible. Laterally loaded fasteners (depending on a single- or double-shear timber-to-timber joint) are to be determined by using the Johansen model with rope effect. The laterally loaded fasteners are mainly dictated by the embedment strength of the timber, the yield moment of the fastener and the joint geometry. These fasteners can be determined by using failure mechanisms as illustrated in Figure 2.16.

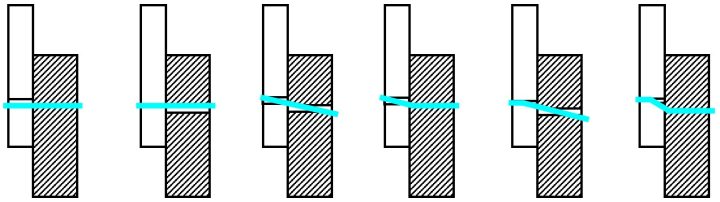

Figure 2.16: Single-shear timber-to-timber joints with their failure modes (Joachim Blaß and Sandhaas, 2017, p. 350)

Johansens yield theory has been expanded by Bejtka and Blaß (2002) in order to evaluate the load-bearing capacity of timber-to-timber connections with inclined fasteners. Roensmaens et al. (2018) developed an analytical model which accounts for a gap between the two connected elements. According to Roensmaens, the ductile failure mechanism f will be governing for the refurbishment of timber floors, see Figure 2.17.

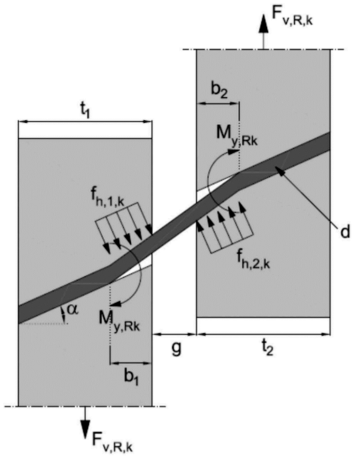

Figure 2.17: Failure mechanism F for an inclined screw with inner gap between the timber elements (Roensmaens et al., 2018)

The maximum load for this failure mechanism is assessed with Equation 2.6.

$$F_{v,Rk} = F_{ax}(\sin\alpha + \mu\cos\alpha) + (1 - \mu\tan\alpha) f_{h,1,k} d \frac{\beta}{\beta+1} \left(\sqrt{g^2 + \frac{4M_{y,Rk}(\cos\alpha)^2}{f_{h,1,k} d} \frac{\beta+1}{\beta}} - g \right) \quad (2.6)$$

In a follow-up study, Roensmaens et al. (2020) demonstrated (for push-out tests Table 4) that the average slip modulus is lowered as the height of the intermediate blocks (gap) is increased. A reduction factor for the slip modulus can be determined from Table 4. Another way to determine the reduction factor for the slip modulus is using the effective stiffness of the system (Table 6) together with the γ-method (for one- or two shear-planes).

Appendix B demonstrates that a reduction of the slip modulus has to be used if the amount of shear-planes is reduced. Figure 2.18 illustrates the factor that has to be used for this reduction. This factor is for fasteners at an angle of 45 degrees and a gap between 0 to 100mm. The dashed line demonstrates the expected reduction factor for gaps larger than 100mm.

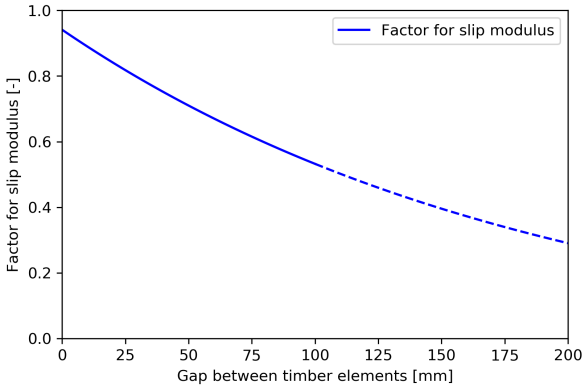

Figure 2.18: Factor slip modulus for increasing gap (at an angle of 45 degrees)

2.3.3. Multiple layered systems

As stated in section 1.2, it is a safe assumption to calculate a traditional timber floor comprising of timber beams, joists and planks, as a simply supported beam structures. If layers are added to strengthen the system, the load-bearing capacity and stiffness of the mechanically jointed system is between the corresponding values of composite beams whose individual components are not jointed and composite beams with rigid (glued) joints. Figure 2.19 clarifies the effect of a semi-rigid joint in terms of overall deformation and stresses over the beam depth.

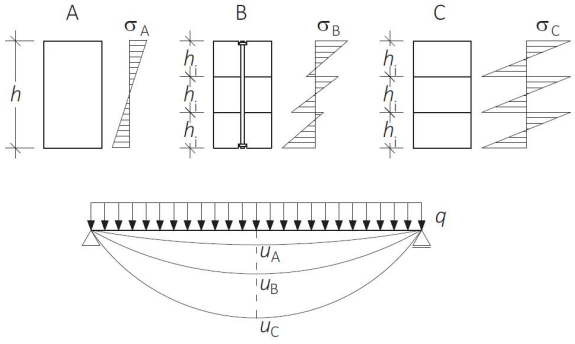

Figure 2.19: Deflection and bending stress distribution of: (A) a fully glued cross-section, (B) a cross-section comprising three individual cross-sections connected via semi-rigid joints, (C) a cross-section comprising three loosely superimposed individual cross-sections (Joachim Blaß and Sandhaas, 2017, p. 250)

Mechanically jointed beams can be calculated by a few methods: the gamma-method (γ), Schelling's method, the shear analogy method and with computer models.

Gamma-method
The γ–method is used in the Appendix of NEN-EN 1995-1-1 (2011). This method offers easily applicable verification rules. However, the γ-method has also a major limitation, as this method only can be used for mechanically composite beams up to only three components. The γ-method incorporates the loss of stiffness by applying the loss factor γ. This loss factor reduces the effect of Steiner's rule on the effective bending stiffness. The value of γ varies between zero and one. When γ has a value of one, the components work together as one and there are no stress losses. With a value of zero, the components do not work together and are considered to be separate components (Joachim Blaß and Sandhaas, 2017).

Möhler (1956) established the γ-method. When using this method, certain assumptions and conditions have to be taken into account:

- The girder is supported by two hinged supports;
- The girder is loaded by a constant load centrally on the girder or by a distributed sinusoidal load;
- The girder is composed of no more than three components;
- The connections are spaced out across the girder with a constant length;
- The components have a constant bending stiffness along their length;
- The shear stresses are negligible.

In the contrary to Möhler's second assumption, the NEN-EN 1995-1-1 (2011) states that his method may also be used with an uniformly distributed load. A beam's behaviour is almost the same, whether applying a sinusoidal or an uniformly distributed load. In both cases, the sinusoidal deflection line is present. A perfectly sinusoidal load rarely occurs, while a uniformly distributed load is common in practice. Therefore, this assumption has been adapted in order to make the method more practical.

Schelling's method
When using more than three components in a multi-layered system, the Schelling's method can be used. This method also determines the effective bending stiffness using the a loss factor γ. In addition this approach takes into account the spacing between the components (Schelling, 1982). The conditions and assumptions set for the Schelling's method are:

- The girder is supported by two hinged supports;
- The girder is loaded by a constant load centrally on the girder or by a distributed sinusoidal load;
- The connections are spaced out across the girder with a constant length;
- The components have a constant bending stiffness along their length;
- The shear stresses are negligible.

Shear-analogy method
In contrast to the γ- and Schelling's method, the shear-analogy method has no limitations regarding the amount of components and the assigned load. The shear-analogy method established by Kreuzinger in 1999, models the mechanically composite beam as a beam made of two components. A real component that adds up all the bending stiffnesses of all the components and a fictitious component that includes all the Steiner portions of the components and the losses due to shear deformation. This model includes both the losses due to the stiffness of the connecting components and the losses due to slip. Kreuzinger provides with his method a more accurate solution to the stresses in the girder than the previous described methods. However, the shear-analogy method can only be calculated by a computer due to its complexity (Joachim Blaß and Sandhaas, 2017).

Computer models

Another method for solving this type of problem is to use a computer model. Such a model can be set up for example in MatrixFrame. Through such a model, the stress in and deflection of the beam can be easily determined.

Software determines the stresses and deflection through the Euler-Bernoulli beam theory, see Equation 2.7, which described the relationship between the deflection and applied load.

$$EI \cdot \frac{d^4w}{dx^4} = q \tag{2.7}$$

2.4. Loads

The ability of a structure to withstand various types of loads - forces which induce stresses, deformations or accelerations - is an important feature of its structural integrity. Loads on a structure are created by factors such as the weight of the structure and the materials used to construct it, the weight of the occupants and their belongings (such as furniture) and the pressure applied by environmental conditions such as wind and rain. The basic concept associated with loads is that they are a ratio of the structure's theoretical strength to the maximum load it is expected to bear.

Based on the intended use, building codes dictate the size of loads for which the structures must be designed. These are based upon three primary categories: dead, live and environmental loads. Floor structures within the building envelop are usually only loaded with dead and live loads. Dead loads are considered to be permanent, as they will not alter during the lifetime of the building. They include the weight of materials used to construct the building, such as beams, flooring components and other fixed parts. Live loads are forces which move through a structure over its lifetime (like books in a library or people going through an office). Engineers should consider maximum loads which are more than the building will probably encounter over the course of its lifetime since loads vary and often are inconsistently applied to the structure.

Live loads can be dived into two categories: concentrated and distributed loads. A concentrated load is a force applied at a negligible area compared to the entire surface of the supporting member that it is considered a single point on the structure. Examples, illustrated in Figure 2.20, include a person where the surface area of its feet is negligible compared to the entire floor, a machine or a statue placed on a specific spot on the floor. A distributed load is one that is spread over a large area, see Figure 2.21. This load can be uniformly or non-uniformly distributed.

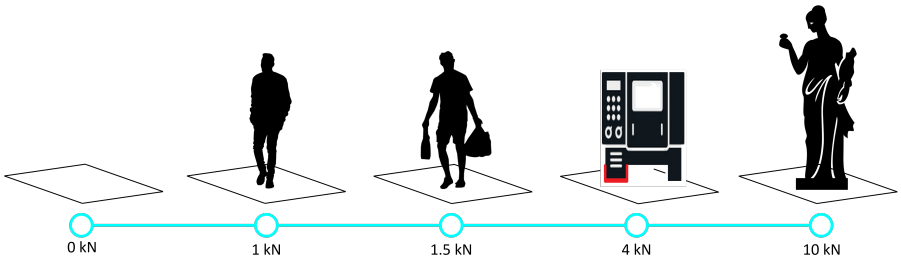

Figure 2.20: Concentrated load

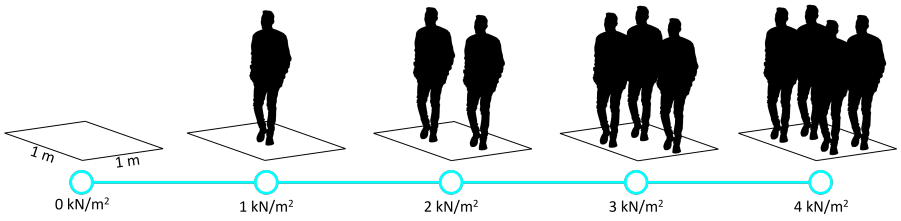

Figure 2.21: Distributed load of persons uniformly distributed over

Whether the concentrated (Q_k) or distributed (q_k) load becomes governing depends on the centre-to-centre distance of the members and their span, which is demonstrated by the following derivation. The larger side is normative.

$$M_{qk} : M_{Qk}$$
$$\frac{1}{8} \cdot q_k \cdot c.t.c. \cdot l^2 : \frac{1}{4} \cdot Q_k \cdot l$$
$$\frac{1}{2} \cdot q_k \cdot c.t.c. \cdot l : Q_k$$

2.5. Case study: Structural performance

To determine the critical structural parameters of timber floors, a case study has been done on the structural performance of the load-bearing components of two floors in the Prinsenhof Museum in Delft (full calculations see Appendix C.) Three aspects of the ultimate limit state (ULS) were considered: bending moment, shear force and compression perpendicular to the grain. In addition, the deflection in serviceability state (SLS) was calculated. Those aspects were examined for three situations, which are: self-weight, added distributed load (30 people) and an added concentrated load (air-handling unit).

The calculations in the appendix demonstrated that for the ULS bending stress was governing. Figure 2.22 shows that unity check for bending failure. The ratio between the unity check of the distributed load (orange bar) and concentrated load (green bar) shows that with a larger area, the distributed load is becoming normative. It is therefore always advisable to put large concentrated loads on the stronger elements.

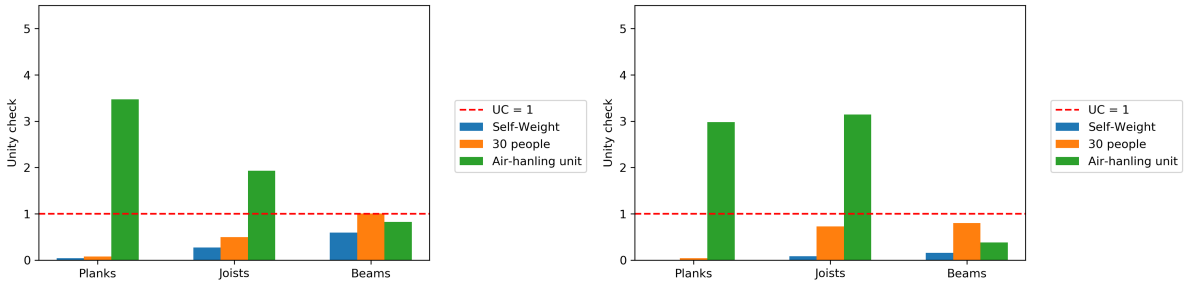

Figure 2.22: Bending stress unity check - (LEFT) floor between the dormitory and attic (RIGHT) floor between the guest quarter and first floor

Figure 2.23 illustrates the unity check on deflection for both floors. Which show the influence the length of an element has on the unity check (difference in length of the green bar for the joists).

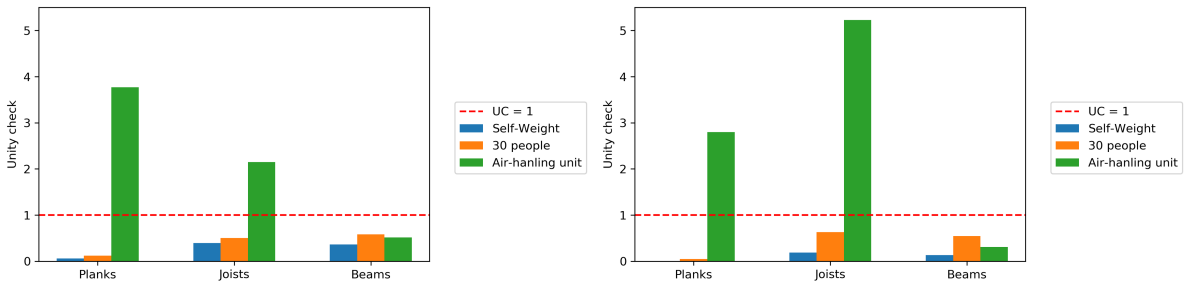

Figure 2.23: Deflection unity check - (LEFT) floor between the dormitory and attic (RIGHT) floor between the guest quarter and first floor

What is evident in both figures is that for large concentrated loads, the planks and joists become normative. And that for large distributed loads the beams become normative.

3

Acoustic transmission

Sounds are perceivable through ears. The subjective way of perceiving sounds is described by what is audible and can be perceived as soft or loud or even annoying. The objective approach of sound deals with pressure changes around the atmospheric air pressure. Sound exists only through a medium (such as air); in a vacuum (space) there is no sound.

3.1. General sound principle

Sound can be described by a wavelength λ, expressed in metres, which is the distance between the two consecutive maxima or minima. The wave number k indicates how many waves (wavelengths) occur per unit length and is therefore the inverse of the wavelength (m^{-1}). The amplitude describes the loudness and the wavelength the frequency of the sound. The frequency of sound is defined as a number of vibrations per second, see Equation 3.1. When the wave speed is constant, lower frequencies will have longer wavelengths (see Figure 3.1). Therefore, low frequencies are harder to insulate than high frequencies.

$$f = \frac{c}{\lambda} \tag{3.1}$$

$$k = \frac{2\pi}{\lambda} \tag{3.2}$$

Where:

f	frequency	Hz
c	wave velocity	m/s
λ	wavelength	m
k	wave number	m^{-1}

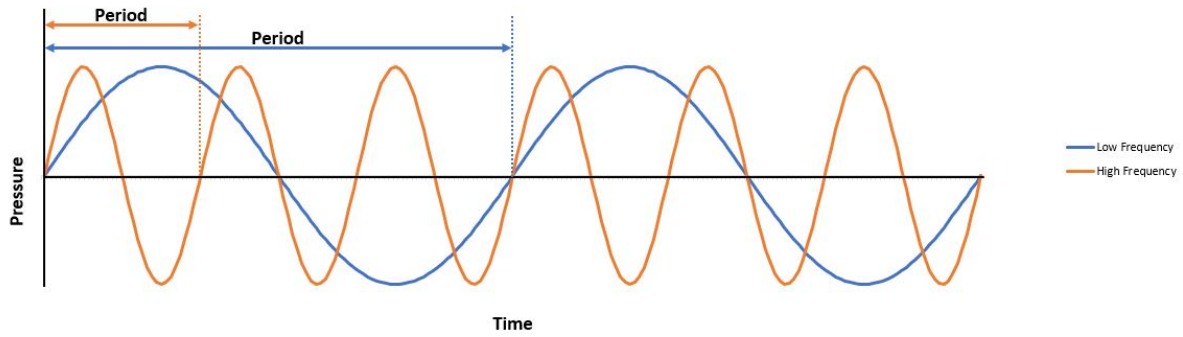

Figure 3.1: Low and high frequency waves

Another regularly used value is the angular frequency ω which describes how fast the waves oscillate and refers to the angular displacement per unit time.

$$\omega = 2\pi f \tag{3.3}$$

Where:

f	frequency	Hz
c	wave velocity	m/s
λ	wavelength	m
ω	angular frequency	Hz

Sound waves can be distinguished into three types. Bending and transverse waves which are dominant for flanking sound transmission and longitudinal waves for direct sound transmission, Figure 3.2 illustrates the most important of the three wave types, the bending wave.

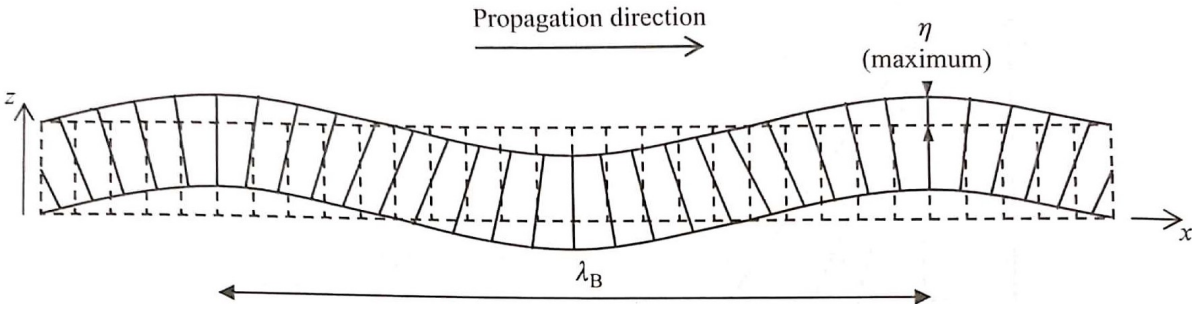

Figure 3.2: Bending waves in solids (Hopkins, 2020, p. 123)

Wave speeds in solids are higher than in air, which causes the wavelengths to be larger than the elements. Since longitudinal waves can only exist in elements that are larger than their wavelength, they often do not exist in building elements. However, there is a different type that exist in elements. This wave is present because of a shear modulus. Shear waves, better known as transverse waves, transfer through a solid due to shear deformation. Their speed is related to the shear modulus G.

Bending waves are caused by transverse deflection of the structural element. They are by far most the important for sound radiation. Their wave speed is related to the bending stiffness of the element, mass and the frequency, as stated in Equation 3.4 (Cremer et al., 1974, p. 55).

$$c_b = \sqrt[4]{\frac{B}{m'}}\sqrt{\omega} \tag{3.4}$$

$$B = E \cdot I \tag{3.5}$$

Where:

c_b	bending wave velocity	m/s
B	bending stiffness	Nm^2
m'	mass per unit area	kg/m^2
ω	angular frequency	Hz
E	modulus of elasticity	N/m^2
I	moment of inertia	m^4

3.2. Quantification of sound

A healthy human ear can detect very small pressure fluctuations around atmospheric pressure (1 bar). The sound pressure at the hearing threshold (20 µPa) and the pain threshold (200 Pa) are too far apart on a linear scale to work with such numbers. Therefore, a quantity is derived on a logarithmic scale (sound pressure level L_p in decibel dB). The hearing threshold corresponds to 0 dB and the pain threshold to 140 dB. ISSO-24 (2018) states that an increase of 2 dB is just perceptible to the human ear. Although, an increase of a 3 dB is more general trend according to acoustic experts within ABT.

In addition to the sound level L_p, the distribution of the sound energy over different frequencies is important. Audible sound is roughly in the range of 20 – 20000 Hz. This range is internationally divided into smaller frequency ranges, which are called octave bands. The subsequent octave band always is a factor 2 bigger: 16 – 31.5 – 63 – 125 – 250 – 500 – 1000 – 2000 – 4000 – 8000 – 16000 Hz. Although a human ear can detect 20 to 20000 Hz, the frequencies from 63 to 4000 Hz are the most important. Lower and upper bass frequencies are between 32 and 500 Hz. The zone between 500 and 2000 Hz is defined by human speech intelligibility and the 2000 Hz to 8000 Hz zone gives presence to speech.

When the sound level L_p (dB) and the frequency range (Hz) is plotted in a graph, a spectrum is created which shows how much sound energy is present in different frequency bands, see Figure 3.3. This is important to determine the action needed for a better reduction of sound, taking in consideration that measures for higher frequencies differ from the lower frequency bands (ISSO-24, 2018).

$$L_{p,total} = 10 \log\left(\sum 10^{\frac{L_{p,i}}{10}}\right) \tag{3.6}$$

Where:

$L_{p,total}$	total sound level in the room	dB
$L_{p,i}$	sound level of source i	dB

Multiple sound sources can be added logarithmically with Equation 3.6, either horizontally or vertically, as demonstrated in Table 3.1 and Figure 3.3. Both clearly demonstrate that when two sound sources with the same sound pressure level are in close proximity, the sound pressure level will not be doubled. When the sound pressure level of both sources is the same, see the first column of Table 3.1, a maximum of 3 dB is added to the total sound pressure level. When the difference between two sound pressure levels is 10 dB or more, see the seventh column of Table 3.1, the total sound pressure level is equal to the highest value.

	Frequency [Hz]							**Total [dB]**
	63	125	250	500	1000	2000	4000	
$L_{p,1}$	71	71	70	64	63	60	60	76
$L_{p,2}$	71	73	75	62	63	58	50	78
$L_{p,total}$	74	75	76	66	66	62	60	80

Table 3.1: Example of adding sound levels of two different sources

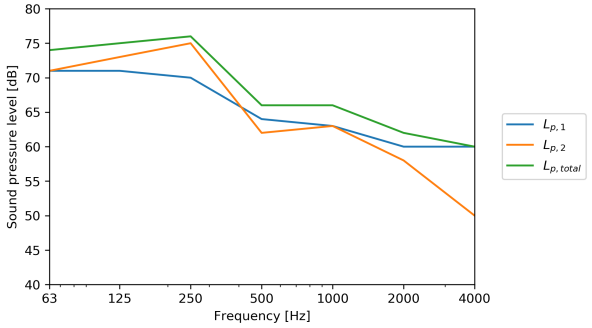

Figure 3.3: Example of adding sound levels of two different sources

3.2.1. Sound spectrum

As explained in the previous section, a sound spectrum shows how much sound energy is present in different frequency bands. Whenever sound insulation of structures has to be optimized, it is important to know which sound spectra a present. When people are talking or an air-handling unit is running some frequencies play a greater role than others. Figure 3.4 illustrates two examples of sound spectra that might occur in buildings. The critical frequencies of human speech are between 250 and 1000 Hz, where clearly the sound pressure level is the highest (DPA microphones, nd). Whereas for air-handling units the lower frequencies, below 250 Hz, play a critical role (Roonasi, 2003, p. 67,68) (Bujoreanu and Benchea, 2016, p. 10). The dashed lines in Figure 3.4 are the expected sound pressure level of the sound spectrum and are not given by the references (Bujoreanu and Benchea, 2016, DPA microphones, nd, Roonasi, 2003).

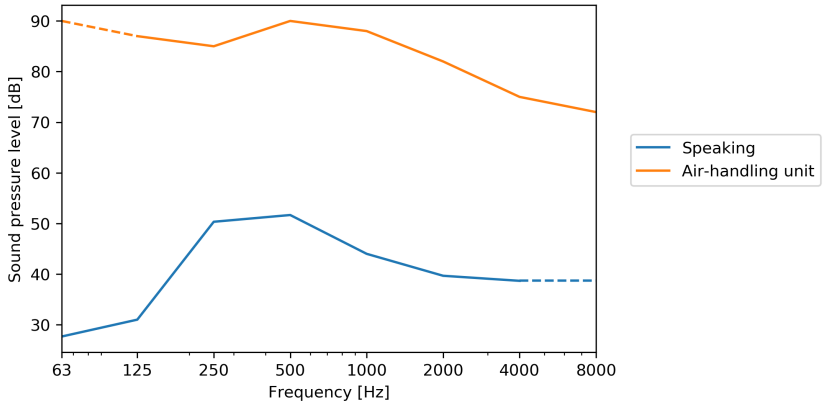

Figure 3.4: Examples of sound spectra of speaking and an air-handling unit (Bujoreanu and Benchea, 2016, DPA microphones, nd, Roonasi, 2003)

3.2.2. Sound perception and rating methods

The perception of loudness is primarily a function of sound pressure and related by frequency. Human ears are not equally sensible to all frequencies (ISSO-24, 2018) .In addition, the ear sensitivity to a specific frequency varies depending on the sound pressure level. Figure 3.5 illustrates these characteristics with a collection of contours in phons. One phone equals one dB at 1000 Hz. Across the frequency range displayed, each contour approximate an equal loudness level. The loudness of a sound is equal to the sound pressure level of a standard sound at 1000 Hz, thus 40 phons which is 40 dB at 1000 Hz is equally as loud as 63 dB at 100 Hz or 34 dB at 3500 Hz (Hyper Physics, nd).

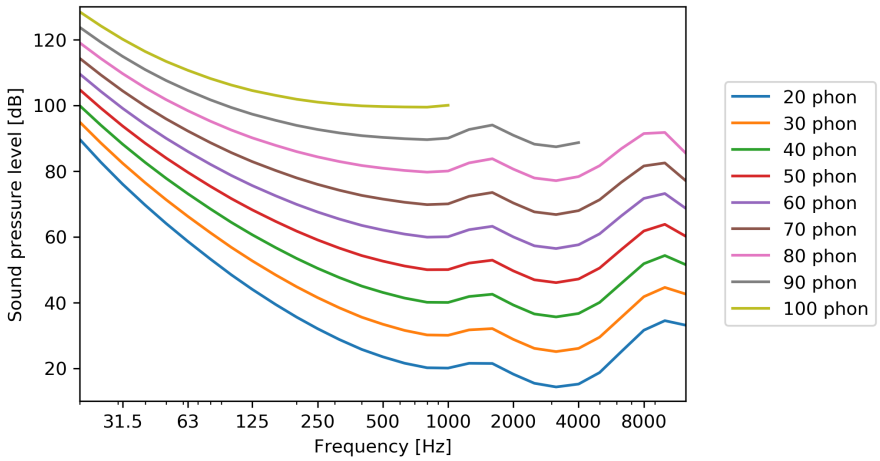

Figure 3.5: Equal-loudness contours Hyper Physics (nd)

The human ear perceives sound in terms of loudness and pitch, but sound-measuring equipment un-

derstands sound as pressure and frequency. As a result, a lot of research has been done to match sound pressure and frequency to sound levels as experienced by the human ear. With the goal to create a single-number system that could represent sound intensity and quality.

Three of the most used single-number descriptors are the A-weighting network, noise criteria (NC) and room criteria (RC). However, they all have the same deficiency: they unavoidably lose crucial information about a sound's character or quality. Each of these descriptors is based on octave band sound data which do not show all the present tones. Furthermore, the conversion from eight octave bands to a single-number excludes even more sound information. Despite this deficiency, the single-number descriptors are useful tools for characterizing sound levels in a room and are commonly used to define its acoustical requirements.

A-B-C Weighting

A-, B-, or C-weighting is a straightforward approach to integrate octave band sound data into a single-number descriptor, see Figure 3.6. A-weighting best approximates human response to sound in the range where no hearing protection is required, it is particularly suited for low-volume sound levels. For medium-volume sound levels, B-weighting is used. For high-volume sound levels, when the ear's response is generally flat, C-weighting is used.

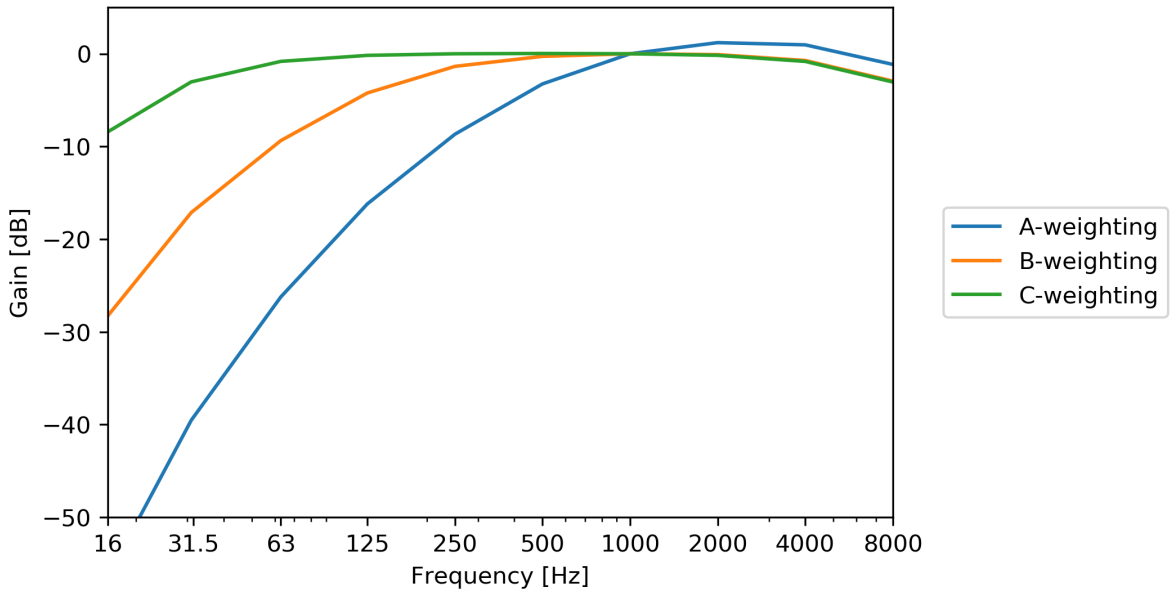

Figure 3.6: A-, B-, C-weighted sound frequency curves (Wikipedia, The Free Encyclopedia, 2005)

A-weighting is therefore the commonly used for indoor environments. The following steps describe how to calculate an A-weighted value. Table 3.2 demonstrates that the sound levels L_p should be corrected to a total A-weighted sound level value, which is then presented as $L_{p,A}$ and expressed in dB(A). The curve in Figure 3.6 shows the correction per frequency and weighting. Similarly, A-weighted sound levels can be added logarithmically.

	Frequency [Hz]							**Total**
	63	125	250	500	1000	2000	4000	
L_p	74	75	76	66	66	62	60	80 dB
A-weighting	-26	-16	-9	-3	+0	+1	+1	
$L_{p,A}$	48	59	67	63	66	63	61	72 dB(A)

Table 3.2: Example of A-weighting

Noise criteria (NC)
Perhaps the most popular single-number descriptor used to assess sound pressure levels in indoor situations are the noise criteria (NC) curves. These curves are displayed in Figure 3.7, where the loudness along each NC curve is roughly the same, just as the equal-loudness curves.

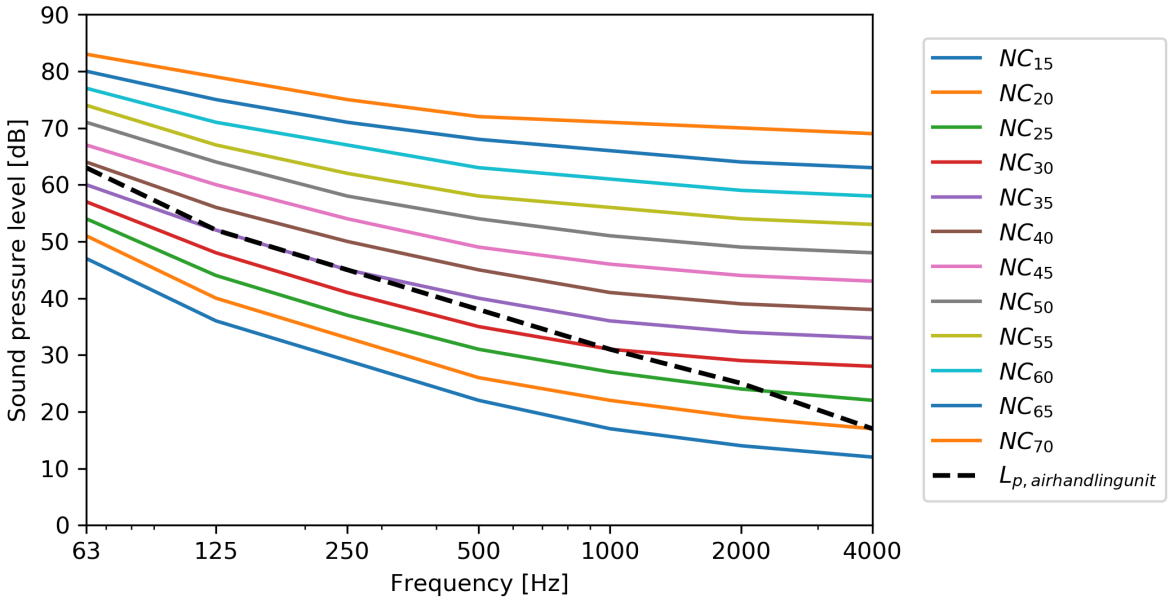

Figure 3.7: NC curves The Engineering Toolbox (nda), with a spectrum of an air-handling unit equal to NC-39

Despite their popularity and ease of use, NC curves have a few deficiencies. They don not take into account the tonal character and overall significance of each octave band. The single-number descriptor of a sound spectrum is given by its highest reached NC level. The black dashed line in Figure 3.7 represents the sound spectrum of an air-handling unit. The resulting NC value, NC-39, is generally accepted. However, high sound pressure levels at low frequencies are often perceived as an annoying rumble. Table 3.3 shows the recommended NC levels and their equivalent dB(A)'s.

Type of room	Recommended NC level	Equivalent dB(A)
Homes, urban	25-30	35-45
Musea	30-35	40-45
Restaurants	40-45	50-55

Table 3.3: Recommended NC level (The Engineering Toolbox, nda)

Room criteria (RC)
The room criteria (RC) curves enable, similar to NC curves, a rating for sound pressure levels indoors. The main distinction is that RC single-number descriptor provides extra information about the sound quality. Sound spectra can be imbalanced in ways that result in poor acoustic quality, as the example for NC-curves in Figure 3.7 demonstrated. A rumble is produced when there is too much low-frequency sound, while a hiss is produced when there is too much high-frequency sound. Both are often perceived as annoying.

The use of RC curves allows to detect these imbalances. There are two descriptors used for RC rating: a number and a letter. The number stand for speech interference level (SIL) of the sound. The letter stand for the character of the sound as described by a subjective observer. The RC uses four letters as a descriptor: N (neutral or balanced spectrum), R (rumble), H (hiss) and RV (perceptible vibration). In addition to the NC level calculation, the RC level calculation also includes the 31.5 Hz octave band.

To calculate the first descriptor SIL of the RC-value, the average sound pressure level of the 500, 1000 and 2000 Hz octave bands needs to be determined. Than three lines need to be drawn:

1. Line C: draw a line with a slop of -5 dB per octave that passes through the SIL at 1000 Hz octave band, this will be the reference line;
2. Line D: draw a line between the 31.5 and 500 Hz that is 5 dB above the reference line (C);
3. Line E: draw a line between the 1000 and 4000 Hz that is 3 dB above the reference line (C).

The line D en E represent a boundary for the maximum permitted deviation to receive a neutral rating. To be able to judge the character of the sound quality the following criteria are used:

- Neutral (N), the sound pressure level of each of the octave bands should be below line D and E;
- Rumble (R), the sound pressure level in any of the octave bands between 31.5 and 500 Hz is above line D;
- Hiss (H), the sound pressure level in any of the octave bands between 1000 and 4000 Hz is above line E;
- Perceptible vibration (RV), the sound pressure level between the octave bands 16 and 63 Hz is located in the shaded regions (A or B). Region A: Noise-induced vibrations in lightweight wall and ceiling structures are likely to be sensed. Region B: Noise-induced vibrations in lightweight wall and ceiling structures may be sensed.

Figure 3.8 displays the RC curves and the sound spectrum of the same air-handling as shown in Figure 3.7. The RC rating for this spectrum is R-31(R).

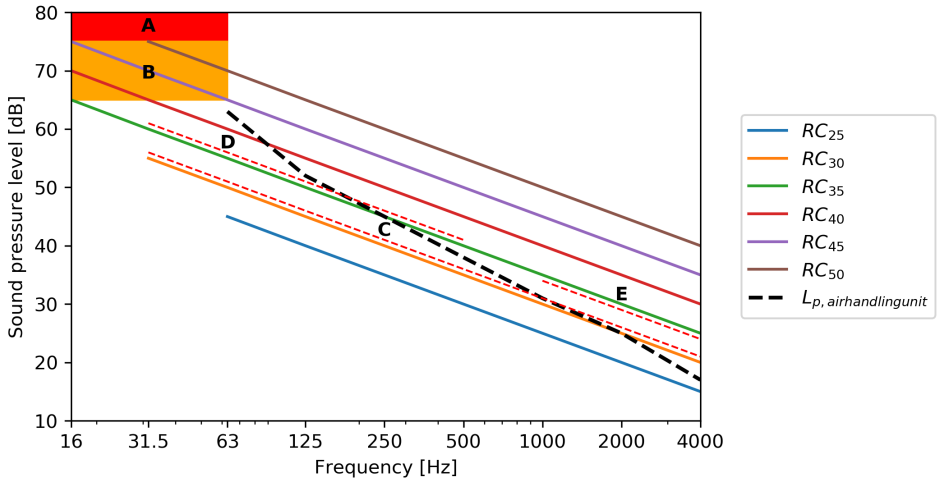

Figure 3.8: RC curves (The Engineering Toolbox, ndb), with a spectrum of an air-handling unit equal to RC-31(R)

Table 3.4 shows the recommended RC and NC values per type of room. When the example is expressed in terms of the NC value (39), it is above the recommended NC level for a museum. However, the more specific calculation of the RC value (31) indicates that this example is within the accepted level for a museum. Although the sound can still be experienced as annoying (R).

Type of room	Recommended RC level	Equivalent NC level	dB(A)
Homes, urban	25-35	25-35	35-45
Musea	30-35	30-35	40-45
Restaurants	40-45	40-45	50-55

Table 3.4: Recommended RC level The Engineering Toolbox (ndb)

3.2.3. Eurocode regarding rating of sounds

NEN-EN-ISO 717-1 (2020) defines single-number quantities for the airborne sound insulation of a building element. And NEN-EN-ISO 717-2 (2020) defines structure-borne sound level in the receiving room of a building. Figure 3.9 illustrates the reference curves described in both standards. These curves are, as well as the sound rating methods, based on octave bands.

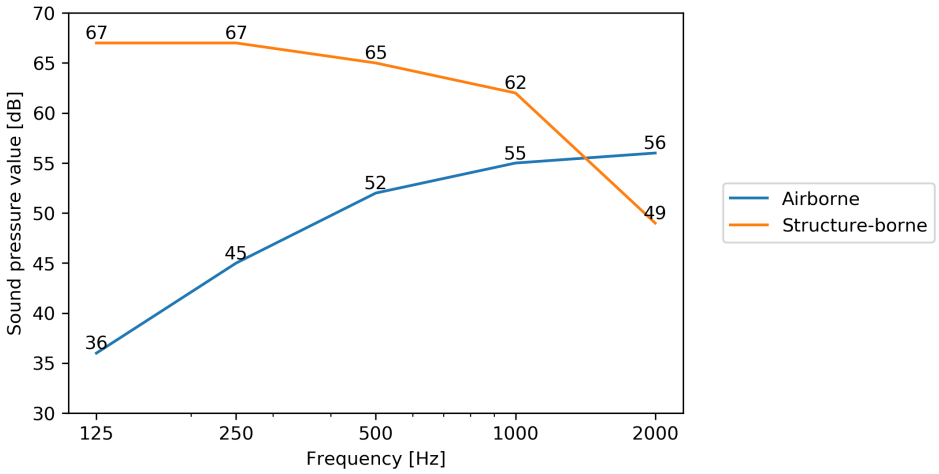

Figure 3.9: Curve of reference values for airborne sound insulation of an element and structure-borne sound pressure level, for octave bands (NEN-EN-ISO 717-1, 2020, NEN-EN-ISO 717-2, 2020)

Airborne sound

The reference curve for airborne sound insulation only indicates the values that a building element must insulate. It does not provide any information about the sound spectra.

According to the method of NEN-EN-ISO 717-1 (2020), the sound pressure level data shall be given to one decimal place per octave band in order to evaluate the results of a sound insulation measurement. Shift the reference curve in increments of 1 dB towards the measured sound pressure levels until the sum of unfavourable deviations is as large as possible but not more than 10 dB (measurement in 5 octave bands). An unfavourable deviation at a particular frequency occurs when the result of measurements **is less than** the reference value. Only the unfavourable deviations shall be taken into account. The value, in decibels, of the reference curve at 500 Hz, after shifting it in accordance with this procedure is R_w.

$$R_w(C; C_{tr}) \geq value\ given\ in\ Table\ 3.5 \tag{3.7}$$

Type of room	Recommended Airborne level	Equivalent RC level	NC level	dB(A)
Homes, urban	43-62	25-35	25-35	35-45
Musea	42-63	30-35	30-35	40-45
Restaurants	42-63	40-45	40-45	50-55

Table 3.5: Recommended airborne sound insulation level (NEN 1070, 1999)

Structure-borne sound

The reference curve for structure-borne sound level indicates the sound pressure level which is present in the receiving room of a building.

According to the method of NEN-EN-ISO 717-2 (2020), the sound pressure level data shall be given to one decimal place per octave band in order to evaluate the results of a sound insulation measurement. Shift the reference curve in increments of 1 dB towards the measured curve until the sum of unfavourable deviations is as large as possible but not more than 10 dB. An unfavourable

deviation at a particular frequency occurs when the results of measurements **exceed** the reference value. Take into account only the unfavourable deviations. The value, in decibels, of the reference curve at 500 Hz, after shifting it in accordance with this procedure and then reducing it by 5 dB is $L_{n,w}$.

$$L_{n,w}(C_I) \leq value\ given\ in\ Table\ 3.6 \tag{3.8}$$

Type of room	Recommended Structure-borne level	Equivalent RC level	NC level	dB(A)
Homes, urban	43-63	25-35	25-35	35-45
Musea	43-63	30-35	30-35	40-45
Restaurants	43-63	40-45	40-45	50-55

Table 3.6: Recommended structure-borne sound pressure level (NEN 1070, 1999)

3.2.4. Conclusion

As described in Section 3.2, sound is made up of a range of frequencies which together form a sound spectrum. In most cases, sound spectra are projected between the range of 63 and 4000 Hz. The frequencies below 63 Hz are excluded because they are difficult to predict as they require a very large reception area due to their long wavelengths. The higher frequencies are often not included because they are perceived as less annoying.

The examples of sound spectra, Figure 3.4, clearly indicate that the sound pressure level produced by an air-handling unit will lead to the most critical situation for sound insulation. In addition, the curves for the single-number descriptors clearly show that high sound pressure levels at low frequencies are being perceived as annoying. Therefore, in the following, only the sound produced by air-handling unit or heavy machines will be considered.

Lastly, the RC-rating should be used for rating the sound spectra is know. This is because all the single-number descriptors leave out a lot of information about the sound quality, but the RC-rating will give more information when imbalanced sounds are present. Otherwise, use the methods of NEN-EN-ISO 717-1 (2020) and NEN-EN-ISO 717-2 (2020).

3.3. Sound transmission through structures

Acoustic sounds which travel through structures can be split into two categories: airborne sounds and structure-borne sounds. Airborne sounds are produced by vibrating air, for example a voice, speaker, machine, etc. Structure-borne sounds are a result of a vibration in an element produced by an impact, for example by a hammer, machine, person, etc. which causes vibration of the construction. The vibrating structural parts emit airborne sounds elsewhere in the building, see Figure 3.10. Heavy structures (such as concrete) are less prone to structural vibrations than light structures (such as timber).

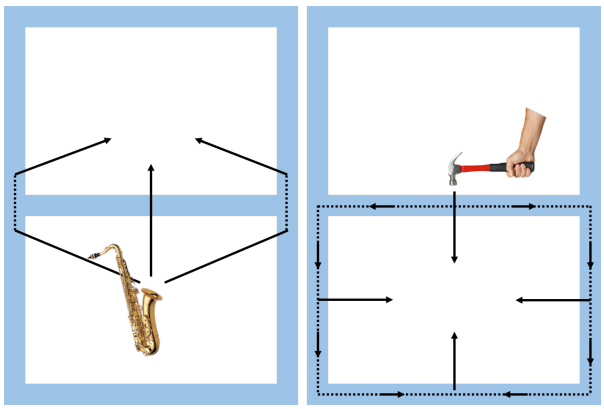

Figure 3.10: Sound transmission of airborne and structure-borne sounds (ISSO-24, 2018, p. 37)

Sound waves which hit the floors or walls get partially reflected, absorbed and transmitted, see Figure 3.11. The incident sound wave is reflected due to the difference in acoustic impedance at the surface boundary. The impedance describes the relation between the applied pressure and the resulting flow. A large difference in acoustic impedance at a boundary results in reflected sound waves. In general waves are not entirely reflected, waves often get partially absorbed and transmitted. The amount of sound energy that is absorbed depends on the absorption coefficient α, its value is between 0 and 1 (one indicates full absorption). The waves which are not absorbed by the material are transmitted by radiation into the neighbouring room. Limiting the amount of transmitted sound waves is the main goal of sound reduction. An important remark is that sound absorption is not equal to sound reduction. Sound absorption affects the sound level inside a room, however it does not influence the sound reduction from one room to another.

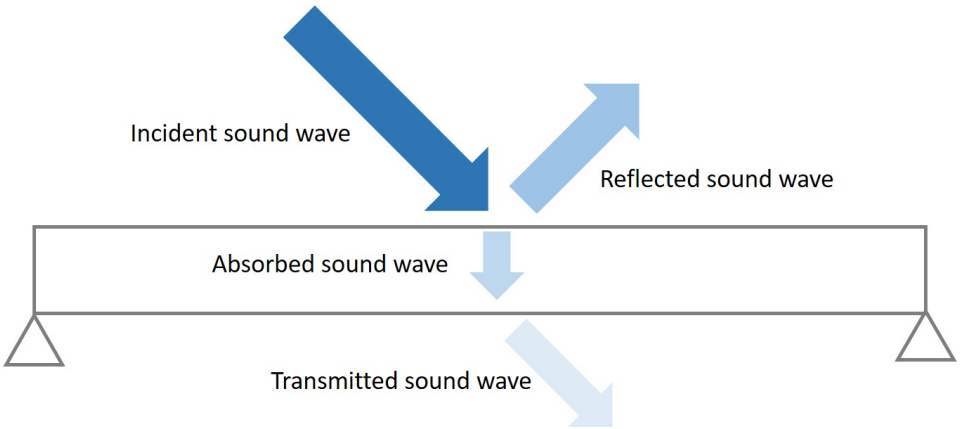

Figure 3.11: Sound wave reflection, absorption and transmission

3.4. Airborne sound

An example of airborne sound is the possibility to hear the music of the neighbours in a multi-story building. The degree to which the music is audible, depends on the degree to which the partition element of the two apartments reduces the airborne sounds. The sound insulation depends on the material properties of the partitioning element and must be independent of the room properties. Sound insulation can be determined by Equation 3.9 which assesses the difference between the emitted and received sound pressure level and adds the sound absorption of the receiving room.

$$R = L_{p,send} - L_{p,receive} + 10\log\left(\frac{S}{A_{receive}}\right) \tag{3.9}$$

Where:

R	direct sound transmission loss	dB
$L_{p,send}$	sound level in the emitting room	dB
$L_{p,receive}$	sound level in the receiving room	dB
S	area of the separating element	m^2
$A_{receive}$	volume of the receiving room	m^3

Sound insulation, also called sound reduction, of a homogeneous element varies along the frequency range and can be divided into three ranges, see Figure 3.12. In the lower range of the frequencies the reduction is governed by the stiffness of the element, in the middle range by the mass and the upper by damping.

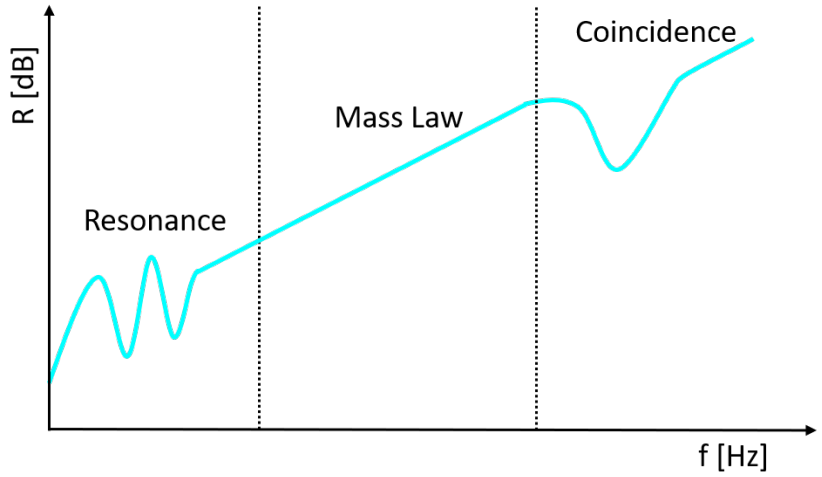

Figure 3.12: Sound reduction over the frequency range of a homogeneous element (Ir. C.J. Janssen, 2019)

3.4.1. Resonance

Building elements have a natural frequency, which is also called the resonance frequency, at which they are susceptible to vibrations. At the resonance frequency, the sound reduction of the system is lowered significantly. When systems are constructed of multiple layers with the same resonance frequency, the vibrations are passed on relatively easily. However, when elements with different resonance frequencies are connected, their resonance frequency is altered. The bending resonance frequency of elements depends on the dimensions and stiffness of an element and the mass per unit area, see Equation 3.10 (NEN-EN 1995-1-1, 2011). As described in Subsection 3.2.2, low frequencies have high hearing thresholds so it is preferable to achieve a low resonance frequency.

$$f_n = \frac{\pi}{2l^2}\sqrt{\frac{(EI)_L}{m'}} \tag{3.10}$$

Where:

f_n	resonance frequency	Hz
l	length element	m
$(EI)_L$	bending stiffness element	Nm^2/m
m'	mass per unit area	kg/m^2

3.4.2. Mass law

Equation 3.12 demonstrates the sound insulation of an element due to the mass law. According to the practical mass law, the sound reduction for homogeneous constructions increases by 6 dB per mass doubling.

$$R_{random} = 20\log\left(\frac{2\pi f m'}{2\rho_0 c_0}\right) - 5 \tag{3.11}$$

Where:

R_{random}	direct sound transmission loss of random incidence	dB
f	sound frequency	Hz
m'	mass per unit area	kg/m^2
ρ_0	density of air	kg/m^3
c_0	speed of air	m/s

3.4.3. Coincidence

The range for where the mass law is valid, is limited nearby the coincidence frequency. Generally, a strong decrease in sound insulation occurs at the coincidence frequency. The coincidence frequency, also known as the critical frequency, is the reason that the mass law does not correctly predict the sound reduction at higher frequencies. When the speed of sound in the air and the element are equal, coincidence of vibrations occurs. As the speed of sound only affects the bending waves, the critical frequency is defined when the bending waves which have the same speed as the waves in the air. It is preferable to obtain the highest critical frequency possible as the higher frequencies are perceived as less annoying. The critical frequency can be determined by Equation 3.12 (Cremer et al., 1974, p. 486).

$$f_c = \frac{c_0^2}{2\pi}\sqrt{\frac{m'}{B}} \tag{3.12}$$

Where:

f_c	coincidence frequency	Hz
c_0	speed of air	m/s
m'	mass per unit area	kg/m^2
B	bending stiffness	Nm^2

3.4.4. Sound radiation

Radiating sound into the receiving room is an important aspect of sound transmission. If sounds or vibrations were not be radiated, sound transmission would be insignificant. The amount of sound radiation can be determined by the critical frequency and expressed as the radiation factor. For estimations, this factor can be taken as 0.1 below critical frequency and as 1 above critical frequency.

In reality the radiation of a plate consists of the vibration modes of the eigen frequencies of the plate. Which depend on the natural modes and boundary conditions. Although the radiation factor of a single frequency induced by a specific vibration pattern may be calculated, it is more practical to take an average over a narrow frequency band. As a result, the average sound radiation factor over an octave range is frequently used to express the sound radiation factor. There are three distinct zones, and the radiation factor is calculated as follows (Vigran, 2008).

$$\sigma = \frac{2(a+b)c_0}{2\pi^2\sqrt{f\cdot f_c}a\cdot b\sqrt{\chi^2-1}}\left(\ln\left(\frac{\chi+1}{\chi-1}\right)+\frac{2\chi}{\chi^2-1}\right) \quad \sigma \le 2 \qquad f < f_c \tag{3.13}$$

$$\sigma = \sqrt{\frac{2\pi f}{c_0}}\sqrt{a}\left(0.5-0.15\frac{a}{b}\right) \quad \sigma \le 2 \qquad f \approx f_c \tag{3.14}$$

$$\sigma = \frac{1}{\sqrt{1-\frac{f_c}{f}}} \quad \sigma \le 2 \qquad f > f_c \tag{3.15}$$

$$\chi = \sqrt{\frac{f_c}{f}} \tag{3.16}$$

Where:

σ	radiation factor	-
f	frequency	Hz
f_c	coincidence frequency	Hz
c_0	speed of air	m/s
a	length of plate (a<b)	m
b	width of plate (a<b)	m

When the plate is vibrated in its natural resonant mode(s) and hence vibrates freely, the above formulas apply. When the plate is subjected to a vibration, the equations above are no longer applicable. Sewell (1970) proposed Equation 3.17 for a radiation factor for forced vibrations.

$$\sigma_f = \frac{1}{2}\left(\ln(k_0\sqrt{ab}) + -\wedge\right) \quad \sigma_f \leq 2 \tag{3.17}$$

$$\wedge = -0.964 - \left(0.5 + \frac{a}{\pi b}\right)\ln\frac{a}{b} + \frac{5a}{2\pi b} - \frac{1}{4\pi k_0^2 ab} \tag{3.18}$$

Where:

σ_f	radiation factor for forced vibrations	-
k_0	wave number for air	1/m
a	length of plate (a<b)	m
b	width of plate (a<b)	m

The forced vibration field is dominant for frequencies below the critical frequency, while the free vibration field is dominant for frequencies above the critical frequency. In the case of direct sound transmission, however, both modes of vibration should be considered.

3.4.5. Internal damping

The energy lost during the transmission of a sound wave through a medium is known as internal damping. NEN-EN-ISO 12354-1 (2017) uses Equation 3.19, which is a simplification of the real situation because damping due to support conditions or radiation is not considered.

$$\eta_{tot} = \eta_{int} + \frac{m'}{485\sqrt{f}} \tag{3.19}$$

Where:

η_{tot}	internal damping	-
η_{int}	initial damping ≈ 0.01	-
m'	mass per unit area	kg/m^2
f	frequency	Hz

3.4.6. Total direct sound transmission

NEN-EN-ISO 12354-1 (2017) defines Equations 3.21 to 3.23 for the total sound reduction index. These are based on the mass law, critical frequency, sound radiation and internal damping.

$$R_d = -10\log(\tau) \tag{3.20}$$

$$\tau = \left(\frac{2\rho_0 c_0}{2\pi f m'}\right)^2 \cdot \left(2\sigma_f\left(\frac{1-f^2}{f_c^2}\right)^{-2} + 2\frac{\pi f_c \sigma^2}{4 f \eta_{tot}}\right) \qquad f < f_c \tag{3.21}$$

$$\tau = \left(\frac{2\rho_0 c_0}{2\pi f m'}\right)^2 \cdot \frac{\pi\sigma^2}{2\eta_{tot}} \qquad f \approx f_c \tag{3.22}$$

$$\tau = \left(\frac{2\rho_0 c_0}{2\pi f m'}\right)^2 \cdot \frac{\pi f_c \sigma^2}{2 f \eta_{tot}} \qquad f > f_c \tag{3.23}$$

3.4.7. Flanking

In addition to direct sound transmission through walls, ceilings and floors, the sound insulation between adjacent rooms is also determined in practice by several other transmission paths which are called flanking transmission paths. As described in Equation 3.24 (NEN-EN-ISO 12354-1, 2017).

$$R_{Total} = -10\log\left(10^{\frac{-R_d}{10}} + \sum 10^{\frac{-R_f}{10}}\right) \tag{3.24}$$

Where:

R_{Total}	total sound transmission reduction	dB
R_d	sound reduction for direct sound transmission	dB
R_f	sound reduction for flanking sound transmission	dB

When a path has a significantly lower sound reduction, it becomes the primary part. As an example Table 3.7 shows the total sound reduction for four scenario's where one index for sound reduction varies. It illustrates how difficult it is to achieve high sound reduction when there is a big difference in one path. It is important to improve both the direct and flanking contributions in order to increase the total sound reduction.

	Scenario 1 [dB]	Scenario 2 [dB]	Scenario 3 [dB]	Scenario 4 [dB]
R_{direct}	50	**40**	**30**	50
R_{f1}	50	50	50	**30**
R_{f2}	50	50	50	50
R_{f3}	50	50	50	50
R_{f4}	50	50	50	50
R_{f5}	50	50	50	50
R_{Total}	42	38	30	30

Table 3.7: Example of dominant transmission path due to flanking

3.5. Structure-borne sound

An example of structure-borne sound is the possibility to hear the neighbour's footsteps in a multi-story building (the downstairs and/or next-door neighbours may also be able to hear this). The extent of structure-borne sound transmission depends on the weight of the object, the way which the impact takes place and the characteristics of the floor and the floor finish. The latter properties lead to a certain impact sound insulation. The difference between impact and structure-borne sounds is that with impact sound the object that causes the vibrations is not in contact with the structure in original situation.

The key challenges in sound control from structure-borne sound are minimization of excitation and propagation of sound. Furthermore, the radiation of sound (transfer from structure-borne to airborne sounds) should be kept as low as possible. Various options are available:

- Insulation of structure-borne sound by means of elastic layers, change of dimensions in the transfer path or discontinuities;
- Dampening of structure-borne sound by means of transferring vibration energy into heat;
- Reduction of the radiation by reducing the radiating surfaces or the radiation efficiency.

3.5.1. Transmission

The exact calculation of the transmission of structure-borne sounds through a floor is complex and elaborate which requires software. However, NEN-EN-ISO 12354-2 (2017) offers Equation 3.25 which can be used to calculate the normalized impact sound pressure level L_n of homogeneous floors. This equation also provides a good approximation for orthotropic plates, like timber joist floors .

$$L_n = L_F + (10\log(Re(Y)) + 10\log(\sigma) - 10\log(m') + 10\log(T) + 10.6) \tag{3.25}$$

Where:

L_n	sound level in receiving room due to impact sound	dB
L_F	sound level of force on the floor	dB
$Re(Y)$	driving-point mobility	m/Ns
σ	radiation factor	-
m'	mass per unit area	kg/m^2
T	reverberation time	s

Equation 3.25 consist of five parts:

- L_F is the force level of the sound which is acting on the floor, measured in decibels (reference 10^{-6}N). This is an empirical equation which is used at ABT for the use of the Equation 3.26.

$$L_F = 10\log(f) + 127.5 \tag{3.26}$$

Where:

L_F	sound level of force on the floor	dB
f	frequency	Hz

- $Re(Y)$ is the driving-point mobility which is a measure of the vibration ability of a structure subjected to dynamic forces. For thin plates with a homogeneous bending stiffenss, the driving-point mobility can be calculated with Equation 3.27 (Cremer et al., 1974, p. 288). For orthotropic plates the driving-point mobility can be calculated with Equation 3.28 (Cremer et al., 1974, p. 266).

$$Y_{thin,plate} = \frac{1}{8\sqrt{m'B}} \tag{3.27}$$

$$Y_{orthotropic,plate} = \frac{1}{8\sqrt[4]{m'^2 B_x B_y}} \tag{3.28}$$

Where:

$Y_{orthotropic,plate}$	driving-point mobility orthotropic plate	m/Ns
$Y_{thin,plate}$	driving-point mobility thin plate	m/Ns
m'	mass per unit area	kg/m^2
B_x	bending stiffness in x-direction	Nm^2
B_y	bending stiffness in y-direction	Nm^2

- σ represents the radiation efficiency of the floor. If sounds or vibrations were not be radiated, structure-borne sound would be insignificant. The radiation factor can be calculated with Equations 3.13-3.15.
- m' reveals the sound reduction by the mass of the floor. It is a smaller amount than the reduction of the mass law with airborne sound insulation.
- T_s denotes the reverberation time. When a sound source in a room suddenly stops, the sound is not interrupted instantly, but gradually decreases in strength depending on the acoustic properties of the room. The time that elapses from the moment that the source stops until L_p has fallen below 60 dB, is called reverberation time. Sabine derived the expression for reverberation time in the 1890's, see Equation 3.29 (ISSO-24, 2018, p. 34). The reverberation time in a room depends on the volume V of the receiving room and the related amount of sound-absorbing material A_a. The total absorbing area can be calculated by multiplying the sound absorption value α and the area of the material S. Sabine's formula is used in the calculation of sound reduction because the reduction has to be corrected for the increased sound level in the room due to reverberation.

$$T_s = \frac{1}{6}\frac{V}{A_a} \tag{3.29}$$

Where:

T_s	reverberation time of the room	s
V	volume of the room (L x W x H)	m^3
A_a	amount of sound-absorbing material in (α x S)	m^2

3.6. Increasing mass or stiffness

Figures 3.13 and 3.14 demonstrate the influence of mass and stiffness increase on the increase of airborne sound insulation and decrease of structure-borne sound transmission respectively. In the figures the mass is increased from 18 to 180 kg/m^2 and the stiffness is increased from 4.5e6 to 45e6 Nm^2.

Thus, for timber floors, it can be concluded that mass has considerable influence on the increase in airborne sound insulation relative to stiffness. In addition, an increase in stiffness is limited and timber floor should therefore be reinforcement to ensure that the floor can carry more mass to improve the sound insulation. Structure-borne sound transmission will have to be solved in a different way than stiffening or adding weight.

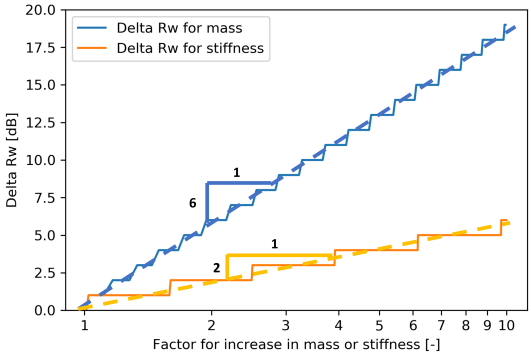

Figure 3.13: Influence of mass and stiffness increase on the airborne sound insulation

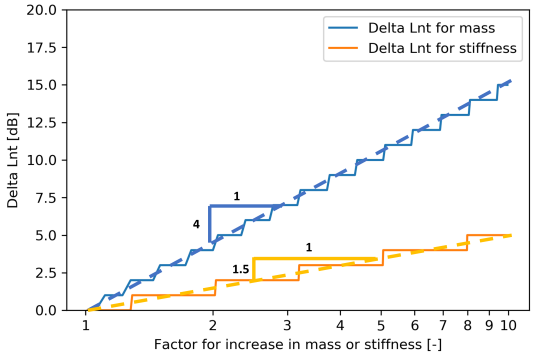

Figure 3.14: Influence of mass and stiffness increase on the structure-borne sound transmission

3.7. Soundproofing measures

When building new structures various soundproofing measures are available on the market. The techniques listed in this section are all based on one concept: floating screed.

A floating screed or floating floor is a floor that is put on a resilient layer and not directly to the underlying surface. This is ideal for monumental timber floors where additional elements can only be placed on top of the floor. There are two types of floating floors: wet and dry. A wet floating floor is obtained by applying wet materials such a concrete screed, see Figure 3.15. The floor of wet screed is more or less load-bearing and in principle to be regarded as a bending floor where tensile stresses occur at the bottom. For a good bending strength a screed is recommended with reinforcement. The use of wet screed increases mass, which lowers the natural frequencies and improves damping (Joostdevree.nl, nd). However, wet floating floors are often difficult to remove (not easily reversible) and very heavy the minimum screed is often 40 mm of concrete.

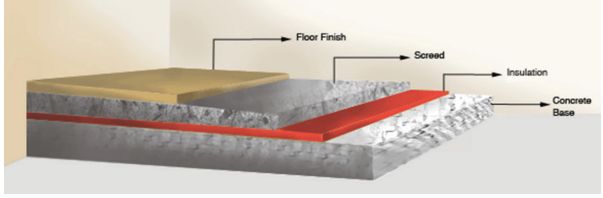

Figure 3.15: Wet screed floating floor (Cemfloor, 2018)

A dry floating floor is a floating screed which is composed of dry materials (cover with sheet material, insulation, edge insulation etc.). Table 3.8 and Figure 3.16 demonstrate six different dry floor options where the airborne sound insulation increases and structure-borne sound transmission decreases with a maximum of 37 dB (Fermacell, 2012).

Option	Dry screed - fermacell	Acoustic insulation	Underlayer - fermacell	Surface mass [kg/m^2]	Rw (Δ) [dB]	Lnt (Δ) [dB]
A	-	-	-	37.0	28 (-)	90 (-)
B	2x 10mm	10mm LM	-	62.8	42 (14)	77 (13)
C	2x 10mm	10mm LM	20mm levelling granules	70.6	47 (19)	71 (19)
D	2x 10mm	10mm LM	60mm levelling granules	86.8	55 (27)	64 (26)
E	2x 12.5mm	20mm LM	30mm honeycomb	114.5	61 (32)	58 (32)
F	2x 12.5mm	20mm LM	60mm honeycomb	155.9	65 (37)	53 (37)

Table 3.8: Fermacell floating floors (Fermacell, 2012)

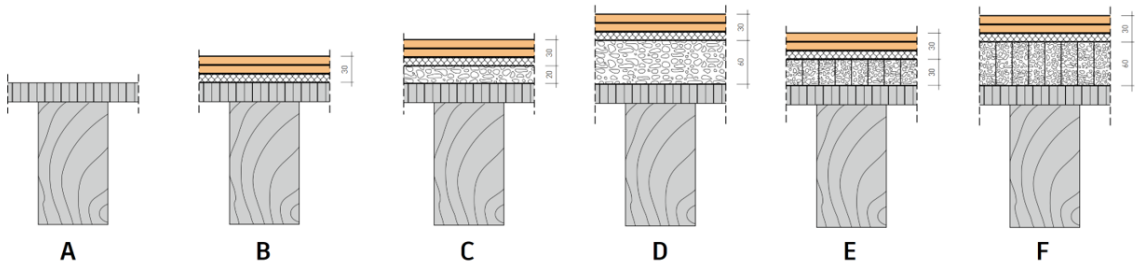

Figure 3.16: Fermacell floating floors Fermacell (2012)

With a floating screed, make sure that the edges of the screed do not touch the walls:

- to prevent the floor from getting a convex due to the rise in temperature;
- to reduce impact sound towards the walls (also use special edge insulation for this).

3.8. Case study: Acoustic performance

To examine the acoustic performance of monumental timber floors, a case study has been done on the airborne and structure-borne sounds performances of two floors in the Prinsenhof Museum in Delft (full calculations see Appendix C). The floor between the dormitory and attic as well as the floor between the guest quarter and first floor are tested on two situations for airborne sound insulation with the RC-curves; in the first situation 30 persons are talking in pairs and the second situation the floor is loaded with an air-handling unit.

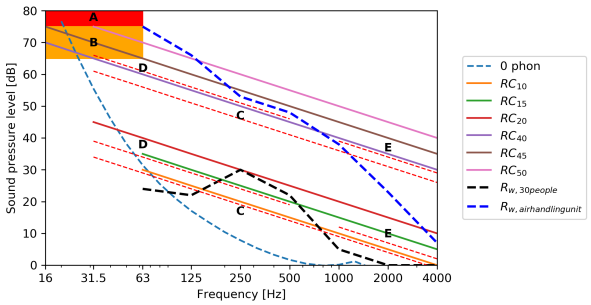

Figure 3.17: RC-curve airborne sound transmitted through the attic floor

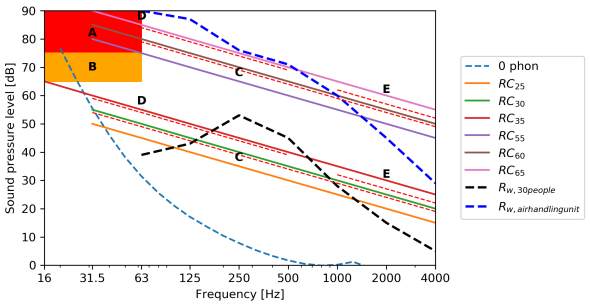

Figure 3.18: RC-curve airborne sound transmitted through the first floor

Figures 3.17 and 3.18 illustrate the airborne sound spectra in relation to the RC-curves of both situations. Table 3.9 shows the single number descriptors of the case study for the RC-curves and the ISO-curves.

The first two rows are related to the two situations of the floor between the dormitory and the attic. The third and fourth rows are related to the floor between the guest quarter and first floor. The airborne sound requirements R_w>42 for the ISO-curve and R<30-35 are only met for the attic floor which can be related to the concrete layer. Talking is acceptable for floor between the guest quarter and first floor, but an air-handling unit would give to much noise. The last column gives the single number descriptor for structure-borne sound transmission. The requirement according to the ISO717-2 is that $L_{n,w}$<63dB. For both floors this is definitely not the case.

Figures 3.17 and 3.18 demonstrate that the spectra of both floors are close to the critical areas A and B in lower frequency range of the RC curves. Furthermore, both spectra of floor between the dormitory and attic in Figure 3.17 are significantly lower than those of the guest quarter. The additional layer of concrete on the floor increases the mass en thus decreases the airborne sound transmission. The RC descriptors have an important additional value, R, which explain that the airborne sound transmission is perceived as a rumble in both situations and on both floors.

Floor between	**Situation**	**ISO717-1** R_w	**RC** R	**ISO717-2** $L_{n,w}$
Dormitory and attic	30 persons	47(-7;-13)	9-R	88(-3)
	Air-handling unit		36-R	
Guest quarter and first floor	30 persons	24(-6;-11)	29-R	116(-3)
	Air-handling unit		59-R	

Table 3.9: Single-number descriptors (in dB) of the case study of the Prinsenhof Museum in Delft

II

Methodological framework

4

Equivalent layer

In order to calculate a beam strengthened by multiple timber plates with the γ-method, the top layers (timber plates) should be transformed to an equivalent layer. This layer should have the same performances as the multiple timber plates. The effective stiffness EI_{eff} $[Nm^2]$ calculated with the γ-method (see Equation 4.1) has two parts. The first part deals with the bending stiffness $E_i I_i$ of each section and the second part addresses the axial stiffness $E_i A_i$ which is translated to a bending stiffness by Steiner's theorem with a_i^2. For the equivalent layer both, a bending and axial stiffness, must be determined.

$$EI_{eff} = \sum (E_i I_i + \gamma_i E_i A_i a_i^2) \tag{4.1}$$

Where:

E_i	Modulus of elasticity	N/m^2
I_i	Moment of inertia	m^4
γ	Joint efficiency coefficient	-
A_i	Area	m^2
a_i	Distance to center of gravity	m

4.1. Influence of bending and axial stiffness

In Equation 4.1 the bending stiffness gets more significant with a bigger moment of inertia and the axial stiffness gets more important when the distance from the centre of gravity is larger. The modulus of elasticity of timber does not have a large variation, so differing in timber types will not have a substantial consequence on the effective stiffness.

Table 4.1 elaborates the effect of different top layer thicknesses of a timber T-beam on the stiffness distribution between the bending and axial stiffness parts. The fourth column shows that the bending stiffness part of the top layer will only be significant when it is larger than 20% of the beam height (60/300=0.2). As the separate plates which will be attached to the beam will have a thickness of 12 to 18 millimetres and the minimum beam height will be 100 millimetre, this part can not be taken out of the effective stiffness with the equivalent layer. The properties of the example are displayed in Table 4.2.

Height [mm]	EI_{beam}/EI_{eff} **[%]**	EA_{beam}/EI_{eff} **[%]**	EI_{top}/EI_{eff} **[%]**	EA_{top}/EI_{eff} **[%]**
15	93.9	0.12	0.02	6.0
30	92.9	0.15	0.15	6.8
60	90.8	0.18	1.14	7.9
120	82.2	0.22	8.22	9.4
240	50.5	0.21	40.44	8.8

Table 4.1: Example; the effectiveness of all parts for different top layer heights in the calculation for EI_{eff} of a T-beam

	Width [mm]	Height [mm]	E-modulus [N/mm2]	Length [mm]	s [mm]	K [N/mm]
Beam	300	400	9000	4000	-	-
Top layer	1000 (effective)	variable	10000	4000	-	-
Connection	-	-	-	-	250	4000

Table 4.2: Example; properties of timber T-beam

4.2. Top layer

Figure 4.1 illustrates the strengthened timber floor by means of multiple layers of separate timber plates which are connected with screws. The red line in the figure illustrates the fasteners which are applied over the effective width of the plate and the green line illustrates the fasteners in the reinforce beam direction. Due to the separate timber plates, two requirements of the γ-method are not met:

- the girder should be composed of no more than three components, which is not met if three or more layers of plates are used;
- the components should have a constant bending stiffness along their length, which is not the case due to the separate plates.

Therefore, the plates need to be transferred into an equivalent layer. Which creates a single continuous top layer that meets the above mentioned requirements.

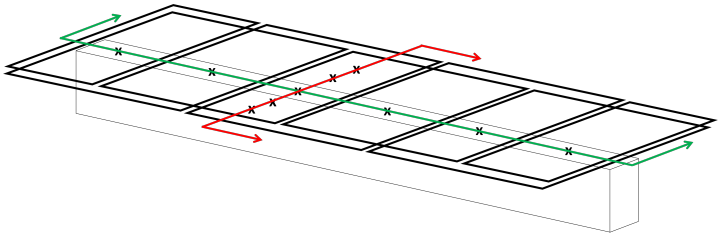

Figure 4.1: Beam strengthened by timber plates

Due to the relative small height of the top layer, the timber plates will generally only be in compression or tension. This allows to use the transform-section method. To establish an equivalent layer, the force and deformation of both (equivalent layer and separate timber plates) will need to be equated.

The deformation is caused by the fasteners (see Equation 4.2) and the elongation of the plates (see Equation 4.3). This last equation is also used for deformation of the equivalent layer. In order to calculate the deformation of the equivalent layer, the displacement of the connections and separate plates must be made equal to the equivalent layer by means of Equation 4.4.

$$u = \frac{F}{K} \tag{4.2}$$

$$\Delta L = \frac{FL}{EA} \tag{4.3}$$

$$\sum u_i + \Delta L_i = \Delta L_{eq} \tag{4.4}$$

Where:

EA	axial stiffness	N
F	force	N
K	stiffness coefficient fastener	-
L	plate length	m
ΔL	elongation plate (length)	m
ΔL_{eq}	elongation equivalent layer (length)	m
u	deformation fastener	m

4.2.1. Segments

The system can be converted to a 2D-system, in the length direction of the beam, where the deformation of the fasteners and plates function as a chain system. Figure 4.2 illustrates this 2D-system for two layered plates connected with two fasteners per plate.

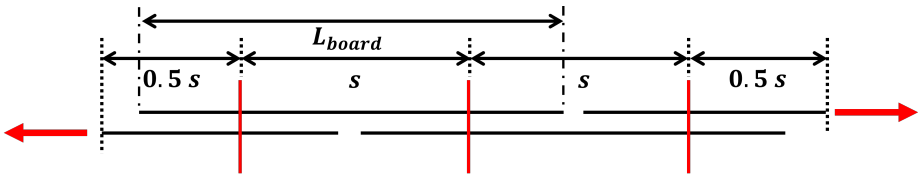

Figure 4.2: Example of an 2D system of two layered plates with two fasteners per plate

In order to create the 2D-system, only fasteners that are within the effective width of the floor will cooperate in the equivalent layer, see Figure 4.3.

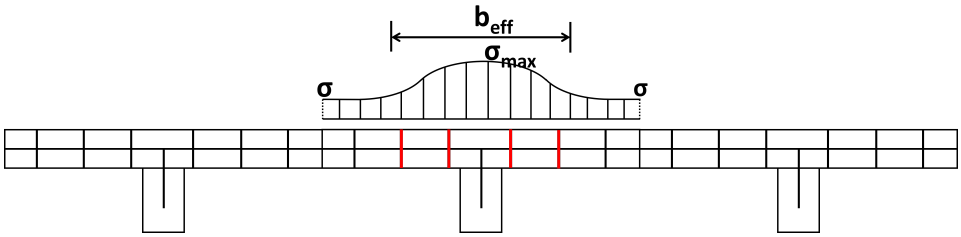

Figure 4.3: Fasteners within the effective width

To analyze the layers, a segment must be chosen that repeats along the length of the floor. Figure 4.4 shows examples of segment parts of 2 to 4 layers that repeat along the length of the floor. In a segment, there are at least the same number of fasteners as the amount of layers and this can be increased by a factor. For example, a segment in a two layered system can contain 2, 4, 6, etc., fasteners. This is due to the requirement of the γ-method, which says that the spacing between the fasteners must be the same.

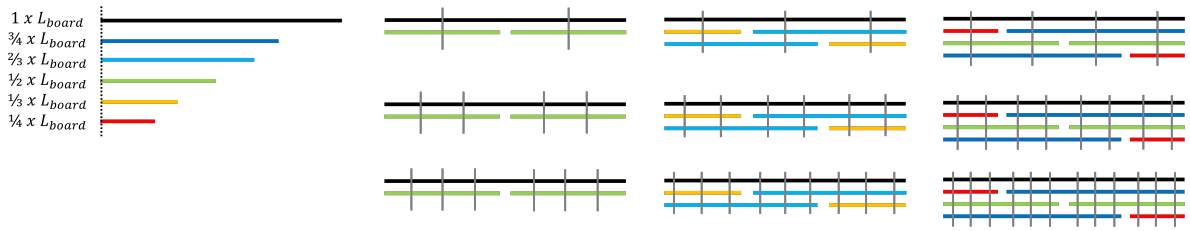

Figure 4.4: Segments of 2, 3 and 4 layered plates with multiple fastener options

4.2.2. Force distribution

The fasteners between the plates will transfer the forces from plate to plate. The distribution of forces between plates is influenced by the number of the fasteners and the stiffness of the plate and fastener. The proportion of the force absorbed by a plate is affected by the relative stiffness between the fastener and the plate. This is be expressed as the joint constant, C (Engineering & Consulting P.C., 2017):

$$C = \frac{K_{fastener}}{K_{fastener} + K_{plate}} \tag{4.5}$$

Where:

C	Joint constant	-
$K_{fastener}$	Stiffness of the fastener	N/mm
K_{plate}	Stiffness of the plate	N/mm

When using thin plates with screws with a diameter up to 10 millimeters, the joint constant reaches a maximum of 2.4% (see the calculation below) where a 100% indicates that the joint is infinite stiff. This implies that the factor which takes the relative stiffness into account (the redistribution of forces due to a stiffer connection) can be neglected.

$$C = \frac{\frac{\rho_m^{1.5} d}{23}}{\frac{\rho_m^{1.5} d}{23} + \frac{EA}{s}} = \frac{\frac{400^{1.5} \cdot 10}{23}}{\frac{400^{1.5} \cdot 10}{23} + \frac{8000 \cdot 750 \cdot 12}{500}} = 2.36\%$$

Since the relative stiffness is neglected, the force distribution for multiple layers of plates can be determined by appointing a relative low stiffness to the fasteners. In Appendix D the force distributions for two, three and four layers of plates are given. Figure 4.5 illustrates the force distribution of one example: a two layered section with six fasteners per plate.

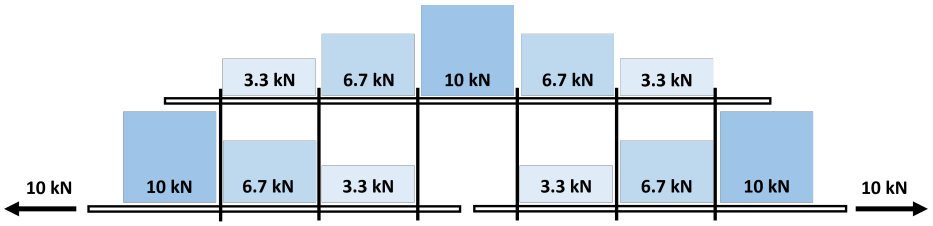

Figure 4.5: Force distribution of two layered timber plates, with six fasteners per plate

With three and four layered segments, *the force introduction phenomenon* occurs. Therefore, multiple segments have to be modelled after which the force distribution of the middle segment is governing. Figure 4.6 shows the force distribution of a four layered segment. The forces are mainly concentrated in the stiffer parts of the layers, which are the layers in the middle. Those layers are always connected with fasteners on both sides.

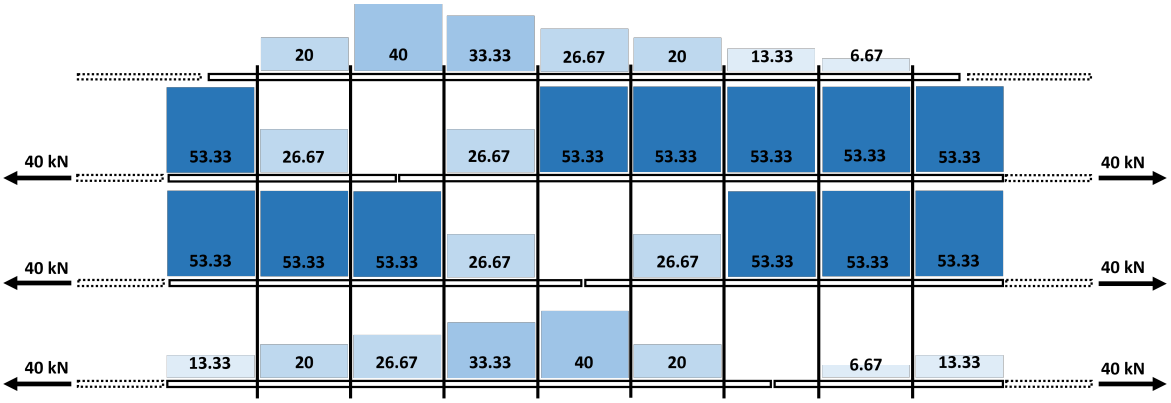

Figure 4.6: Force distribution of four layered timber plates, with eight fasteners per plate

4.2.3. Equivalent layer equations

By using Equations 4.2 and 4.3 together with the force distributions in Appendix D, the Equations 4.6, 4.7 and 4.8 are determined. These equations give the elongation of a segment to a certain force. The elongation calculated with the equations, is checked with the software MatrixFrame (for calculations see Appendix D). The check proved that the equations are in good agreement with the software.

$$\Delta L_{total,2,plates} = \frac{2F}{n_{fpp} n_y K} + \frac{(n_{fpp}+1)FL}{n_p n_{fpp} E A_{plate}} \tag{4.6}$$

$$\Delta L_{total,3,plates} = \frac{3F}{4 n_{fpp} n_y K} + \frac{(3n_{fpp}+1)FL}{2 n_p n_{fpp} E A_{plate}} \tag{4.7}$$

$$\Delta L_{total,4,plates} = \frac{4F}{9 n_{fpp} n_y K} + \frac{(8n_{fpp}+3)FL}{6 n_p n_{fpp} E A_{plate}} \tag{4.8}$$

Where:

$\Delta L_{total,np,plates}$	elongation of the segment with n_p amount of plates	mm
F	reference force	N
n_p	number of plates	-
n_{fpp}	number of fasteners on 1/n_p of the segment	-
n_y	number of fasteners in width direction	-
K	stiffness of a fastener	N/mm
L	length of one plate	mm
EA_{plate}	axial stiffness of a plate	N

4.2.4. Equivalent axial stiffness EA

Through these equations, the equivalent axial stiffness (EA_{eq}) can be determined in two ways: either by calculating an equivalent area or an equivalent modulus of elasticity.

When calculating an equivalent area, two options can be considered: width and height (see Figure 4.7). The first option is with an effective width and the height remains the same as the height of the layers. The second option is with an effective height, which is lower than the height of the layers and the width remains the same. The latter affects the effective stiffness more, because the height is affected in the bending and axial stiffness to the power of three. Therefore, by choosing an effective height, the effective stiffness will most likely not be an adequate approximation.

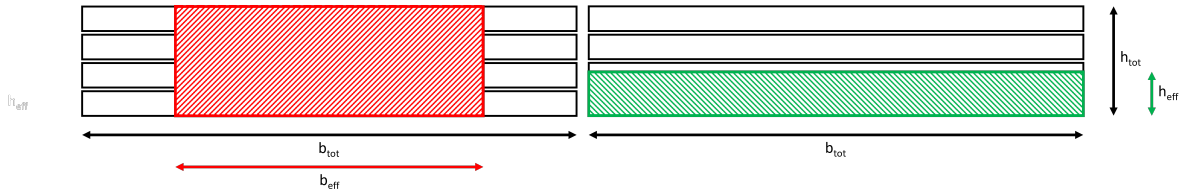

Figure 4.7: Equivalent area: width (left) and height (right)

On the other hand, when calculating an equivalent modulus of elasticity, the dimensions of the system will not change. With an equivalent modulus of elasticity, the effective stiffness is considered to be the same as with an effective width. However with an equivalent modulus of elasticity, the maximum stresses in the outer fibres of the equivalent layer will be lower.

It is expected that the equivalent layer with an equivalent width or modulus of elasticity will represent the complete model the closest and this will be further investigated in Chapter 5.

4.2.5. Equivalent bending stiffness EI

In addition to an equivalent axial stiffness, an equivalent bending stiffness must be determined. Figure 4.8 illustrates that with a smaller spacing and consequently more fasteners, the layers will have a larger effective bending stiffness. Because with more fasteners the layers will cooperate better. For two and three layers this effective bending stiffness could be determined by the γ-method. However, this is no longer possible for four layers. Therefore, it is preferable to use Schelling's method (see Subsection 2.3.3). The effective stiffness is determined with the dimensions and characteristics established from the equivalent axial stiffness.

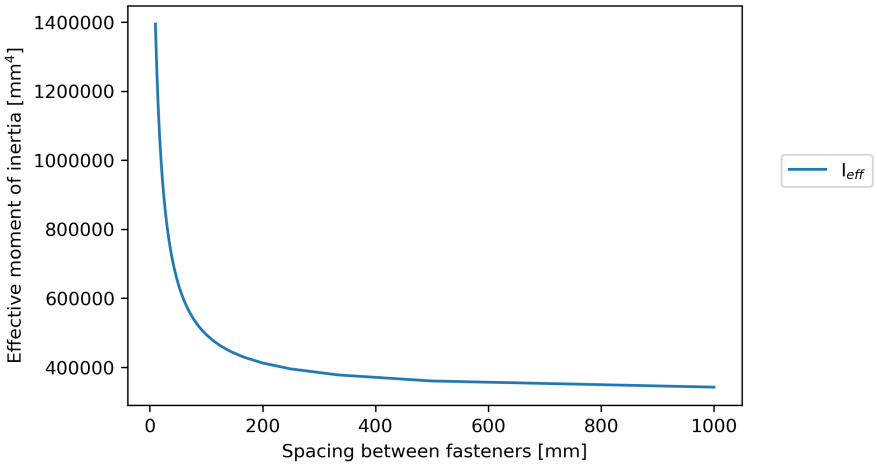

Figure 4.8: Effective moment of inertia, for three plates with different fasteners spacings

4.2.6. Effective stiffness

In order to include the separate timber plates in the calculation of the effective stiffness of the system with the γ-method, these plates have to be translated to an equivalent layer. The equations 4.6, 4.7 and 4.8 calculate the equivalent axial stiffness based on the strain due to a tensile force on the layer. The formulas are based on the distribution of forces between the plates and joints, but leave out the relative stiffness between them. The equation have been verified with MatrixFrame models where the deformations of all formulas match the models. Therefore, the formula's can be used to calculate an equivalent EA.

5

Verification model

The verification of the previous created method (using an equivalent layer to be able to calculate the effective stiffness of the system) is done by creating a 2D framework with the calculation software MatrixFrame.

5.1. Boundary conditions

To verify the equivalent layer method, the boundary conditions of both Maple and MatrixFrame models must be the same. These boundary conditions are defined by the input parameters, which are element properties (beam, plate and fastener), connections, supports and load.

5.1.1. Element properties

MatrixFrame models elements with lines, see Figure 5.1. Properties can be given to these lines such as: area, moment of inertia and modulus of elasticity.

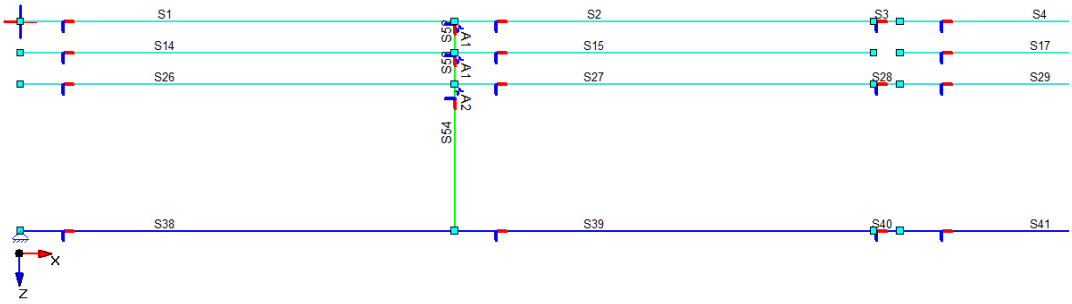

Figure 5.1: Part of the MatrixFrame model where a beam is strengthened by three layers of plates

Table 5.1 demonstrates the properties of all line elements of MatrixFrame. Section 4.1 demonstrates that the effectiveness of the strengthening technique is larger with more plates. This relates to the area and Steiner's rule. Therefore, the beam is modeled with dimensions of 100x100mm and strength class D18. The plates are made of plywood with a size of 750x12mm.

Element	**Area [mm^2]**	**Moment of inertia [mm^4]**	**Modulus of elasticity [N/mm^2]**
Beam	10000	8333333	9500
Plate	9000	108000	8000
Fastener	infinite $\approx 10^8$	infinite $\approx 10^{12}$	8000

Table 5.1: Element properties of the MatrixFrame model

The beam and plates are connected with fasteners. These fasteners can be modelled in three ways: clamped, hinged or spring connections. Clamped and hinged connections negatively affect plates due to bending of the fastener, as Mulder (2019) showed in his undergraduate final report. Therefore, they are excluded in this thesis. For fasteners modelled with springs, the spring constant determines the shear resistance. In order to avoid bending of the fastener, the bending stiffness must approximate infinity.

In addition, the fasteners could shorten due to compression. However, shortening is avoided since this is not possible in reality due to the material of the plates and beam. Shortening of the fastener can be calculated by Equation 4.3. In order to avoid shortening, the product of the modulus of elasticity multiplied by the area should be infinite. As infinite values cannot be chosen in MatrixFrame, the product of the modulus of elasticity and the area of the fastener must be approximated to infinity. Thus the area should be many orders of magnitude greater than that of the plates and beam.

5.1.2. Connections

To realize the interaction between the beam and plates, the proper connection for the fasteners must be appointed. The connection for the fasteners is defined by the shear resistance which can be calculated using Equation 2.4. This shear resistance is introduced as a horizontal spring into the system at one end of the fastener.

5.1.3. Supports

The system is a simply supported structure which means that the beam must be able to rotate freely at its ends. Therefore, it is modelled with hinged supports. To avoid additional forces due to horizontal displacements, one of these hinged supports becomes a rolling support.

The student-license of MatrixFrame has one major limitation: the software can only support 100 elements. The more layers of plates and fasteners that are added, the faster this limitation is reached. There are two possibilities to avoid the limitation of 100 elements:

- Reducing the number of fasteners in MatrixFrame by placing fasteners with a larger spacing. As a result, the stiffness of the fasteners will have to be scaled to the actual amount of fasteners over the length (see Equation 5.1). However, as Jong (2018) described in his undergraduate final report, increasing the distance between the connecting bars has a major impact on the accuracy of the model. By reducing the number of fasteners, thus increasing the distnace between connecting bars, the fasteners will have more bending. Therefore, reducing the number of fasteners should be avoided;

$$K_{MatrixFrame} = \frac{K_{Reality} \cdot s_{MatrixFrame}}{s_{Reality}} \tag{5.1}$$

- Modelling only half of the system. This is only possible if the model is symmetrical. Exact symmetry is only possible for two layered plates (see Figure 5.3 in Subsection 5.2.2). Nevertheless, it is possible to model only half of the system for more than two layers, but its accuracy is reduced.

When modelling only half of the system, two adjustments to the supports must be made: adding a clamped roller and changing the fixed hinged support to a rolling hinged support. A clamped roller which can move in vertical direction must be placed in the middle. This adjustment keeps the angular deflection zero. Furthermore, it enables the beam to move only vertically. As there is no horizontal displacement in the middle, this must be enabled at the other end of the beam. In other words, the fixed hinged support should be changed into a rolling hinged support to prevent horizontal forces. Another way to prevent these horizontal forces in the beam is placing the fixed hinged support in the neutral line of the system. Because every strengthening variation results in a different position of the neutral line, the rolling hinged support is the easier method and is chosen when modelling half of the system.

5.1.4. Load

In practice elements transmit normal forces and moments without being affected by the fasteners. However in MatrixFrame, the force transmission from plate to plate or plate to beam passes through

the fasteners. Therefore, to prevent deformation of the top element, the load is only applied to the fasteners. Since the load no longer acts on the whole beam, the model is slightly inaccurate. The load no longer engages at its original shape. A possible solution for better accuracy is to add more fasteners, which are scaled according to Equation 5.1.

The floor must be loaded with a sinusoidal load according to Equation 5.2, because the effective stiffness is calculated with the γ-method. Since the load is only allowed to act above the fasteners, it is necessary to integrating the sinusoidal load over the elements around the fastener based on Equation 5.3, which calculates the point load for each fastener. The factor Q is taken as 10 in this verification model.

$$q = Q \cdot \frac{\pi}{2} \cdot \sin\left(\frac{x \cdot \pi}{L}\right) \quad with \quad 0 \leq x \leq L \tag{5.2}$$

$$F = \int_{x1}^{x2} Q \cdot \frac{\pi}{2} \cdot \sin\left(\frac{x \cdot \pi}{L}\right) dx \tag{5.3}$$

5.2. Verifying the effective stiffness

5.2.1. Simplified model

The first step for the verification model is to model the equivalent layer as a single continuous layer. Figure 5.2 illustrates the simplified model for two layered plates with a spacing between the screws of 500 mm. Due to the continuous top layer, the model can be made symmetric without accuracy loss.

As mentioned in Chapter 4, the equivalent layer can be calculated with two approaches: with an equivalent area or an equivalent modulus of elasticity. The equivalent width should have the same result in effective stiffness as an equivalent modulus of elasticity. Therefore, the simplified model is only verified for the equivalent area method with an equivalent height or width. Both will be verified for two, three and four layered plates with different spacings between the fasteners. The spacing between the fasteners is governed by $n_p \cdot n_{fpp}$ which stands for the amount of fasteners per plates. N_p is the amount of layers and n_{fpp} is a factor for fasteners per plate (n_{fpp} ranges from 1 to 5).

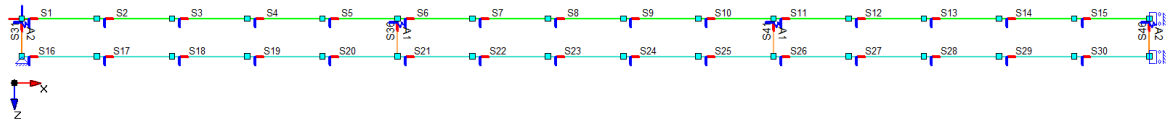

Figure 5.2: Simplified model with the equivalent layer modelled as one continuous layer

Tables 5.2 and 5.3 show the deflections of the Maple script and MatrixFrame model for two layers of plates with the equivalent height and equivalent width method respectively. The difference between the Maple script and MatrixFrame model (final rows of Tables 5.2 and 5.3) is larger for the equivalent height method. This deviation is due to the modelled distance between beam and equivalent layer which is half of the equivalent height (rounded to the millimeter). Nonetheless, the deviations in both Tables are acceptable and explainable (rounding).

		n_{fpp} **= 1**	n_{fpp} **= 2**	n_{fpp} **= 3**	n_{fpp} **= 4**	n_{fpp} **= 5**
s	[mm]	500	250	167	125	100
h_{eq}	[mm]	0.4	1.6	3.2	5.1	7.0
Maple h_{eq}	[mm]	155.5	139.0	123.7	111.1	101.0
MatrixFrame	[mm]	154.0	138.6	123.3	110.5	100.3
$\frac{Maple}{Matrixframe}$	[%]	+ 1.0	+ 0.3	+ 0.3	+ 0.5	+ 0.7

Table 5.2: Deflection [mm] in the middle of the floor, 2 layers of plates, with the equivalent height method

		n_{fpp} = 1	n_{fpp} = 2	n_{fpp} = 3	n_{fpp} = 4	n_{fpp} = 5
s	[mm]	500	250	167	125	100
b_{eq}	[mm]	13.1	49.0	100.6	159.6	220.1
Maple b_{eq}	[mm]	151.1	129.3	111.7	98.8	89.4
MatrixFrame	[mm]	149.7	129.1	111.7	98.8	89.4
$\frac{Maple}{Matrixframe}$	[%]	+ 0.9	+ 0.2	+ 0	+ 0	+ 0

Table 5.3: Deflection [mm] in the middle of the floor, 2 layers of plates, with the equivalent width method

The final rows of Tables 5.2 and 5.3 demonstrate that the deviations between Maple and MatrixFrame are on the same order of magnitude. As a result, only the model with the equivalent width approach will be included for checking the three and four layered MatrixFrame models. This approach is chosen because the rounding error in dimensions is smaller, which results in a lower deviation between Maple and MatrixFrame.

Tables 5.4 and 5.5 display the deflection for the equivalent width method for three and four layered plates respectively. The deviations in both Tables are negligible. Therefore, a complexer model can be created as the boundary conditions are correct for both Maple and MatrixFrame.

		n_{fpp} = 1	n_{fpp} = 2	n_{fpp} = 3	n_{fpp} = 4	n_{fpp} = 5
s	[mm]	333	167	111	83	67
b_{eq}	[mm]	33.0	108.3	189.1	257.0	308.9
Maple b_{eq}	[mm]	126.9	96.3	79.7	69.8	63.4
MatrixFrame	[mm]	126.8	96.3	79.7	69.8	63.4
$\frac{Maple}{Matrixframe}$	[%]	+ 0.1	+ 0	+ 0	+ 0	+ 0

Table 5.4: Deflection [mm] in the middle of the floor, 3 layers of plates, with the equivalent width method

		n_{fpp} = 1	n_{fpp} = 2	n_{fpp} = 3	n_{fpp} = 4	n_{fpp} = 5
s	[mm]	250	125	83	63	50
b_{eq}	[mm]	53.8	164.2	267.2	343.5	396.7
Maple b_{eq}	[mm]	104.3	73.6	59.5	51.6	46.6
MatrixFrame	[mm]	104.3	73.6	59.5	51.6	46.6
$\frac{Maple}{Matrixframe}$	[%]	+ 0	+ 0	+ 0	+ 0	+ 0

Table 5.5: Deflection [mm] in the middle of the floor, 4 layers of plates, with the equivalent width method

5.2.2. Complex model - symmetric

The last step in the verification process is to model the system as in reality. Figure 5.3 illustrates a complete model of two layered plates on top of a beam which are connected with fasteners with a spacing of 100 mm. The MatrixFrame models will be created for two, three and four layered plates with n_{fpp} from 1 to 5. This will allow to check whether the calculation method for the equivalent layer is comparable to the complete model.

As mentioned in Section 5.1.3, the complete system is only symmetric for two layered plates and is less accurate with more layers. This inaccuracy can be verified by modelling a full beam, see Subsection 5.4.

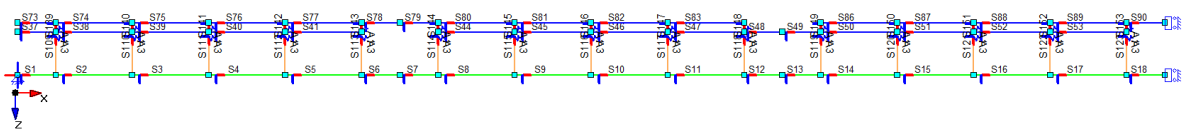

Figure 5.3: Complete symmetric model, with two layered plates

Tables 5.6, 5.7 and 5.8 show the deflection for two, three and four layered plates respectively. The deflections are calculated with Maple and MatrixFrame. Maple uses three different approaches: equivalent height, equivalent width and equivalent modulus of elasticity.

		n_{fpp} = 1	n_{fpp} = 2	n_{fpp} = 3	n_{fpp} = 4	n_{fpp} = 5
Maple h_{eq}	[mm]	155.5	139.0	123.7	111.1	101.0
Maple b_{eq}	[mm]	151.1	129.3	111.7	98.8	89.4
Maple E_{eq}	[mm]	151.0	129.1	111.4	98.4	89.1
MatrixFrame	[mm]	146.8	126.4	110.0	98.0	89.4

Table 5.6: Strengthening with 2 layers of plates; Deflection in the middle of the beam for the equivalent height, width and modulus of elasticity and complex symmetric MatrixFrame model [mm]

		n_{fpp} = 1	n_{fpp} = 2	n_{fpp} = 3	n_{fpp} = 4	n_{fpp} = 5
Maple h_{eq}	[mm]	141.5	116.0	98.4	86.4	78.1
Maple b_{eq}	[mm]	126.9	96.3	79.7	69.8	63.4
Maple E_{eq}	[mm]	126.5	95.5	78.9	69.1	62.8
MatrixFrame	[mm]	122.4	94.8	78.9	69.0	62.4

Table 5.7: Strengthening with 3 layers of plates; Deflection in the middle of the beam for the equivalent height, width and modulus of elasticity and complex symmetric MatrixFrame model [mm]

		n_{fpp} = 1	n_{fpp} = 2	n_{fpp} = 3	n_{fpp} = 4	n_{fpp} = 5
Maple h_{eq}	[mm]	128.7	98.3	79.5	67.7	60.1
Maple b_{eq}	[mm]	104.3	73.6	59.5	51.6	46.6
Maple E_{eq}	[mm]	103.4	72.3	58.4	50.7	45.9
MatrixFrame	[mm]	105.8	73.7	58.7	50.3	45.2

Table 5.8: Strengthening with 4 layers of plates; Deflection in the middle of the beam for the equivalent height, width and modulus of elasticity and complex symmetric MatrixFrame model [mm]

Tables 5.9, 5.10 and 5.11 demonstrate the deviations for deflection between the Maple methods and the complete symmetric MatrixFrame model. The first row for deviations in all three tables show the difference between the equivalent height method and the complete symmetric model. This deviation proves that the effective stiffness of the complete symmetric model is not representative using an equivalent height, as the latter influences the distance to the centre of gravity of the equivalent layer. This distance influences the effective stiffness to the power of three in the γ-method (see Equation 4.1).

The second and third rows for deviations in all three tables show the difference between the equivalent width and equivalent modulus of elasticity compared to the complete symmetric model respectively. The deviations for the equivalent width and modulus of elasticity method for Maple and MatrixFrame are both low. Positive deviations are acceptable because larger deflections are conservative in the calculations. The differences between the mean deviations (last column) for equivalent width and modulus of elasticity demonstrate that the deviations of the equivalent modulus of elasticity are in accordance with the MatrixFrame model. Especially for the four layered plates some deviations are negative, see first two column of the second and third rows for deviation in Table 5.11. This negative deviation indicates that the equivalent method calculates a higher effective stiffness than the complete symmetric MatrixFrame model.

		n_{fpp} = 1	n_{fpp} = 2	n_{fpp} = 3	n_{fpp} = 4	n_{fpp} = 5	**Mean dev.**
$\frac{Maple\ heq}{Matrixframe}$	[%]	+ 5.9	+ 10.0	+ 12.5	+ 13.4	+ 13.0	+ 11.0
$\frac{Maple\ beq}{Matrixframe}$	[%]	+ 2.9	+ 2.3	+ 1.5	+ 0.8	+ 0	+ 1.5
$\frac{Maple\ Eeq}{Matrixframe}$	[%]	+ 2.9	+ 2.1	+ 1.3	+ 0.4	- 0.3	+ 1.3

Table 5.9: Strengthening with 2 layers of plates; Deviation in deflections (based on Table 5.6) for the equivalent height, width and modulus of elasticity with the complex symmetric MatrixFrame model [%]

		n_{fpp} = 1	n_{fpp} = 2	n_{fpp} = 3	n_{fpp} = 4	n_{fpp} = 5	Mean dev.
$\frac{Maple\ heq}{Matrixframe}$	[%]	+ 15.6	+ 22.4	+ 24.7	+ 25.2	+ 25.2	+ 22.6
$\frac{Maple\ beq}{Matrixframe}$	[%]	+ 3.7	+ 1.6	+ 1.0	+ 1.2	+ 1.6	+ 1.8
$\frac{Maple\ Eeq}{Matrixframe}$	[%]	+ 3.3	+ 0.7	+ 0	+ 0.1	+ 0.6	+ 0.9

Table 5.10: Strengthening with 3 layers of plates; Deviation in deflections (based on Table 5.7) for the equivalent height, width and modulus of elasticity with the complex symmetric MatrixFrame model [%]

		n_{fpp} = 1	n_{fpp} = 2	n_{fpp} = 3	n_{fpp} = 4	n_{fpp} = 5	Mean dev.
$\frac{Maple\ heq}{Matrixframe}$	[%]	+ 21.6	+ 33.4	+ 35.4	+ 34.6	+ 33.0	+ 31.6
$\frac{Maple\ beq}{Matrixframe}$	[%]	- 1.4	- 0.1	+ 1.4	+ 2.6	+ 3.1	+ 0.6
$\frac{Maple\ Eeq}{Matrixframe}$	[%]	- 2.3	- 1.9	- 0.5	+ 0.8	+ 1.5	- 0.5

Table 5.11: Strengthening with 4 layers of plates; Deviation in deflections (based on Table 5.8) for the equivalent height, width and modulus of elasticity with the complex symmetric MatrixFrame model [%]

5.3. Verifying the stresses

In addition to the equivalent stiffness and deflection, it is also important that the stresses of the strengthened beam match. The stresses of the components in the MatrixFrame model are calculated with Equation 5.4. The normal force and moment are extracted from the MatrixFrame components; the area, moment of inertia and z from the element input. z is the distance from the centre of an element to any other position in the same element.

$$\sigma = \frac{N}{A} + \frac{M \cdot z}{I} \tag{5.4}$$

Where:

σ	stress	N/m^2
N	normal force	N
A	Area	m^2
M	moment	kNm
z	half of the element height	m
I	moment of inertia	m^4

The stresses for Maple are determined with Equation 5.5. As a first step, the strain has to be calculated with Equation 5.6. In this equation, the loss factor has to be taken into account for every part. Where a_i is the distance from the center of gravity of the system to the position where the stress is determined and z is the distance from the centre of gravity of the element to the point where the stress in the element is determined. With the strains multiplied by the modulus of elasticity, the stresses are determined by Equation 5.5.

$$\sigma = E \cdot \epsilon \tag{5.5}$$

$$\epsilon_{i,neutralaxis} = \kappa \cdot a_i$$

$$\epsilon_{i,\gamma} = \gamma_i \cdot \epsilon_{i,neutralaxis}$$

$$\epsilon_i = \epsilon_{i,\gamma} + \kappa \cdot z_i \tag{5.6}$$

5.3.1. Simplified model

Similar to the process of verifying the effective stiffness, the strains and stresses are to be verified in the simplified model. Tables 5.3, 5.4 and 5.5 demonstrate that the effective stiffness for all Maple scripts match the simplified MatrixFrame models. Since the mean deviation in Tables 5.9, 5.10 and 5.11 are the lowest for the equivalent modulus of elasticity, the strains and stresses are only verified with this simplified MatrixFrame model.

Figure 5.4 illustrates the strains for strengthening the beam with 4 plates and 8 fasteners per plate. The strains for the equivalent layer and the beam with both methods, Maple script (A) and MatrixFrame model (B), are parallel to each other which is correct according to Hooke's law. Figure 5.5 illustrates the stresses for the equivalent layer and the beam with both, the Maple script (A) and MatrixFrame model (B). As the outcome (C) for both models, see Figures 5.4 and 5.5, match perfectly, the boundary conditions are correct.

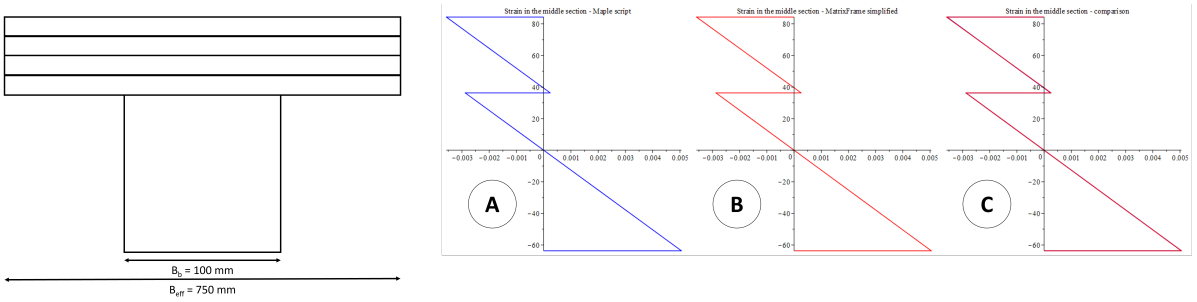

Figure 5.4: Strains in Maple script (A) and MatrixFrame model (B). Comparison of A+B (C)

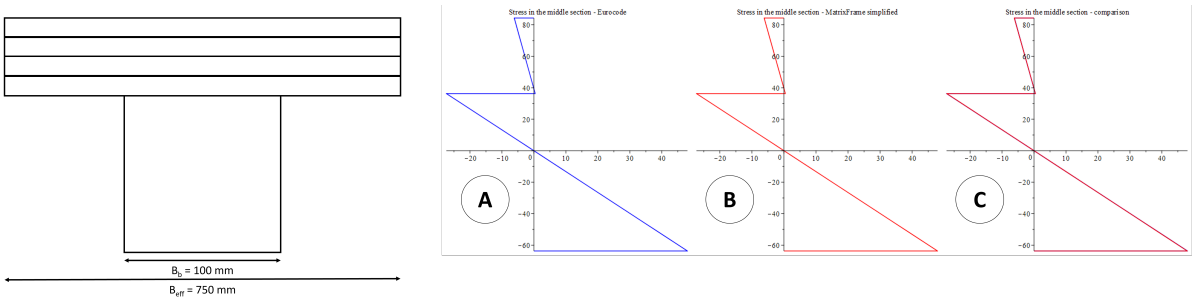

Figure 5.5: Stresses in Maple script (A), MatrixFrame model (B). Comparison of A+B (C)

From the stresses, the horizontal forces are determined. The summation of the horizontal forces must be equal to zero in each section, because the supports do not allow horizontal forces. The calculation of the horizontal equilibrium is shows ith the summation of the horizontal forces equal to zero.

Furthermore, the moment of a segment has to be verified. The moment is calculated with the distance to the centre of gravity of the horizontal force multiplied with the horizontal force. The moment must be equal to the moment which is determined with the load on the system and its boundary conditions. The moments in the Maple script and MatrixFrame model match. Therefore, the boundary conditions are correct.

5.3.2. Complex model - symmetric

Since the strains and stresses of the simplified model and maple script match, the complex model can be compared. Both, the effective stiffness of the equivalent width and equivalent modulus of elasticity, have the same deviation from the complex model. Therefore, the stresses are compared for both.

Figures 5.6, 5.7 and 5.8 illustrate the stress diagrams of two, three and four layered timber plates (n_{fpp}=2) respectively. The three figures show that the stresses in the main beam for all three strengthening techniques match for the Maple script and the MatrixFrame model. However, for the equivalent width method (A), the normal stresses in the equivalent layer are larger than the average normal stress in the separate plates. The explanation for this phenomenon is that the area of the equivalent layer with an equivalent width is smaller than the total of the separate plates. However, the moment needs to be the same which causes the normal force to be the same. To get the same normal force, the normal stresses need to be higher with a smaller area. Furthermore, the figures illustrate that average normal stress of the equivalent modulus of elasticity matches that of the separate plates. However, the method does not match the peak stresses in the plates. A solution to be able to calculate these peak stresses is to take the average normal stress of the equivalent layer and use "$+/-\kappa \cdot z \cdot E$" to determine the maximum stresses in the separate plates.

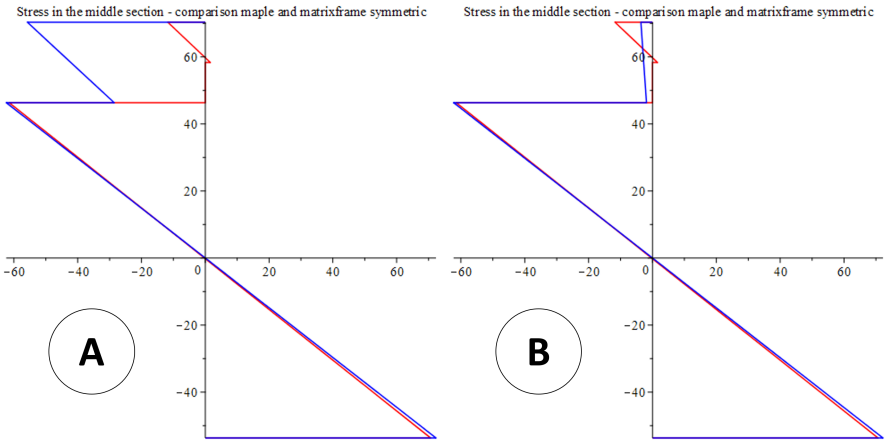

Figure 5.6: Stress comparison between Maple and MatrixFrame for two plates with four fasteners; equivalent width (A); equivalent modulus of elasticity (B)

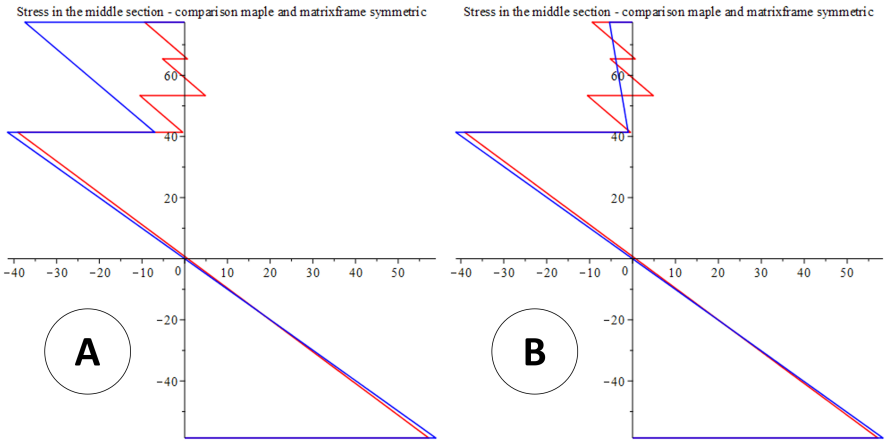

Figure 5.7: Stress comparison between Maple and MatrixFrame for three plates with six fasteners; equivalent width (A); equivalent modulus of elasticity (B)

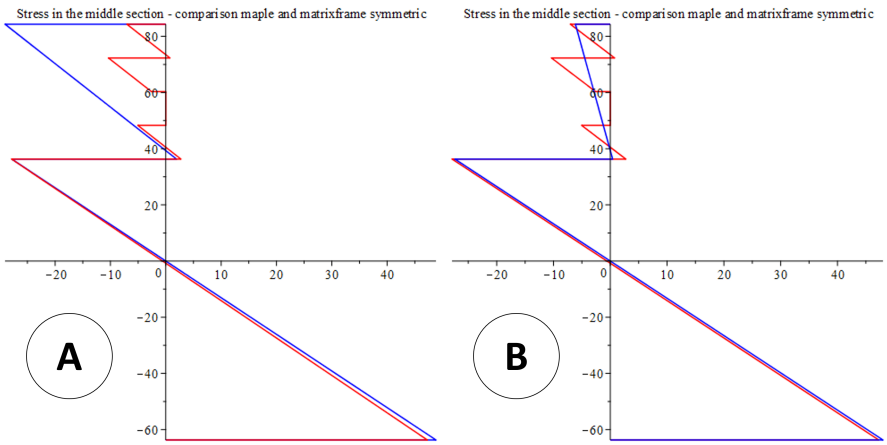

Figure 5.8: Stress comparison between Maple and MatrixFrame for four plates with eight fasteners; equivalent width (A); equivalent modulus of elasticity (B)

5.4. Changing boundary conditions

To check that the models are not only applicable to the used symmetric boundary conditions, dimensions of the system and dimensions of the plates; a few adjustments are verified for all layers.

Symmetric boundary conditions

To check the influence of modelling the beam symmetric, complete models for two, three and four layered plates with $n_{fpp} = 2$ are created. The deflection in the center of the MatrixFrame model for two, three and four layered plates is shown in Table 5.12. It is clear that there is almost no deviation between the symmetrical model and complete model of the two layered timber plates, which is expected since the build-up of the plates is symmetrical. However, large differences appear between the three and four layered complete models.

		2 layers	3 layers	4 layers
Maple E_{eq}	[mm]	129.1	95.5	72.3
MatrixFrame symmetric	[mm]	126.4	94.8	73.7
MatrixFrame complete	[mm]	126.7	96.7	74.9
$\frac{MF\ Eeq}{MF\ complete}$	[%]	+ 1.9	- 1.2	- 3.4
$\frac{MF\ symmetric}{MF\ complete}$	[%]	- 0.2	- 2.0	- 1.6

Table 5.12: Deflection [mm] in the middle of the floor, $n_{fpp} = 2$, comparing the symmetric MatrixFrame model to the complete MatrixFrame model

Dimension of the system

To check the influence of the dimensions of the system, the length of the beam will be enlarged. The length is chosen because it is taken to the power of four in de equations for deflection. Every parameter is kept the same as before, but the length is increased to 5 metres (it was 3 metres). Table 5.13 demonstrates the difference in deflection between the Maple script and the MatrixFrame models. It can be concluded that the equivalent method for a 1.7x span overestimates the effective stiffness by three to four percent.

		2 layers	3 layers	4 layers
Maple E_{eq}	[mm]	841.7	540.0	382.0
MatrixFrame complete	[mm]	867.5	562.9	397.2
$\frac{Maple\ Eeq}{MF\ complete}$	[%]	- 2.9	- 4.0	- 3.8

Table 5.13: Deflection [mm] in the middle of the floor, $n_{fpp} = 2$, comparing the symmetric MatrixFrame model to the complete MatrixFrame model

5.5. Conclusion

During the verification of the different methods, the deflections and stresses showed that the equivalent modulus of elasticity best matched the real situation. As can be seen in the different tables, the deviations of deflection vary between -4 and +4 percent. This deviation is acceptable because the variation in material properties is of the same order of magnitude. In addition, for the stresses, it can be seen that the method correctly reflects the reduction in stresses in the main beam. Therefore, the method with equivalent modulus of elasticity is used to do the parameter study.

III

Results

6

Parameter study

This chapter includes the parameter study which is conducted to investigate the influence of the previous mentioned strengthening technique on strength, stiffness and acoustic transmission.

6.1. Parameters

There are two types of parameters used in this study: nominal and discrete variables. There are three nominal variables used in this study: systems, plates and fasteners.

6.1.1. Systems

The system is divided into three floors with different dimensions, which are common in monumental buildings. These three floors demonstrate similar results in their unity check for bending strength and deflection, with a uniform distributed load of 1 kN/m^2). The three systems used in this parameter study are:

- System 1: A=100x100mm^2; L=2500mm; c.t.c.=500mm; C18;
- System 2: A=200x200mm^2; L=5000mm; c.t.c.=1000mm; C18;
- System 3: A=300x300mm^2; L=7500mm; c.t.c.=1500mm; C18.

The systems have one fixed property: the beams are simply supported. In general the above mentioned systems 2 and 3 often contain joists, because their respective centre-to-centre distance is too large to carry the load with plates only. However, the joists do not influence the strength of the beam. Therefore, the joists are omitted in this study.

6.1.2. Plates

The plates have two fixed properties: type and size. As described in Subsection 2.3.1, the best non-structural plate for this application is plywood. Their length and width dimensions is based on commonly available sizes (Plyterra Group, nd). In this study the plate will contain the full width of the centre-to-centre distance and their length will be 1000 mm so that all spans are realised with whole and half plates.

The plates have two discrete variables: number of layers and thickness. The number of layers (n_p) ranges for two to four. The thickness of the plates is based on commonly available sizes and ranges from 4 to 50 mm (Mestawood, 2015, Plyterra Group, nd).

6.1.3. Fasteners

The fasteners have two fixed properties: type and size. As described in Subsection 2.3.2, the best type of fastener for this application is a self-tapping screw. The fasteners used in this study have a diameter of 10 mm and is determined by commonly available sizes (Rothoblaas, nd, Österreichisches Institut für Bautechnik, 2012). The strength of the fasteners are assumed not to be governing in this study. Therefore, their length is excluded.

The fasteners have two discrete variables: the factor for number of fasteners per plate and their respective angle. The factor for the number of fasteners per plate (n_{fpp}) is multiplied by the number of plates to get the total number of fasteners per plate. This determines the spacing between the fasteners. According to Table 8.6 from NEN-EN 1995-1-1 (2011), the minimal spacing between fasteners in the grain direction should be 7 times the diameter. The minimal spacing determines the maximum amount of fasteners per plate. The angle of the fastener ranges from 0 to 60 degrees, where 0 degrees is perpendicular to the direction of the beam. Angles bigger than 60 degrees are often impractical. In this study, the angle is increased with increments of 15 degrees.

6.1.4. Combinations

Figure 6.1 and Table 6.1 demonstrate all the combinations of the discrete variables. Figure 6.1 shows the combination in the program AutoStudy AI which used an excel sheet that calculates all the options. The program shows colors that are linked to the first parameter: the factor for numbers of fasteners per plate.

System [-]	n_p [-]	n_{fpp} [-]	Plate thickness [mm]	Fastener angle [◦]
1-3	2	1-20	4/6.5/9/12/15/18/21/24/27/30/35/40/45/50	0/15/30/45/60
1-3	3	1-13	4/6.5/9/12/15/18/21/24/27/30/35/40/45/50	0/15/30/45/60
1-3	4	1-10	4/6.5/9/12/15/18/21/24/27/30/35/40/45/50	0/15/30/45/60

Table 6.1: Discrete variables

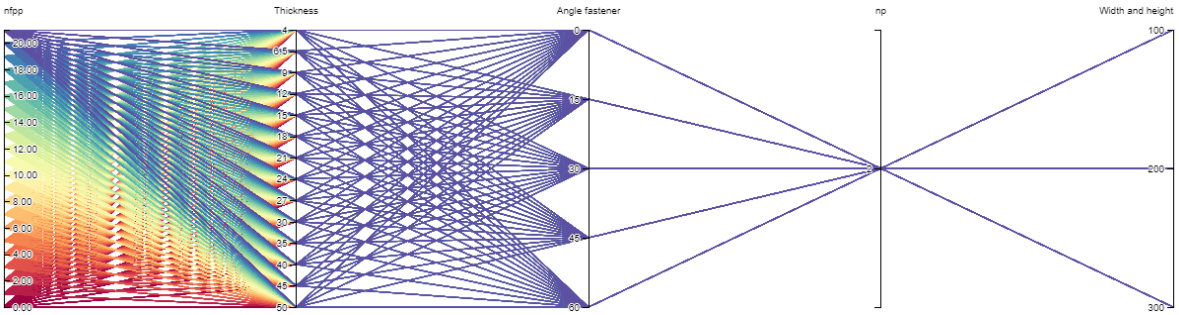

Figure 6.1: All combinations between the discrete parameters, setting n_p=2 (software: Autostudy AI)

6.1.5. Output

As explained, the program AutoStudy is used to calculate all different combinations. To compare the different results four output parameters are selected. The output is expressed as a percentage difference [%] between the strengthened beam and the bare beam. The four output parameters are:

1. Increase in effective stiffness of the section, ΔEI;
2. Increase in load carrying capacity, Δq;
3. Increase in airborne sound insulation, ΔR_w;
4. Decrease in structure-borne sound transmidded, $\Delta L_{n,w}$.

These parameters are chosen as a result of the case study described in Sections 2.5 and 3.8.

6.2. Parameter study

All discrete variables will be compared to the output parameters. In order to illustrate the influence of each variable, all other variables will be set to a control (constant) value.

6.2.1. Individual parameters

Table 6.2 shows the values of an un-strengthened floor, these values can be compared with the output in the following subsections.

System [−]	EI [Nmm^2]	q [kN/m^2]	R_w [dB]	$L_{n,w}$ [dB]
1	5.0x10^{10}	1.18	16	114
2	8.0x10^{11}	1.15	21	106
3	4.1x10^{12}	1.12	24	102

Table 6.2: Parameters before strengthening

The control variable that are chosen for the individual parameter study:

- System 1: 100x100 mm^2;
  It is expected that the influence on the output parameters (Δ) is bigger for a smaller beam with a smaller span;
- Fastener spacing of 83.33 mm;
  In order to get an identical spacing for all numbers of layers, the amount of fasteners per plate equals 12, which implies $n_p = 2 > n_{fpp} = 6$, $n_p = 3 > n_{fpp} = 4$ and $n_p = 4 > n_{fpp} = 3$;
- Plate thickness of 12 mm;
  This plate thickness will not affect the deflection due to the system's own weight for the large beam;
- Fastener angle of 0°;
  A more inclined screw causes the influence Δ to be larger for the parameter study.

As described in Subsection 3.2.3, the Eurocode describes the following requirements for acoustic values. For airborne sound insulation R_w > 42 dB and for structure-borne sound transmission L_{nt} < 63 dB. This implies that for system 1 the airborne sound insulation has to be increased by 163% and the structure-borne sound transmission decreased by 44%. For system 3 these are 75% and 38% respectively.

System

Table 6.3 shows the control variables used to check the influence of the system.

Fastener spacing [mm]	Plate thickness [mm]	Fastener angle [$\circ$]
83.33	12	0

Table 6.3: All control variables for spacing

Figures 6.2 to 6.5 illustrate the output parameters with the influence of the system. The y-axis of the figures show the difference with the original non-strengthened beam which values are given in Table 6.2. Figures 6.2 and 6.3 illustrate that the increase in stiffness and load-bearing capacity (strength) decreases as the system size increases, which was expected.

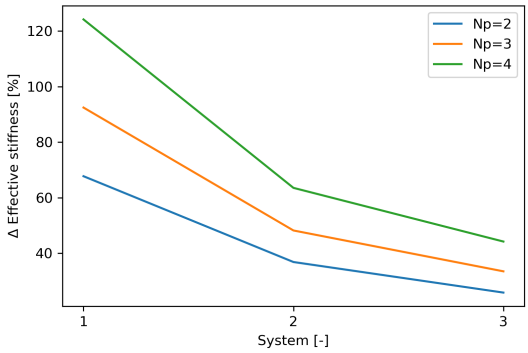

Figure 6.2: Influence of nominal variable system [-] on the effective stiffness, ΔEI [%]

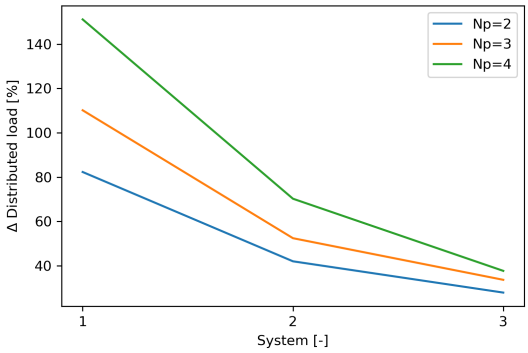

Figure 6.3: Influence of nominal variable system [-] on the distributed load, Δq [%]

Figure 6.4 illustrates that the increase in airborne sound insulation is higher for system 1 than for systems 2 and 3. Figure 6.5 illustrates that the type of floor does not affect the structure-borne sound transmission.

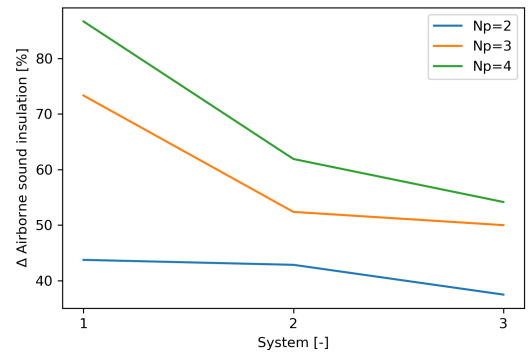

Figure 6.4: Influence of nominal variable system [-] on the airborne sound insulation, ΔR_w [%]

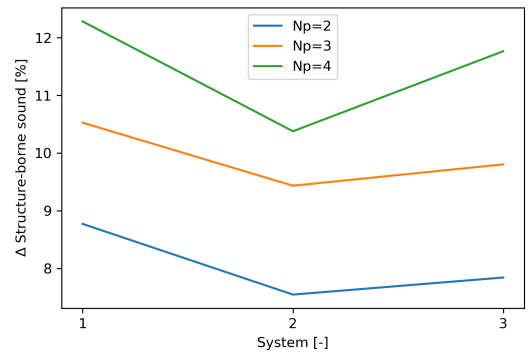

Figure 6.5: Influence of nominal variable system [-] on the structure-borne sound transmitted, $\Delta L_{n,w}$ [%]

Fastener spacing

Table 6.4 shows the control variables used to check the influence of spacing between the fasteners (amount of fasteners).

System [−]	Plate thickness [mm]	Fastener angle [$\circ$]
1	12	0

Table 6.4: Control variables for spacing

Figures 6.6 to 6.9 illustrate the influence of the spacing between fasteners. The y-axis of the figures show the difference with the original non-strengthened beam which values are given in Table 6.2. The three different types of number of layers (n_p) start at different initial spacing distances, as described in Chapter 4. Figures 6.6 and 6.7 illustrate the exponential relationship between the fastener spacing and effective stiffness and distributed load respectively.

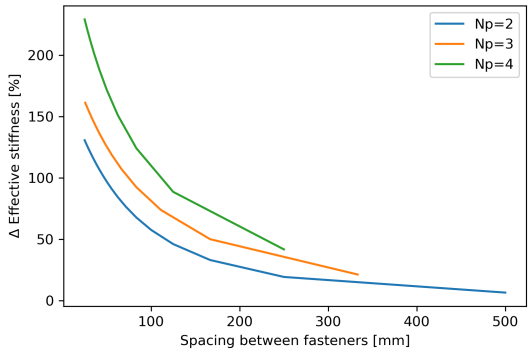

Figure 6.6: Influence of discrete variable fastener spacing [mm] on the effective stiffness, ΔEI [%]

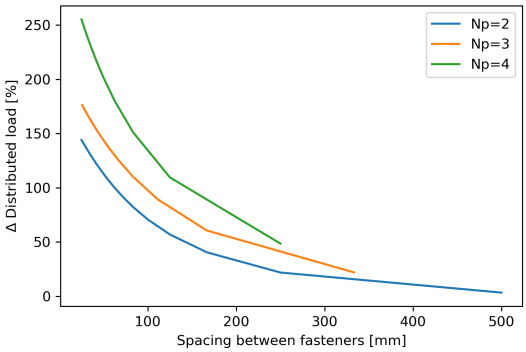

Figure 6.7: Influence of discrete variable fastener spacing [mm] on the distributed load, Δq [%]

Figures 6.8 and 6.9 illustrate the relation between the fastener spacing and the acoustic properties. Both figures illustrate that a smaller fastener spacing has a positive effect on the increase in airborne sound insulation as well as on the decrease in structure-borne sound transmission.

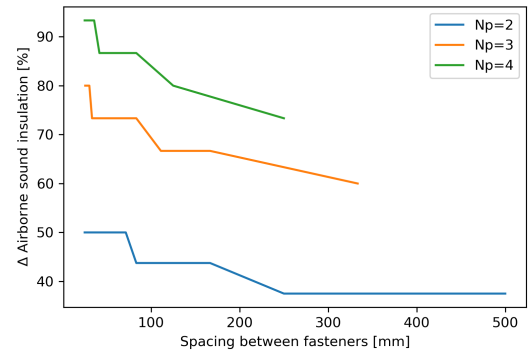

Figure 6.8: Influence of discrete variable fastener spacing [mm] on the airborne sound insulation, ΔR_w [%]

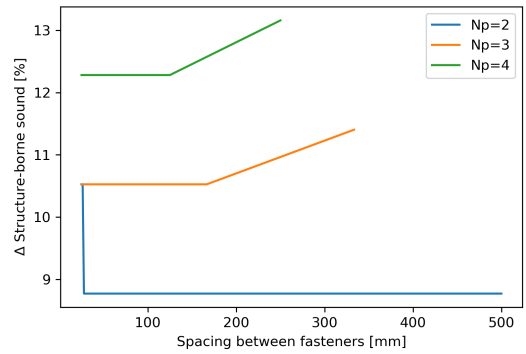

Figure 6.9: Influence of discrete variable fastener spacing [mm] on the structure-borne sound transmitted, $\Delta L_{n,w}$ [%]

Plate thickness

Table 6.5 shows the control variables used to check the influence of the plate thickness.

System [−]	Fastener spacing [mm]	Fastener angle [◦]
1	83.33	0

Table 6.5: Control variables for plate thickness

Figures 6.10 to 6.13 illustrate the influence of the plate thickness. The y-axis of the figures show the difference with the original non-strengthened beam which values are given in Table 6.2. Figures 6.10 and 6.11 illustrate a linear relationship between the plate thickness and the effective stiffness and distributed load respectively.

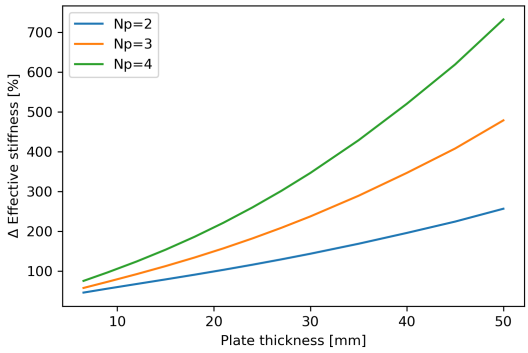

Figure 6.10: Influence of discrete variable plate thickness [mm] on the effective stiffness, ΔEI [%]

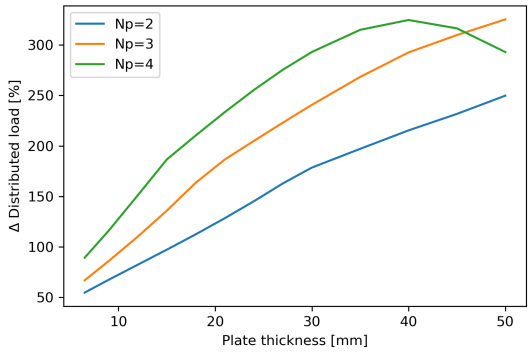

Figure 6.11: Influence of discrete variable plate thickness [mm] on the distributed load, Δq [%]

Figures 6.12 and 6.13 illustrate the relation between the plate thickness and the acoustic properties, which demonstrate a linear relationship.

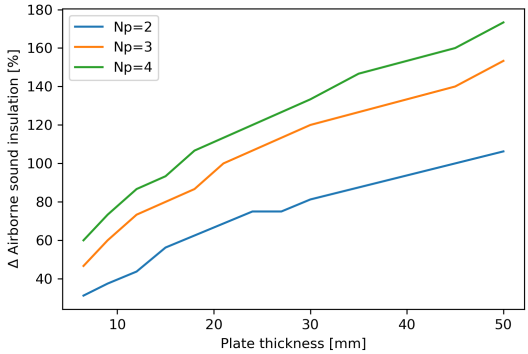

Figure 6.12: Influence of discrete variable plate thickness [mm] on the airborne sound insulation, ΔR_w [%]

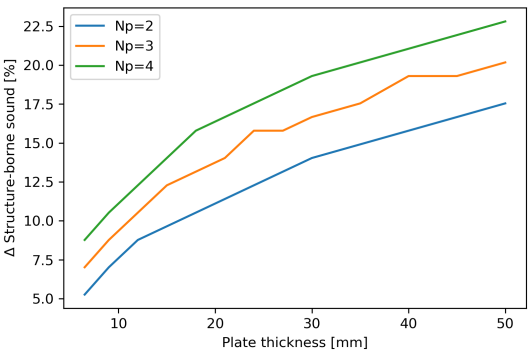

Figure 6.13: Influence of discrete variable plate thickness [mm] on the structure-borne sound transmitted, $\Delta L_{n,w}$ [%]

Fastener angle

Table 6.6 shows the control variables used to check the influence of the angle of the fasteners.

System [−]	Fastener spacing [mm]	Plate thickness [mm]
1	83.33	12

Table 6.6: Control variables for fastener angle

Figures 6.14 to 6.17 illustrate the influence of the angle of the fastener. The y-axis of the figures show the difference with the original non-strengthened beam which values are given in Table 6.2. Figures 6.14 and 6.15 illustrate a linear relationship between the angle of the fastener and the effective stiffness and distributed load respectively. These figures demonstrate, similar to Figures 6.6, 6.7, 6.10 and 6.11, that the effective stiffness correlates with the load-carrying capacity.

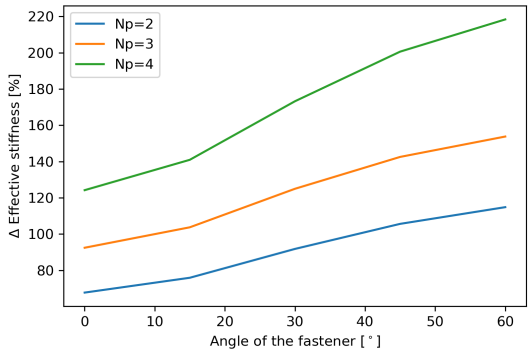

Figure 6.14: Influence of discrete variable fastener angle [◦] on the effective stiffness, ΔEI [%]

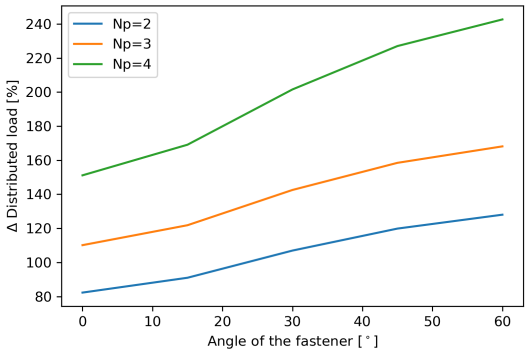

Figure 6.15: Influence of discrete variable fastener angle [◦] on the distributed load, Δq [%]

Figures 6.16 and 6.17 illustrate the relation between the angle of the fastener and the acoustic properties. Generally they show no relationship.

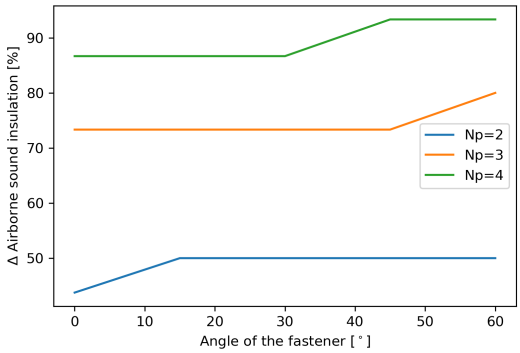

Figure 6.16: Influence of discrete variable fastener angle [◦] on the airborne sound insulation, ΔR_w [%]

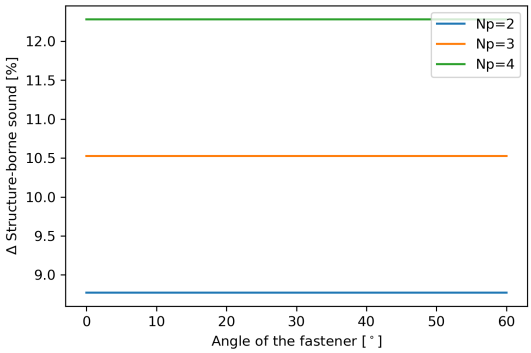

Figure 6.17: Influence of discrete variable fastener angle [◦] on the structure-borne sound transmitted, $\Delta L_{n,w}$ [%]

6.2.2. Comparison of the systems

The individual parameters are now checked only for system 1. In general, this also applies to systems 2 and 3. However, there are still a few options to be described as they influence the decision for the next steps in this research. Because the plate thickness affects all four output parameters, it will be used to compare the three types of floors.

Figures 6.18 to 6.20 illustrate the influence of the plate thickness on increase in the effective stiffness of the system. The decreasing trend in the ΔEI between system 1 to 3, demonstrates that strengthening a floor by plywood plates has more impact on smaller beams with shorter spans than on larger beams.

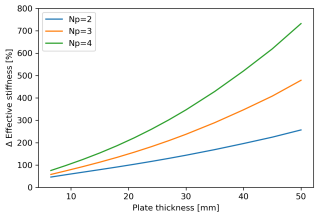

Figure 6.18: Influence of discrete variable plate thickness [mm] on the effective stiffness of system 1, ΔEI [%]

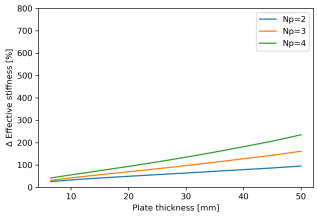

Figure 6.19: Influence of discrete variable plate thickness [mm] on the effective stiffness of system 2, ΔEI [%]

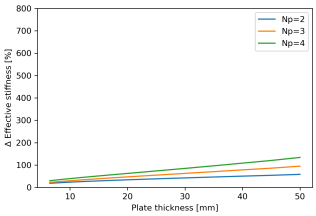

Figure 6.20: Influence of discrete variable plate thickness [mm] on the effective stiffness of system 3, ΔEI [%]

Figures 6.21 to 6.23 illustrate the influence of the plate thickness on decrease in structure-borne sound transmission. A difference between system 1, 2 and 3 is sightly present but can be considered nil. This furthermore indicates that with a timber floors the structure-borne sound transmission is mainly dominated by the airborne sound insulation part.

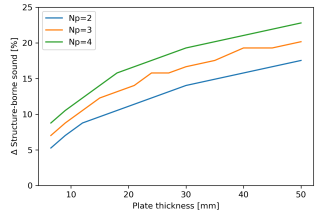

Figure 6.21: Influence of discrete variable plate thickness [mm] on the structure-borne sound transmitted of system 1, $\Delta L_{n,w}$ [%]

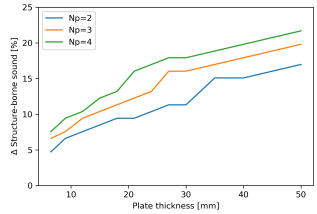

Figure 6.22: Influence of discrete variable plate thickness [mm] on the structure-borne sound transmitted of system 2, $\Delta L_{n,w}$ [%]

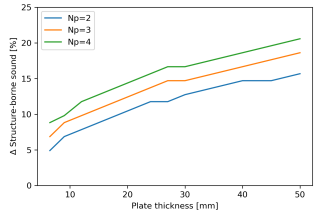

Figure 6.23: Influence of discrete variable plate thickness [mm] on the structure-borne sound transmitted of system 3, $\Delta L_{n,w}$ [%]

However, not every reinforcement increases the load-carrying capacity of the system. Figures 6.24, 6.25 and 6.26 illustrate this case. In these figure the added self-weight of the plates has a significant role in the deflection calculations (SLS) of the system, resulting in a lower load-bearing capacity when the added plates become too thick. As described, one type of fastener spacing and angle was applied in this case. If the spacing was reduced or the angle was increased, it would have a positive effect on the maximum load-bearing capacity for these systems with thicker plates.

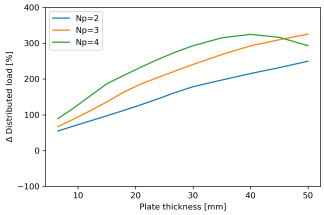

Figure 6.24: Influence of discrete variable plate thickness [mm] on distributed load on system 1, Δq [%]

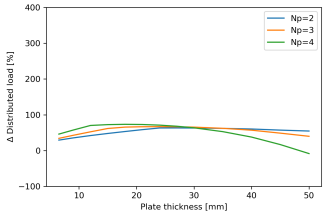

Figure 6.25: Influence of discrete variable plate thickness [mm] on distributed load on system 2, Δq [%]

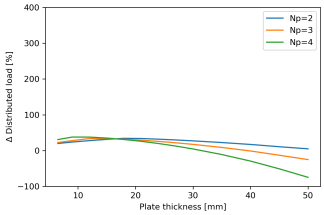

Figure 6.26: Influence of discrete variable plate thickness [mm] on distributed load on system 3, Δq [%]

The last comparison is to keep the total height of all three different layered plates the same. Figure 6.27 illustrates this phenomenon, where the maximum allowable distributed load remains the same for all n_p (thickness of the plate; ($n_p = 2$)=18mm; ($n_p = 3$)=12mm; ($n_p = 4$)=9mm). Hence, it is easier to strengthen the floor with two thick layers of plates than with four thin layers. If possible less fasteners can be used with two layered reinforcement.

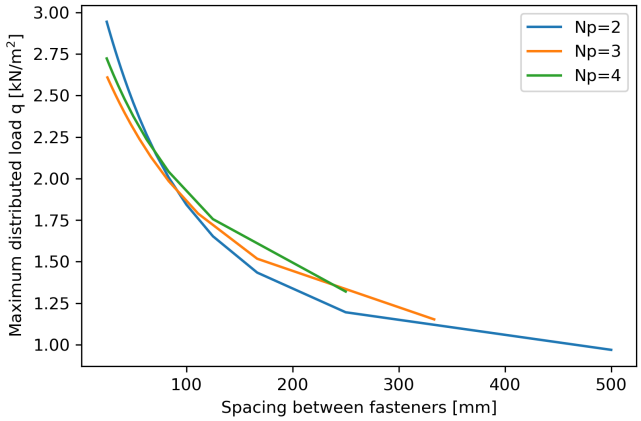

Figure 6.27: Influence of fastener spacing [mm] between 2, 3 and 4 layered plates with the same total height on the maximum distributed load [kN/m^2] for system 1

6.2.3. Overall plot

In the following visualizations, the correlation between the individual parameters is described. Figure 6.28 displays an overview of the different scatter-plots which are visualized with the output parameters. The plots on the diagonal of the matrix are represented by histograms corresponding to output parameters. The colours blue, orange and green are the three nominal variables of the three systems.

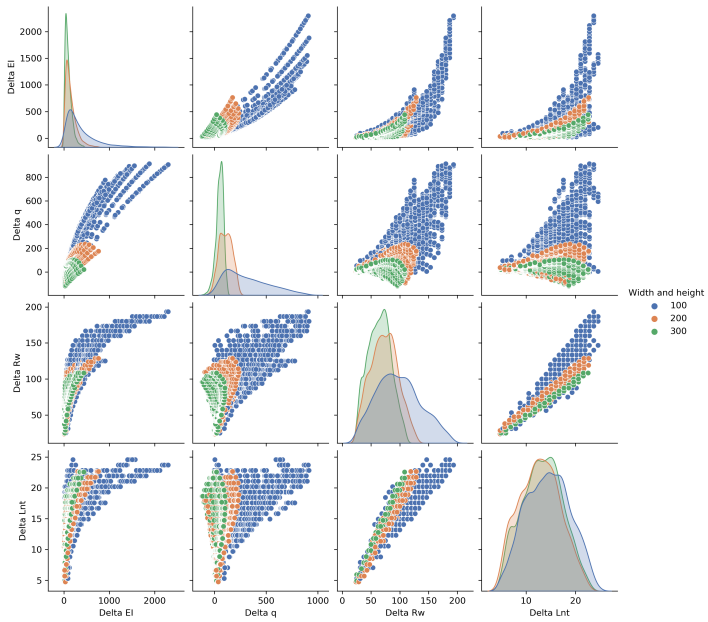

Figure 6.28: A matrix containing all the possible scatter-plots when the discrete variables in the parameter study are considered. The blue dots represent system 1, orange dots system 2 and green dots system 3

Figure 6.28 displays a general overview between the dependency among discrete variables. This overview is mainly visual and lacks a numerical representation. Figure 6.28 is is only capable of showing dependency between nominal variables. Categorical variables can not be accounted for. Therefore the Cramérs V correlation was computed between all the discrete variables and all output variables. The results of the computation Cramérs V correlations are demonstrated in Figure 6.29.

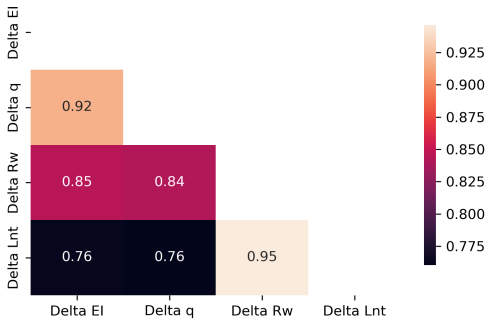

Figure 6.29: A heat map displaying the Cramérs V correlation between the four output variables

7

Case study

In this chapter, the strengthening technique is applied to an existing floor so that the influence of additional intermediate layers or the direction of reinforcement can be investigated.

7.1. Prinsenhof

Prinsenhof is a museum in Delft in which a historic moment of Delft took place: the assassination of Prince Willem van Oranje in 1584. The construction and occupation of the Prinsenhof dates back to the early 1400s. The Prinsenhof has like many traditional buildings timber floor structures. The floor between the dormitory and the attic is relevant because in the new situation an air-handling unit needs to be installed on the attic floor. Which is often not possible without reinforcement for monumental timber floors.

Figure 7.1: Monumental timber floor ceiling of the dormitory in the Prinsenhof Museum in Delft [Figure from ABT]

7.1.1. Overview, floor between the dormitory to attic

Figure 7.2 on the next page illustrates the build-up of the floor between the dormitory and attic in the Prinsenhof. The attic floor consists of beams, joists and planks. In the present state, there is a concrete layer on the existing floor. If the floor should be strengthened with timber plates as described in this case study, this concrete layer would have to be removed. Table 7.1 shows the properties of these components.

		Planks (C18)	**Joists (C18)**	**Beams (D18)**
Width	[mm]	200	110	300
Height	[mm]	20	110	280
Length	[mm]	380	2500	9000 (7000)
$E_{m,0,k}$	[N/mm^2]	6000	6000	8000
ρ_k (ρ_m)	[kg/m^3]	320 (380)	320 (380)	475 (570)
$f_{m,k}$	[N/mm^2]	18	18	18
$f_{v,k}$	[N/mm^2]	3.4	3.4	3.5
$f_{c,90,k}$	[N/mm^2]	2.2	2.2	4.8

Table 7.1: Properties of the attic floor

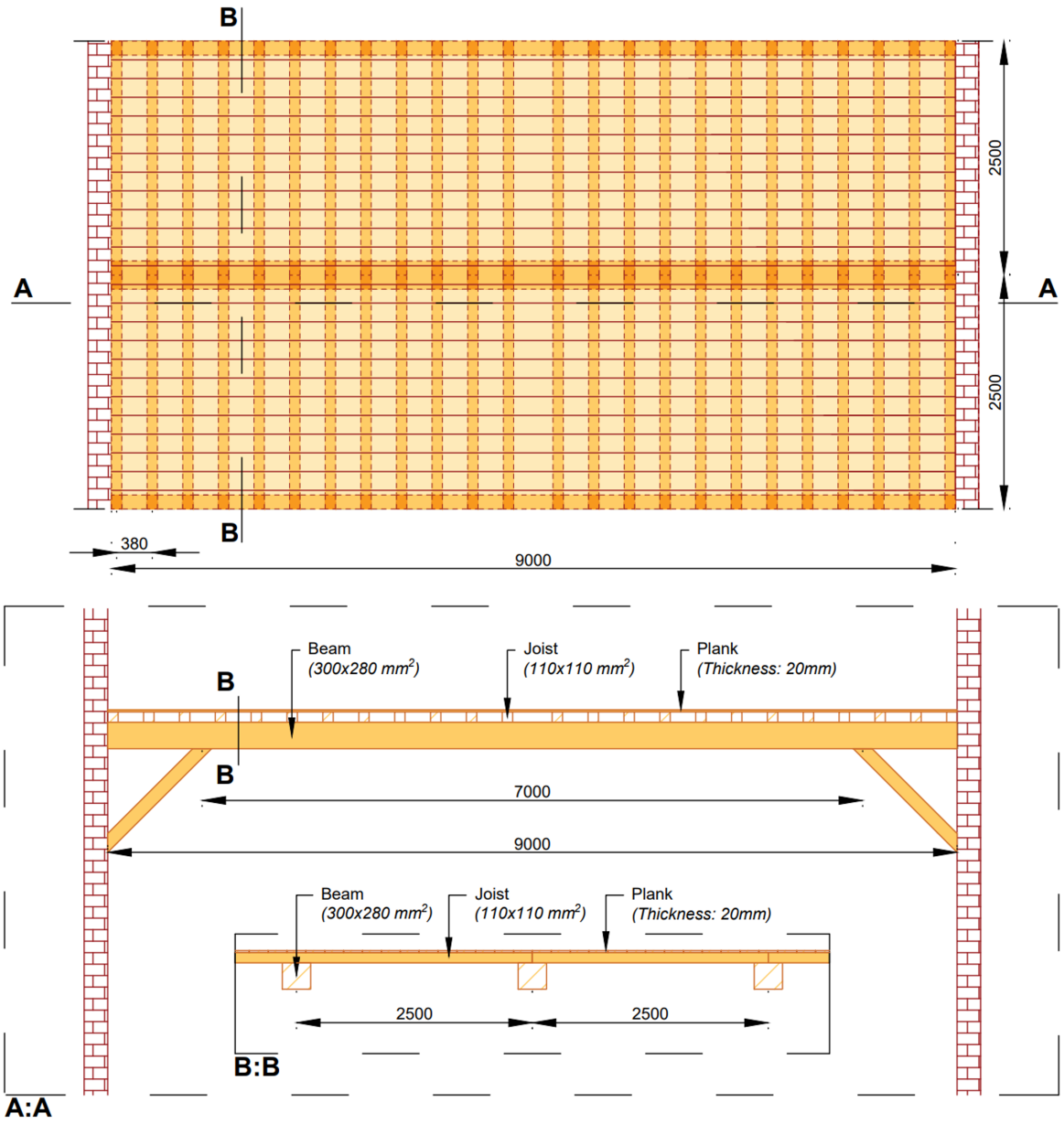

Figure 7.2: Top and side view of the attic floor current situation

7.1.2. Load cases

The attic floor must accommodate an air-handling unit. As illustrated in the preceding case study (see Appendix C), the point loads on the planks and joists are the most significant.

This case study considers two load cases in order to future proof the attic floor. One load case where the attic is considered as storage and a second for the air-handling unit combined with a person. These load cases are described as:

- Load case 1:
  Storage - distributed load of 4 kN/m^2 ($k_{mod} = 0.6$; $\Psi_0 = 1.0$; $\Psi_2 = 0.8$)
- Load case 2:
  Air-handling unit - point loads of 4 kN ($k_{mod} = 0.6$; $\Psi_0 = 1.0$; $\Psi_2 = 0.8$)
  +
  Person - distributed load of 1 kN/m^2 ($k_{mod} = 0.8$; $\Psi_0 = 0.4$; $\Psi_2 = 0.3$)

Figures 7.3 to 7.5 illustrate load case 2 for the planks, joists and beams respectively. Only the beam supports two point loads.

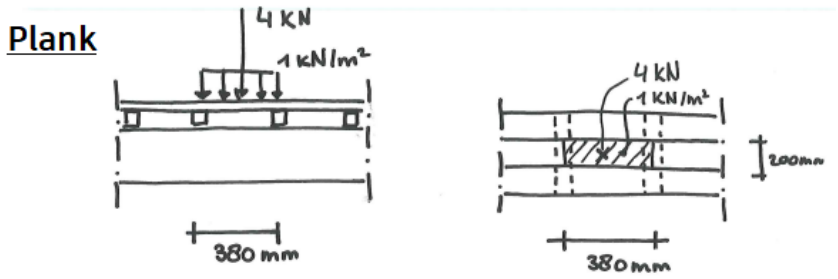

Figure 7.3: Load case 2 on the plank. Left: side view and Right: top view

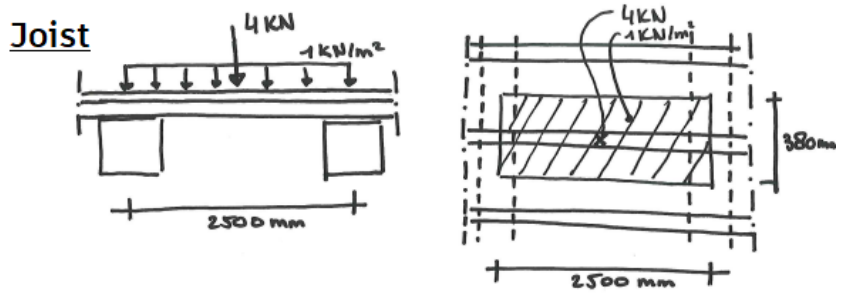

Figure 7.4: Load case 2 on the joist. Left: side view and Right: top view

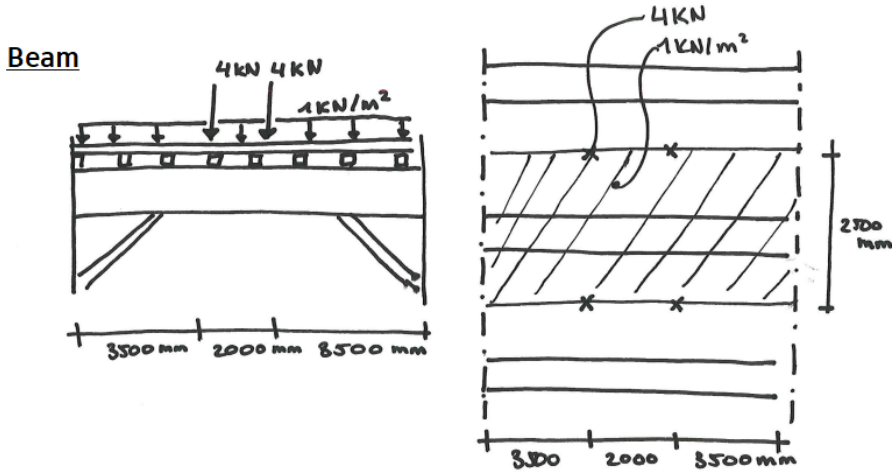

Figure 7.5: Load case 2 on the beam. Left: side view and Right: top view

Figures 7.6 and 7.7 illustrate the bending and deflection unity checks for all three components. Similar to the case study in Section 2.5, the planks and joists are normative for the point load and the joists and beams are normative for the distributed load.

Table 7.2 shows the maximum loads on all three components. From these numbers, the joists and beams should be strengthened to carry the distributed load and the planks and joists should be strengthened to carry the point load. When the joists or beams are strengthened, the planks will be automatically reinforced as well. Therefore, the joists are taken as the governing element in these calculations.

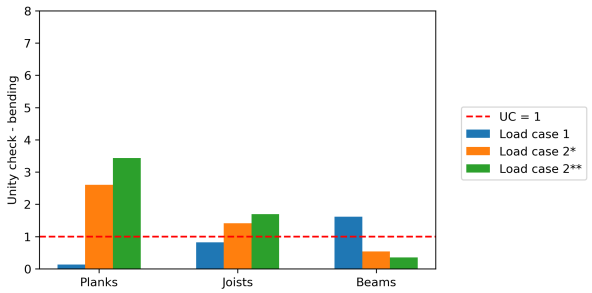

Figure 7.6: Bending stress unity check for both load cases on the attic floor (* $k_{mod} = 0.6$ en ** $k_{mod} = 0.8$)

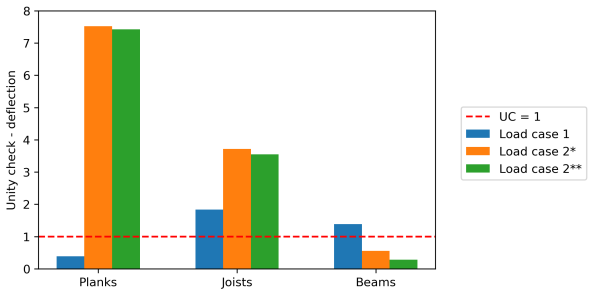

Figure 7.7: Deflection unity check for both load cases on the attic floor (* $k_{mod} = 0.6$ en ** $k_{mod} = 0.8$)

Load type		Plank	Joist	Beam
Distributed load [kN/m^2]	ULS	30.6	4.9	**2.4**
	SLS	11.3	**1.9**	2.9
Point load [kN]	ULS	1.2	2.3	15.0
	SLS	**0.5**	**1.1**	16.0

Table 7.2: Maximum loads on the elements according to the case study from Appendix C

7.2. Strengthening

The reinforcement consist of 2-layered plywood plates with a thickness of 30 mm each. As Figure 6.26 illustrates, thicker plates than 30 mm will be negative for the large beam with 2 layers. In addition, Figure 6.27 illustrates that more layers with thinner plates do not create a more positive effect and in addition only produce more labor. The reinforcement layer will be placed in the direction of the joists as described in the previous subsection. To connect the new plates to the existing structure self-tapping screws with a diameter of 9 mm are used. These fasteners are placed at an angle of 45 degrees and have a spacing of 140 mm.

As there is a void between the planks and the beam, timber blocks have to be placed in order to create the pratt truss between the reinforcement layer and the beam with the fasteners.

7.2.1. Properties of the strengthening layer

Table 7.3 describes the mechanical properties of the plates and self-tapping screws (Mestawood, 2015, Plyterra Group, nd, Österreichisches Institut für Bautechnik, 2012).

Plywood plates			**Self-tapping screws**		Joist	Beam
$E_{m,0,k}$	$[N/mm^2]$	6025	Diameter	$[mm]$	9	9
$E_{0,mean}$	$[N/mm^2]$	8000	Length	$[mm]$	200	355
Thickness	$[mm]$	30	α	$[\circ]$	45	45
ρ_k	$[kg/m^3]$	630	Penetration length	$[mm]$	85	85
ρ_{mean}	$[kg/m^3]$	680	Spacing between screws	$[mm]$	140	140
$f_{m,k}$	$[N/mm^2]$	36.8	$M_{y,Rk}$	$[Nmm]$	19200	19200
$f_{v,k}$	$[N/mm^2]$	2.57	$K_{ser,\perp}$	$[N/mm]$	4485	6080
			$K_{ser,\parallel}$	$[N/mm]$	23550	29957
			K_{ser}	$[N/mm]$	8993	7867
			K_u	$[N/mm]$	5995	5245
			$f_{ax,k}$	$[N/mm^2]$	12.8	12.8

Table 7.3: Plywood plates and self-tapping screws characteristics

7.2.2. Overview structure

Figure 7.8 illustrates the strengthened beam layer in the direction of the joists. The plywood plates are (1000 x 2500 mm^2) with 2500 mm in the direction of the joists and 1000 mm in the direction of the

beam. The joist direction indicates that the plates are overlapping in the joist direction and are stacked in lanes in the beam direction.

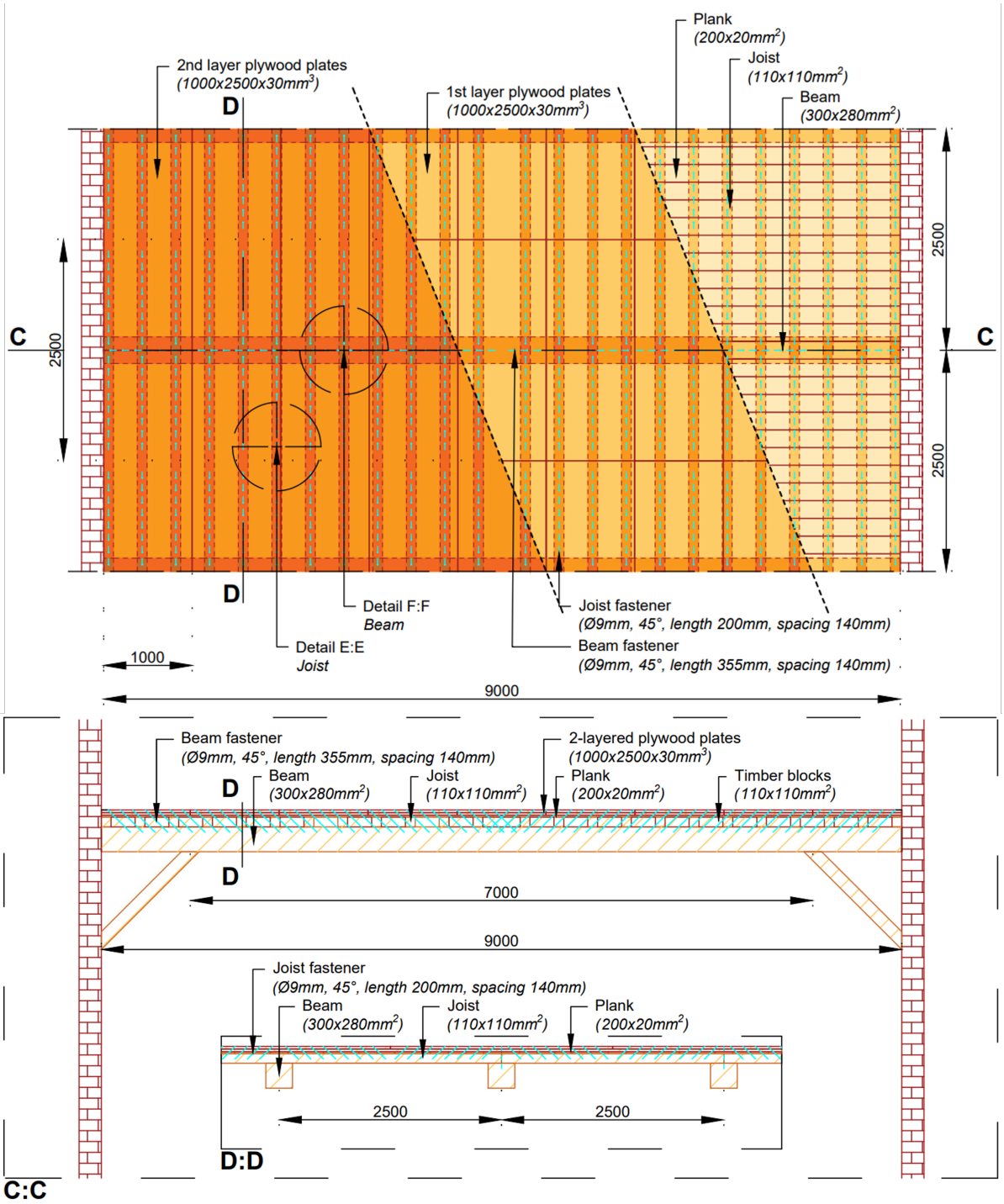

Figure 7.8: Top and side view of the attic floor after strengthening the joist direction

7.2.3. Plank

The planks are strengthened by the plates, just by the increase of EI of the plates. Table 7.4 shows the unity checks for strength in the ultimate limit state (ULS) of the planks, none of the values are above 1. Table 7.5 shows the unity checks for stiffness in the serviceability limit state (SLS) of the planks, the unity check for load case 2 are sightly below 1.

			Max. value	Calculated value	Unity check
	$EI_{eff,ULS,plank}$	$[Nmm^2]$	-	6.22 x 10^9	-
Load case 1	$\sigma_{plank,max}$	$[N/mm^2]$	10.80	0.20	0.02
*Load case 2**	$\sigma_{plank,max}$	$[N/mm^2]$	10.80	4.78	0.44
*Load case 2***	$\sigma_{plank,max}$	$[N/mm^2]$	14.40	4.83	0.34

Table 7.4: Calculated and maximum stresses of reinforced floor in joist direction ULS
(* k_{mod} = 0.6 en ** k_{mod} = 0.8)

			Max. value	Calculated value	Unity check
	$EI_{eff,SLS,plank}$	$[Nmm^2]$	-	6.22 x 10^9	-
Load case 1	$w_{plank,first}$	$[mm]$	1.14	0.05	0.05
*Load case 2**	$w_{plank,first}$	$[mm]$	1.14	1.09	0.96
*Load case 2***	$w_{plank,first}$	$[mm]$	1.14	1.10	0.97

Table 7.5: Calculated and maximum stresses of reinforced floor in joist direction SLS
(* k_{mod} = 0.6 en ** k_{mod} = 0.8)

7.2.4. Joist

Figures 7.9 illustrates detailed sections of the joists with the strengthening plates.

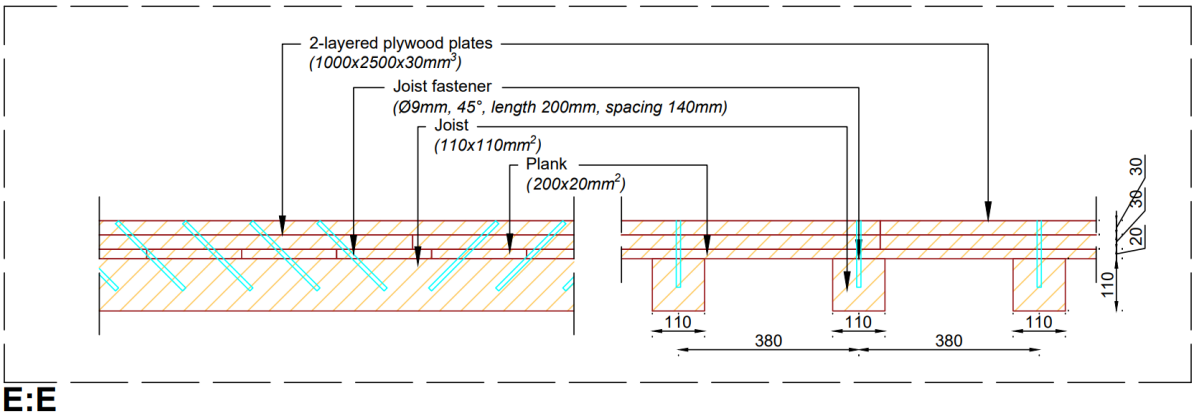

E:E

Figure 7.9: Detail E:E of Figure 7.8, strengthened joist

Table 7.6 shows the unity checks for strength in the ULS of the joists, none of the values are above 1. The slip reduction factor (Sub-subsection 2.3.2) is 0.84 for the 20mm of planks between the joists and the additional plates.

			Max. value	Calculated value	Unity check
	$EI_{eff,ULS,joist}$	$[Nmm^2]$	-	2.50 x 10^{11}	-
Load case 1	$\sigma_{joist,max}$	$[N/mm^2]$	8.84	2.60	0.29
	$V_{connection,joist}$	$[kN/screw]$	4.27	2.40	0.56
*Load case 2**	$\sigma_{joist,max}$	$[N/mm^2]$	8.84	5.12	0.58
	$V_{connection,joist}$	$[kN/screw]$	4.27	2.51	0.59
*Load case 2***	$\sigma_{joist,max}$	$[N/mm^2]$	11.79	5.98	0.48
	$V_{connection,joist}$	$[kN/screw]$	5.69	3.00	0.53

Table 7.6: Calculated and maximum stresses of reinforced floor in joist direction ULS
(* k_{mod} = 0.6 en ** k_{mod} = 0.8)

Table 7.7 shows the unity checks for stiffness in the SLS of the joists, for the second load case the unity check is slightly above 1.

			Max. value	Calculated value	Unity check
	$EI_{eff,SLS,joist}$	$[Nmm^2]$	-	2.94 x 10^{11}	-
Load case 1	$w_{joist,first}$	$[mm]$	7.50	4.10	0.54
*Load case 2**	$w_{joist,first}$	$[mm]$	7.50	6.76	0.90
*Load case 2***	$w_{joist,first}$	$[mm]$	7.50	7.54	**1.01**

Table 7.7: Calculated and maximum stresses of reinforced floor in joist direction SLS
(* k_{mod} = 0.6 en ** k_{mod} = 0.8)

7.2.5. Beam

Figures 7.10 illustrates detailed sections of the beam with the strengthening plates.

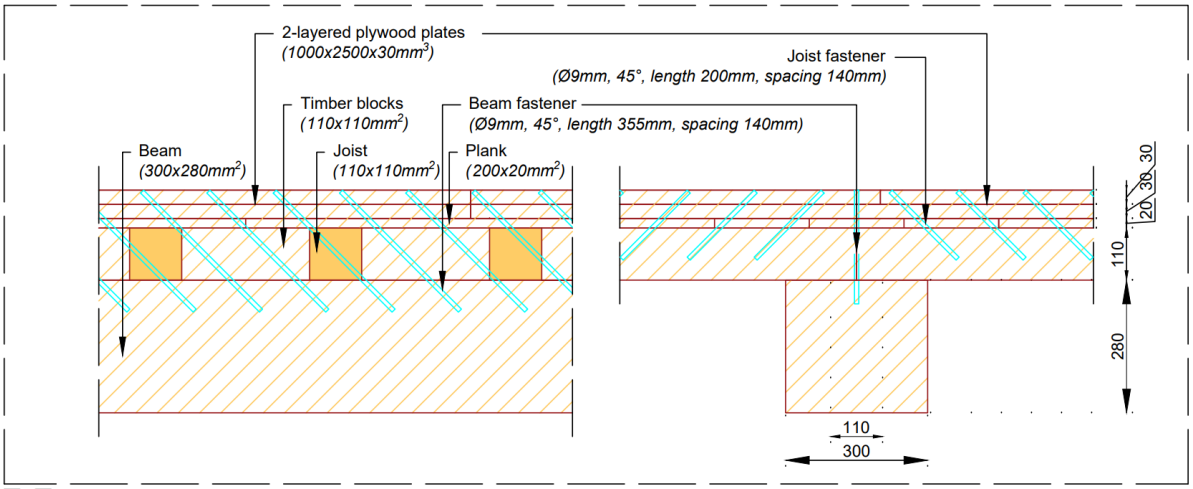

Figure 7.10: Detail F:F of Figure 7.8, strengthened beam

Table 7.8 shows the unity checks for strength in the ULS of the beam. The effective stiffness of the beam was calculated with the program MatrixFrame. The effective stiffness is only increased by approximately 5% compared to the stiffness of the beam. As load case 1 demonstrated load case 1, large distributed loads are still not possible. Furthermore, the connections become governing both load cases.

			Max. value	Calculated value	Unity check
	$EI_{eff,ULS,beam}$	$[Nmm^2]$	-	4.47 x 10^{12}	-
Load case 1	$\sigma_{beam,max}$	$[N/mm^2]$	8.31	16.02	**1.87**
	$V_{connection,beam}$	$[kN/screw]$	4.04	19.09	**4.73**
*Load case 2**	$\sigma_{beam,max}$	$[N/mm^2]$	8.31	4.40	0.53
	$V_{connection,beam}$	$[kN/screw]$	4.04	5.36	**1.33**
*Load case 2***	$\sigma_{beam,max}$	$[N/mm^2]$	11.08	7.44	0.67
	$V_{connection,beam}$	$[kN/screw]$	5.38	8.82	**1.64**

Table 7.8: Calculated and maximum stresses of reinforced floor in joist direction ULS
(* k_{mod} = 0.6 en ** k_{mod} = 0.8)

Table 7.9 shows the unity checks for stiffness in the SLS of the beam, none of the values are above 1.

			Max. value	Calculated value	Unity check
	$EI_{eff,SLS,beam}$	$[Nmm^2]$	-	4.61 x 10^{12}	-
Load case 1	$w_{beam,first}$	$[mm]$	21.00	19.68	0.94
*Load case 2**	$w_{beam,first}$	$[mm]$	21.00	5.00	0.24
*Load case 2***	$w_{beam,first}$	$[mm]$	21.00	9.66	0.46

Table 7.9: Calculated and maximum stresses of reinforced floor in joist direction SLS (* $k_{mod} = 0.6$ en ** $k_{mod} = 0.8$)

7.2.6. Total overview

Tables 7.4 to 7.9 demonstrate the results of the strengthening technique for both load cases on every component for ULS and SLS. Figures 7.11 and 7.12 summarize these tables in the form of graphs. These show that for the ULS the floor is not strengthened sufficiently to accommodate the bending stresses in the beam.

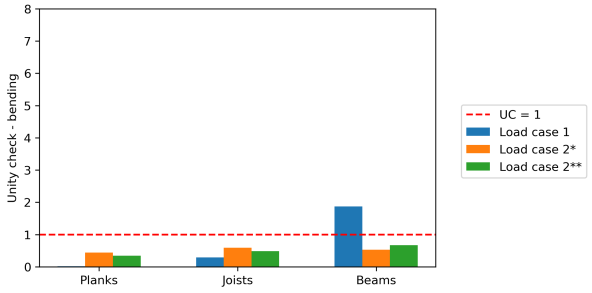

Figure 7.11: Bending stress unity check for both load cases on the attic floor (* $k_{mod} = 0.6$ en ** $k_{mod} = 0.8$)

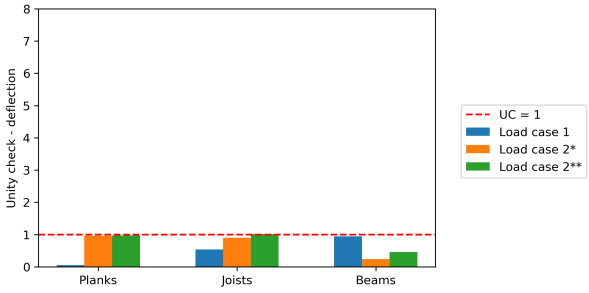

Figure 7.12: Deflection unity check for both load cases on the attic floor (* $k_{mod} = 0.6$ en ** $k_{mod} = 0.8$)

Furthermore, the large shear forces cause the forces between the beam and the reinforcing layer to become normative. Figure 7.13 shows the unity checks for these fasteners at the large shear forces.

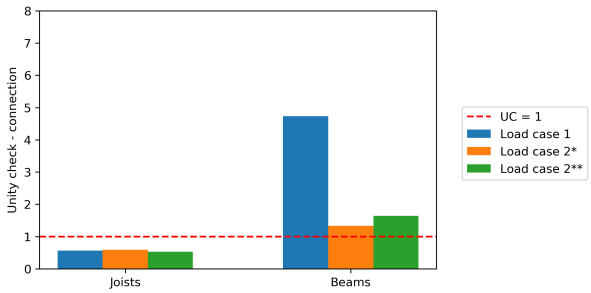

Figure 7.13: Fastener unity check for both load cases on the attic floor (* $k_{mod} = 0.6$ en ** $k_{mod} = 0.8$)

Equation 7.1 shows the effectiveness of the strengthening technique. The effectiveness of concrete strengthening techniques on refurbished timber floors are often found between 0.4-0.7, according to Roensmaens et al. (2018). Which implies that the strengthening technique in this case study is in a similar range.

$$\eta_{joists} = \frac{EI_{eff} - EI_0}{EI_1 - EI_0} = \frac{2.50 \cdot 10^{11} - 0.89 \cdot 10^{11}}{4.43 \cdot 10^{11} - 0.89 \cdot 10^{11}} = 0.45 \tag{7.1}$$

To satisfy the unity check of the beam on bending and connection failure, the following variables could be adjusted:

- Stronger fasteners
  Stronger fasteners do not have a significant effect on the connection failure force because the

connection failure is mainly governed by the embedment strength of the plate. Furthermore, stronger fasteners often imply a larger diameter which causes the minimum fastener spacing to be larger. Therefore, less fasteners would be used which then lower the effective stiffness.

- More inclined fasteners
  Increasing the angle of the fastener will create a higher effective stiffness. Furthermore, increasing the angle implies that the distance between successive fasteners is smaller and the minimal fastener spacing is reached earlier. A higher effective stiffness also causes the forces on the fastener to increase.

- Smaller fastener spacing
  Applying more fasteners will increase the effective stiffness which has a positive effect on the bending stresses and a negative on the force on the fastener.

- More fasteners in width direction
  Applying more fasteners in the width direction causes the floor to be stiffer and divides the force over the fasteners in width direction. However, the minimum distance between the fasteners as well as and between the fasteners and the edge of the beam must be taken into account. The minimum spacing between fasteners is 5x the diameter and the minimum edge distance is 4x the diameter.

- Increasing the plate thickness
  Thicker plates would be another option. However, thicker plate do not increase the effective stiffness for the beam since the plates do not create a continuous layer.

- Applying a continuous strengthening layer over the beam
  Applying a continuous strengthening layer over the beam increases its effective stiffness considerably. At the beginning and end of the joists the plywood plates have to be shortened to create the space for this continuous layer. At the ends of the joists, the moments are small and shear forces are high and these can be handled by the cross-section of the joist only.

7.2.7. Acoustics

Table 7.10 demonstrates the changes in acoustics. Both airborne as well as structure-borne sound requirements are not met.

	R_w $[dB]$		$L_{n,w}$ $[dB]$	
	Joist	Beam	Joist	Beam
Before	17	26	113	101
After	32	40	95	89

Table 7.10: Acoustic properties of the floor, before and after strengthening in the joist direction

7.3. Optimization for effective stiffness of the beam

In the previous section, multiple variables were discussed which could be adjusted to increase the effective stiffness of the beam. From these variables, applying a continuous strengthening layer over the beam will be the most effective. Therefore, an optimization for the effective stiffness of the beam is created by shortening the strengthening layer of the joists with 0.5 meters at both ends and applying a continuous layer in the direction of the beam.

By increasing the effective stiffness of the beam through a continuous layer, the forces on the fastener also increase. As Figure 7.13 illustrates, the fasteners are already governing. Therefore, multiple fasteners in width direction need to be applied in the beam.

7.3.1. Properties of the strengthening layer

Table 7.11 sums up the mechanical properties of the plates and the mechanical properties of the self-tapping screws (Mestawood, 2015, Plyterra Group, nd, Österreichisches Institut für Bautechnik, 2012).

Plywood plates			**Self-tapping screws**		Joist	Beam
$E_{m,0,k}$	$[N/mm^2]$	6025	Diameter	$[mm]$	9	9
$E_{0,mean}$	$[N/mm^2]$	8000	Length	$[mm]$	200	355
Thickness	$[mm]$	30	α	$[\circ]$	45	45
ρ_k	$[kg/m^3]$	630	Penetration length	$[mm]$	85	85
ρ_{mean}	$[kg/m^3]$	680	Spacing between screws	$[mm]$	125	140
$f_{m,k}$	$[N/mm^2]$	36.8	$M_{y,Rk}$	$[Nmm]$	19200	19200
$f_{v,k}$	$[N/mm^2]$	2.57	$K_{ser,\perp}$	$[N/mm]$	4485	6080
			$K_{ser,\parallel}$	$[N/mm]$	23550	29957
			K_{ser}	$[N/mm]$	8993	7867
			K_u	$[N/mm]$	5995	5245
			$f_{ax,k}$	$[N/mm^2]$	12.8	12.8

Table 7.11: Plywood plates and self-tapping screws characteristics

7.3.2. Overview structure

There are two sizes of plywood plates:

1. Plywood for joists (1000 x 1500 mm^2), with 1500 mm in the direction of the joists;
2. Plywood for beams (1000 x 2500 mm^2), with 2500 mm in the direction of the beams.

Figures 7.14 and 7.15 illustrate the top and side view where the plates strengthen the joists and the beams. Figures 7.16 and 7.17 illustrate the details of the strengthened joist and beam.

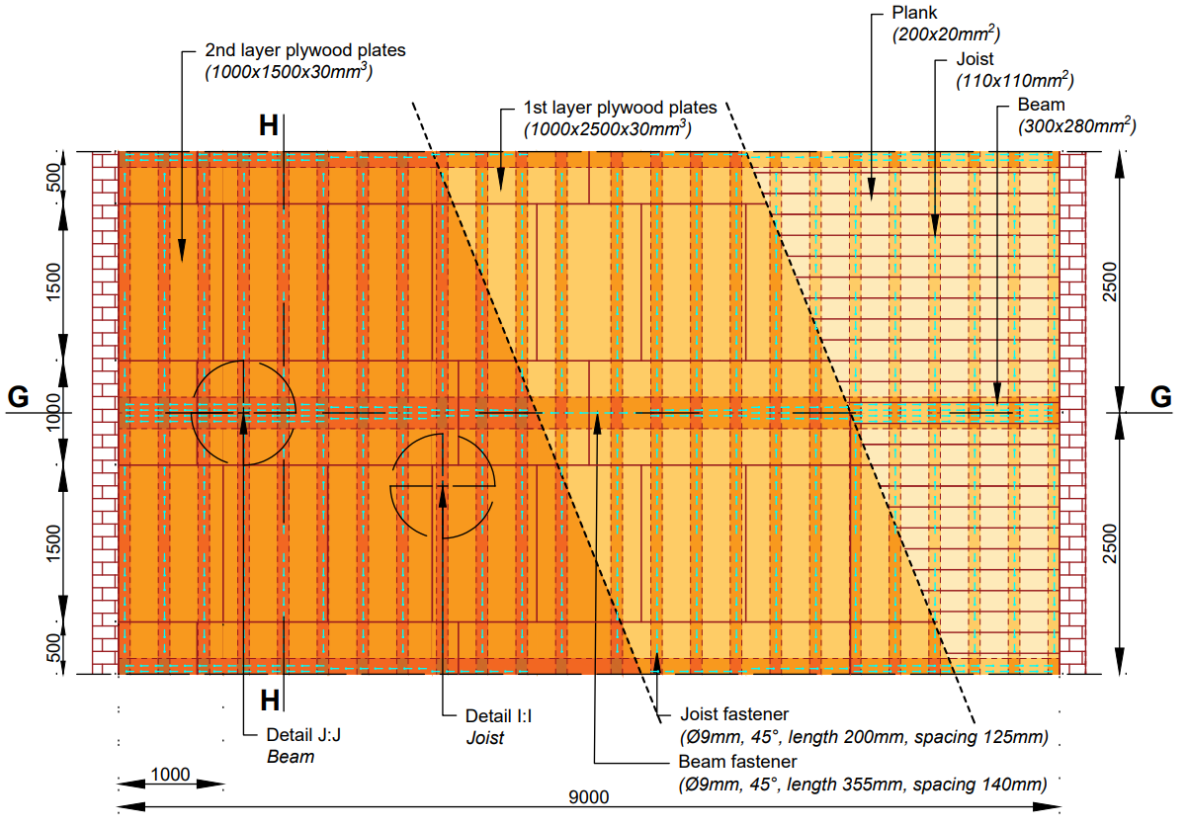

Figure 7.14: Top view of the attic floor after strengthening the joist direction

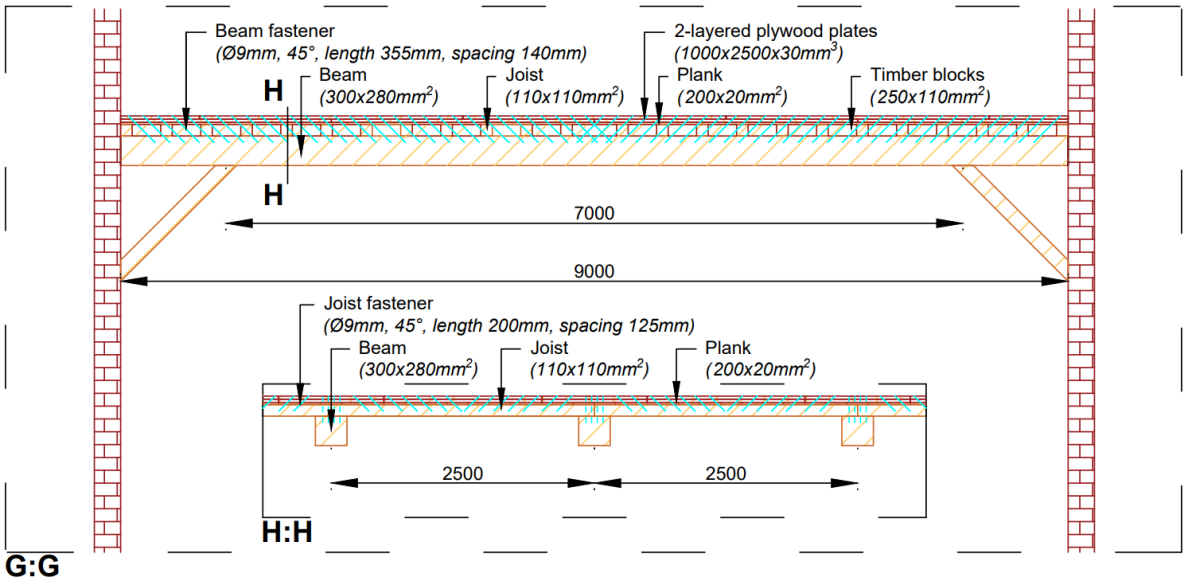

Figure 7.15: Side view of the attic floor after strengthening the joist direction

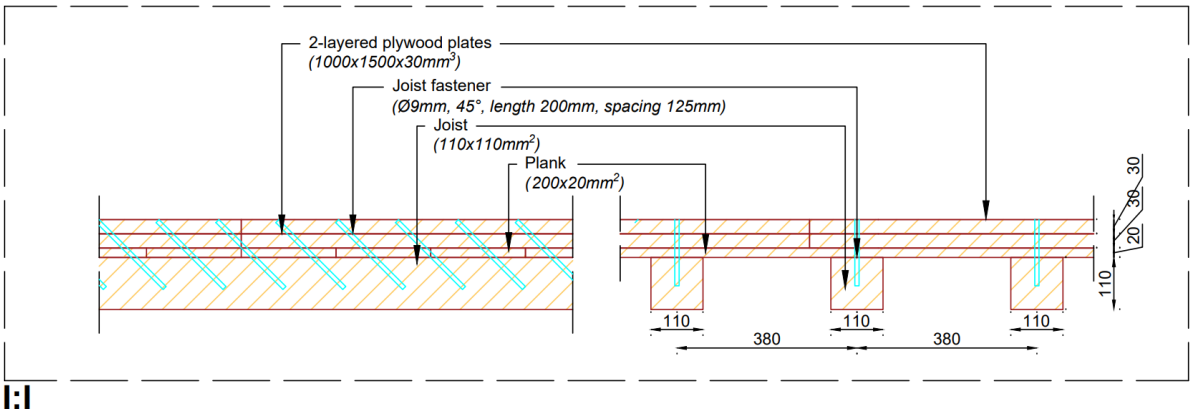

Figure 7.16: Detail I:I of Figure 7.14, strengthened joist

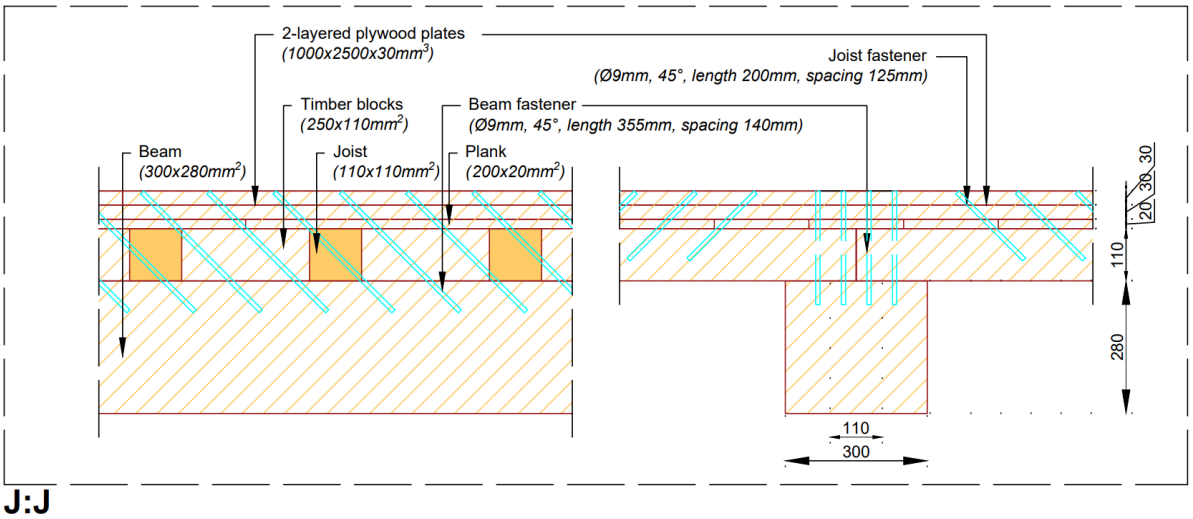

Figure 7.17: Detail J:J of Figure 7.14, strengthened beam

7.3.3. Total overview

Figures 7.18 and 7.19 summarize the unity checks for bending and deflection, indicating that ULS as well as SLS of the floor are sufficiently strengthened regarding all three elements: planks, joists and beams. With a minor reservation regarding the unity check of the joists resulting in 1.05 (load case 2, with short duration), which is considered acceptable. The slip reduction factor (Sub-subsection 2.3.2) is 0.84 for the joists (20mm of planks) and 0.42 for the beam (20mm of planks + 110mm joists).

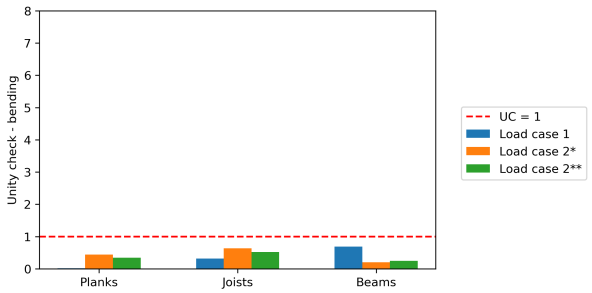

Figure 7.18: Bending stress unity check for both load cases on the attic floor (* $k_{mod} = 0.6$ en ** $k_{mod} = 0.8$)

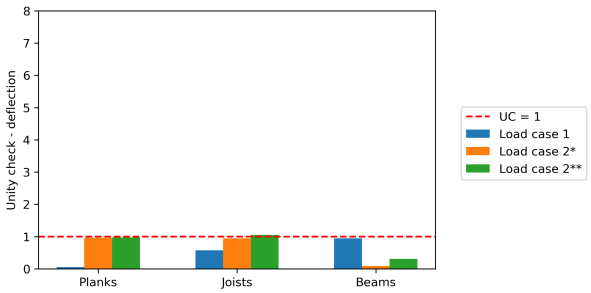

Figure 7.19: Deflection unity check for both load cases on the attic floor (* $k_{mod} = 0.6$ en ** $k_{mod} = 0.8$)

Furthermore, the beam is connected to the strengthening layer by multiple fasteners. This is up to four fasteners at the sections where the shear forces are the highest. Figure 7.20 illustrates the unity checks for these fasteners at the section where the shear forces are the highest and this demonstrates that of these fasteners only the beam reach their limit (UC=1.06). For the next optimization five fasteners need to be installed at these locations in the beam.

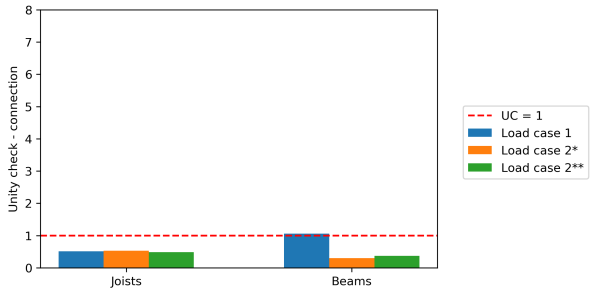

Figure 7.20: Fastener unity check for both load cases on the attic floor (* $k_{mod} = 0.6$ en ** $k_{mod} = 0.8$)

Equations 7.2 and 7.3 show the effectiveness of the strengthening technique. The joist results in the average of the 0.4-0.7 range (Roensmaens et al., 2018), the beam preforms above average. Furthermore, the effectiveness of the joists is increased.

$$\eta_{joist} = \frac{EI_{eff} - EI_0}{EI_1 - EI_0} = \frac{2.38 \cdot 10^{11} - 0.84 \cdot 10^{11}}{3.74 \cdot 10^{11} - 0.84 \cdot 10^{11}} = 0.53 \tag{7.2}$$

$$\eta_{beam} = \frac{EI_{eff} - EI_0}{EI_1 - EI_0} = \frac{1.39 \cdot 10^{13} - 0.44 \cdot 10^{13}}{1.62 \cdot 10^{13} - 0.44 \cdot 10^{13}} = 0.81 \tag{7.3}$$

7.3.4. Acoustics

Table 7.12 demonstrates the changes in acoustics. Both airborne as well as structure-borne sound requirements are not met. Furthermore, this optimization increased R_w with +2dB and decreased L_{nt} with -2dB. A change of 2 dB is just about to be perceived with the human ear (Section 3.2) and is therefore insignificant. The increase in structure-borne sound transmitted by the joists is +3dB. This increase is related to the decrease of the stiffness and therefore increase of the coincidence frequency.

	R_w $[dB]$		$L_{n,w}$ $[dB]$	
	Joist	Beam	Joist	Beam
Before	17	26	113	101
After	32	42	98	87

Table 7.12: Acoustic properties due to strengthening in joist and beam direction

7.4. Optimization acoustics

Floating floors as described in Section 3.7 are an option to improve the acoustic sound insulation. Since load case 1 for the beam and for load case 2 for the joists are normative and already around UC=1, two options are possible if floating floors are applied. The load from both load could be reduced or the joist and beams need to be propped during reinforcement of the floor. The latter compensates for the present deflection and to ensures that the deflection due to the self-weight of the structure is supported by the effective stiffness of the reinforced system.

Section 3.7 describes five types of dry floating floors. For the purpose of meeting the acoustic requirements only the heaviest option (F, 160kg/m2) should be applied, if the lowest insulation value (joist and beam) is chosen. This only possible if the beams will be propped during reinforcement. Furthermore, it is advised to place the air-handling unit directly on top of the beam. However, is this is not executed the floor could support the point loads but only when the joists are propped during reinforcement. In addition, to bear the load five fasteners need to be installed in the beam at the locations where shear forces are high with the fastener spacing in the beam and joist decreasing to 113mm. Figures 7.21 and 7.22 illustrate the side and top view of the air-handling unit on the attic floor.

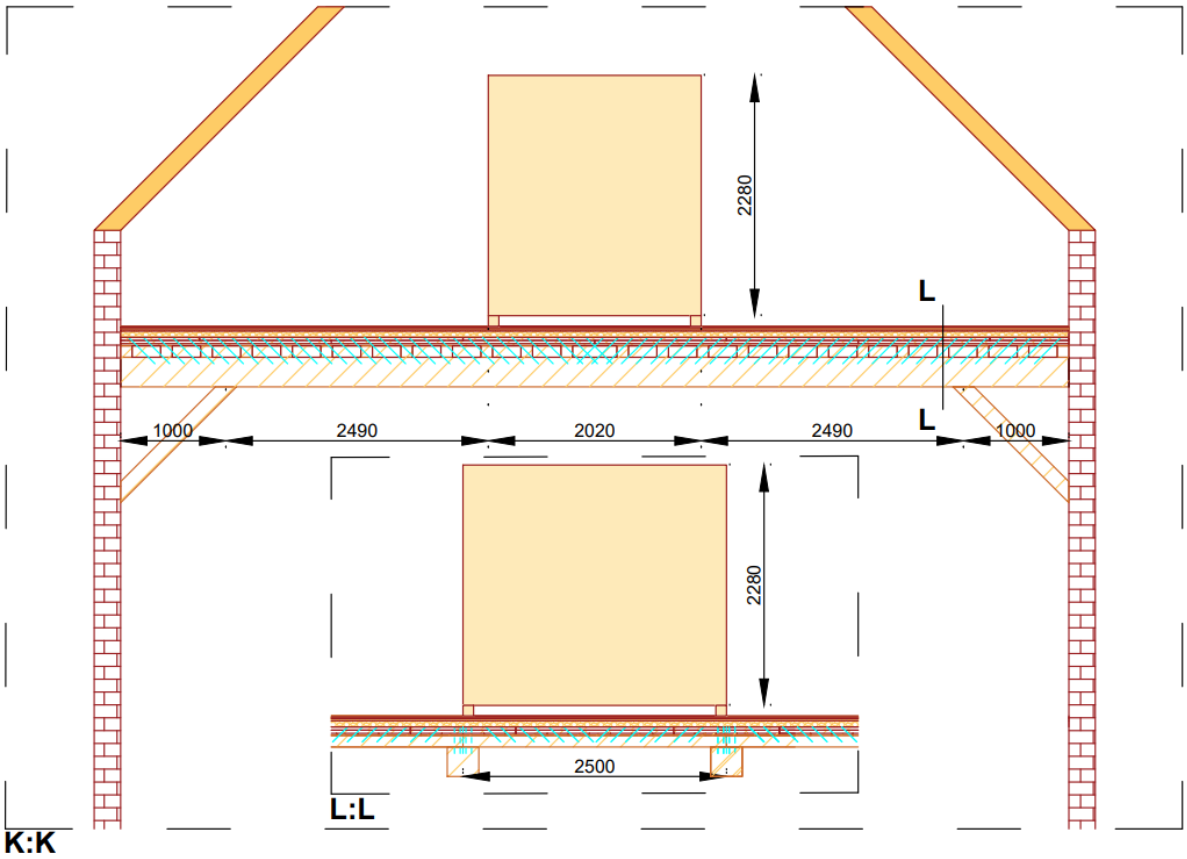

Figure 7.21: Side view of the attic floor after strengthening + acoustic measures

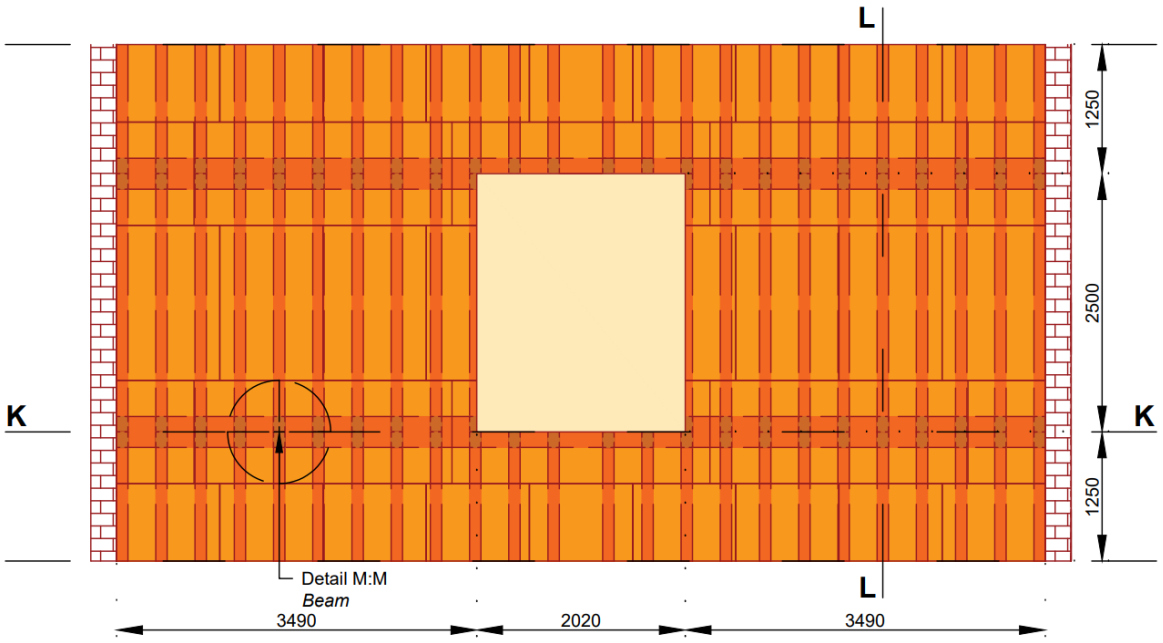

Figure 7.22: Top view of the attic floor after strengthening + acoustic measures

Figure 7.23 illustrates a detail of the floating floor on top of the existing floor. It is evident that a large increase in the height on top of the existing floor is necessary to achieve the strength and acoustic requirements.

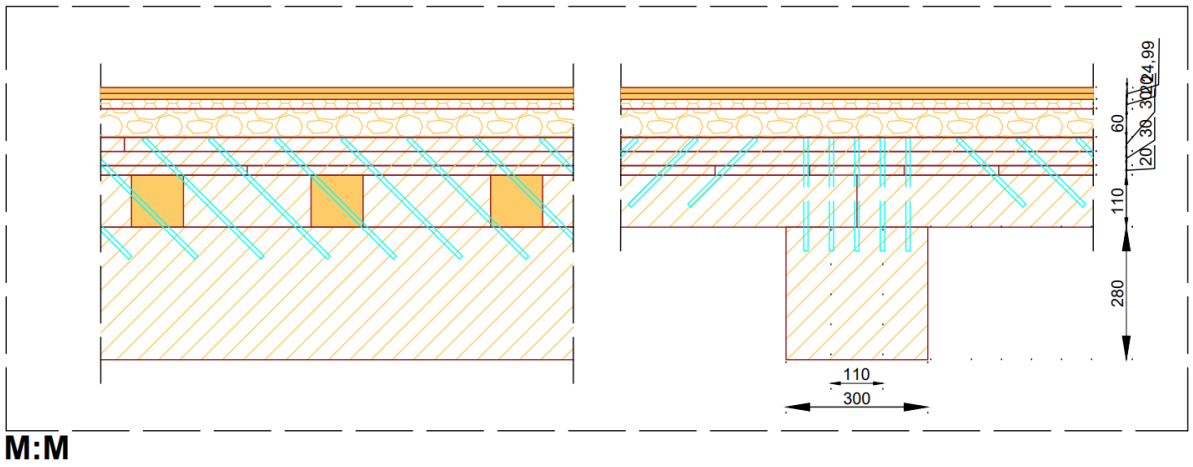

Figure 7.23: Detail M:M of Figure 7.22, strengthened beam + floating floor

7.4.1. Total overview

Figures 7.24 and 7.25 summarize the unity checks for bending and deflection, indicating that ULS as well as SLS of the floor are sufficiently strengthened regarding all three elements: planks, joists and beams.

Furthermore, the beam is connected to the strengthening layer by multiple fasteners. This is up to five fasteners at the sections where the shear forces are the highest. Figure 7.26 illustrates the unity checks for these fasteners at the section where the shear forces are the highest and this demonstrates that non these fasteners of only the beam reach their limit.

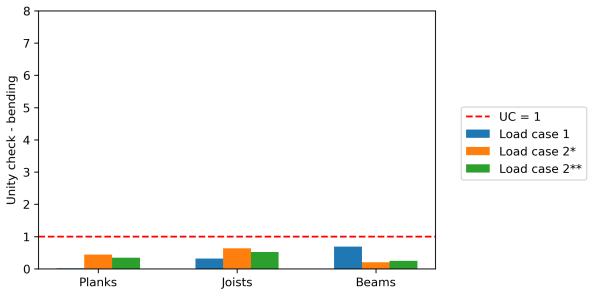

Figure 7.24: Bending stress unity check for both load cases on the attic floor (* $k_{mod} = 0.6$ en ** $k_{mod} = 0.8$)

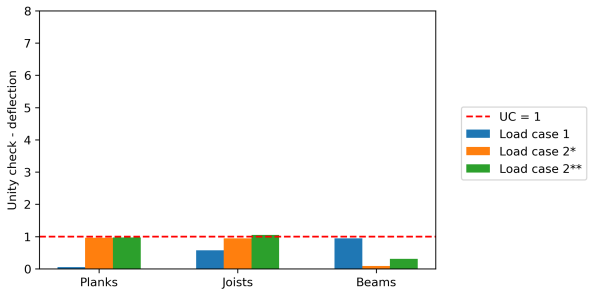

Figure 7.25: Deflection unity check for both load cases on the attic floor (* $k_{mod} = 0.6$ en ** $k_{mod} = 0.8$)

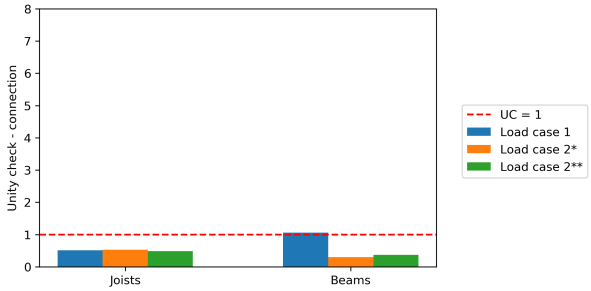

Figure 7.26: Fastener unity check for both load cases on the attic floor (* $k_{mod} = 0.6$ en ** $k_{mod} = 0.8$)

7.4.2. Acoustics

Table 7.13 demonstrates the end values of acoustics properties of the floor. Both airborne as well as structure-borne sound requirements are met. But it must be noted that flanking sounds might become more dominant. Figure 7.27 illustrates the RC-curve after acoustic optimization for the values of the joist. The value RC-11 demonstrates that the requirements are met. However, due to high sound pressure levels in the low frequency range, the sound may still be perceived as a rumble (R).

	R_w $[dB]$		$L_{n,w}$ $[dB]$	
	Joist	Beam	Joist	Beam
After	69	79	61	50

Table 7.13: Acoustic properties due to strengthening in joist and beam direction after acoustic optimization

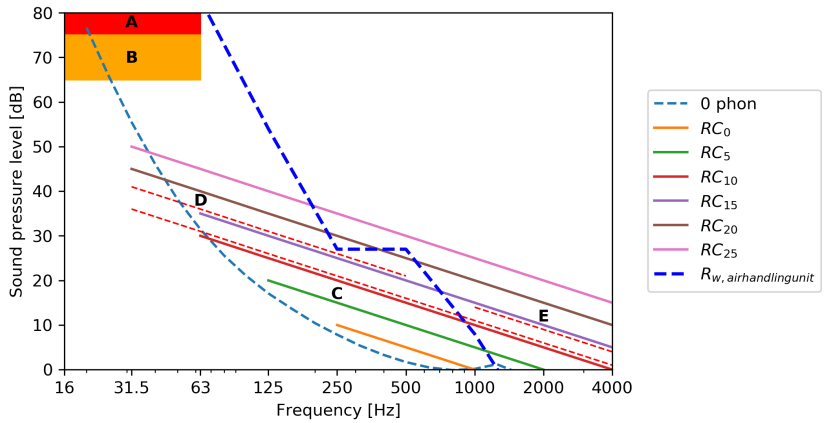

Figure 7.27: RC-curve airborne sound transmitted through the attic floor for the air-handling unit RC-11(R)

IV

Conclusions

8

Discussion

8.1. Validity

This thesis is divided into four parts: theoretical background, methodological framework, results and conclusions. These parts are based on various articles, studies, books, etc. written by researchers who are authoritative in their fields.

The equivalent layer is based on the general laws of physics. The deformation of the plates and fasteners, based on the elastic region, is only to be calculated by Hooke's law. Subsequently, to calculate a mechanically connected system, Möhlers' γ-method was used (Möhler, 1956). The γ-method can only be used with certain conditions. The NEN-EN 1995-1-1 (2011), in addition to the conditions set by Möhler, state that the γ-method can be used with an uniformly distributed load. These conditions prevent reality from being exactly replicated. A more precise alternative is the shear-analogy method which has no limitations regarding the amount of components and the assigned load. However, computer models must be used in order to calculate the fictitious component that includes all the Steiner parts and losses due to shear deformation.

When it comes to calculate the effective stiffness of the system, the connection between the timber components by fasteners has to be determined. The slip modulus in this thesis is based on the research from Betjka, Blaß, Keverinmaki, Roensmaens and Tomasi and the Eurocode 5 (Blaß and Bejtka, 2001, 2003, Blaß and Steige, 2019, Kevarinmäki, 2002, NEN-EN 1995-1-1, 2011, Roensmaens et al., 2020, 2018, Tomasi et al., 2010). The only alternative to determine the slip modulus would be by means of experiments, which are a more precise approach. However, this approach is often costly and time consuming and its outcome generally does not deviate far from the equations for the slip modulus. To verify the mechanically connected system, the Euler-Bernoulli beam model is used. It is stated that if the length to thickness ratio is greater than 10, this model is correct. However, if the ratio is less than 10 the Timoshenko beam theory provides more accurate results. In this thesis the length to thickness ratio was greater than 10. For the case study, the influence of a non-cooperating intermediate layer had to be taken into account for the slip modulus. This factor was determined on the basis of research and experiments by Roensmaens et al. (2020, 2018). This factor reduces multiple shear-planes to a single shear-plane. As using the γ-method only allows a maximum of three components with a constant bending stiffness, this reduction factor had to be implemented. Although its results are considerably accurate, the shear-analogy method would be more precise.

At last, the acoustics for airborne and structure-borne sounds are based on equations from the standards (ISSO-24, 2018, NEN-EN-ISO 12354-1, 2017, NEN-EN-ISO 12354-2, 2017, NEN-EN-ISO 717-1, 2020, NEN-EN-ISO 717-2, 2020). Herein, the coincidence frequency plays a significant part in reducing the airborne sound insulation. This coincidence frequency is determined on laws of physics which are uncertain for bio-based structures like timber beams, since the material properties can vary along its length. In addition, the structure-borne sound transmission is based on equations for homogeneous floor constructions from NEN-EN-ISO 12354-2 (2017). For the orthotropic timber floor structures, the calculated structure-borne sounds transmitted are an overestimation, as demonstrated between the difference of the $L_{n,w}$ values from the case study and the value from the Fermacell floor (Figure 3.16 (A)). Acoustic computer models or experiments would probably provide more accurate acoustic values

for timber floor structures.

8.2. Interpretation

The expectations of this thesis are discussed throughout the theoretical background in Chapter 2 and 3. The parameter study (Chapter 6) and the case study (Chapter 7) present the results regarding the research questions. The main finding is that monumental timber floors can be strengthened by separate timber plates fastened on top of the existing floor to improve their strength and stiffness. However, the acoustic transmission properties are not considerably improved. Therefore, strengthening should be used to apply additional acoustical measures so that the acoustic requirement is met. The result that increasing stiffness by strengthening does not contribute much to acoustic improvement was expected by research from Section 3.6 and by the Subsections 7.2.7 and 7.3.4 from the case study.

Both the parameter and case study demonstrate a few interesting results. According to the parameter study, it is beneficial to strengthen the floor, with as many and as thick plates as possible, as well as with as many and as inclined fasteners as possible. This is supported by the calculation methods for mechanically connected systems in Subsection 2.3.3. However, there is a limit to the thickness of the plates when it comes to large spans (see Figures 6.24 to 6.26). The maximum additional load is limited by the additional weight of the plates. The deflection of the structure's self-weight (including the additional plates) is determined by the stiffness of the beam and not by the stiffness of the effective system. The result that the system therefore cannot bear more load actually gives a biased view. The serviceability requirement does not indicate that the floor will fail, only that it will deflect more than is acceptable. Therefore, an increased load can still be achieved, although the structural engineer must demonstrate that an increased deflection is not seen as relevant. A final essential finding from the parameter study is that reinforcing added layers of timber plates is most efficient on smaller spans (see Figure 6.18). This is supported by the γ-method where for smaller cross-sections relatively more area is added. Furthermore, the results of the case study show that, in addition to the bending stresses and the deflection, the connection between the plates and the beam are decisive for the strength. This corresponds to study of Roensmaens et al. (2018).

8.3. Limitations

The limitations of this study are based on three parts: the calculation method for the equivalent layer (Chapter 4), the verification of the equivalent layer (Chapter 5) and the case study (Chapter 7).

For the equivalent layer, equations are established to determine an effective axial stiffness and an effective moment of inertia. The equations for the axial stiffness (Equation 4.6 to 4.8) are based on the deformation of an equivalent layer. The separate timber plates are approached in a two-dimensional system, where the width of the plates is factored out. The stiffness of the fasteners in width direction (over the effective width of the plate) are added with the factor n_y in these equations. This may be an overestimation, as with large amount of fasteners, not all are equally effective. Overestimating the number of fasteners in the effective width direction will lower the deformation, as the greatest deformation is determined by the fasteners and not the elongation of the plates. Due to this lower deformation, the equivalent modulus of elasticity will be higher, resulting in an overestimation of the effective stiffness of the system. This ultimately leads to lower stresses and strains in the beam. This overestimation implies that the equations may produce more positive results than in reality. In addition, these equations do not include the relative stiffness between the plates and fasteners. This relative stiffness is only important with more than two layers and will become more significant when larger fasteners (diameter>10mm) are used. The exclusion of the relative stiffness leads to higher forces in the stiffer section of force distribution. This results in a lower equivalent modulus of elasticity than in reality. However, the latter limitation is not relevant for the case study at hand because the applied fasteners have a diameter of 9 mm. Furthermore, the equations are based on Hooke's law (Equation 4.2 and 4.3) and the force distribution from MatrixFrame. The deformations obtained by these equations are checked with MatrixFrame. Although the equations are based on physical laws, there is still a limitation due to the fact that the force distribution and verification is done with the same program which is based on a two-dimensional approach.

For the verification of the equivalent layer, the effective stiffness of a beam strengthened by separate timber plates is determined by the γ-method (Subsection 2.3.3). This effective stiffness is used in combination with the Euler-Bernoulli beam theory to determine the stresses and deflections of the

system. These stresses and deflections are compared with a complete model in MatrixFrame (Subsections 5.2.2 and 5.3.2). The MatrixFrame model approximates the system with a two-dimensional perspective by modelling it as a beam connected to multiple beams which are the separate timber plates. In general, models tend to simplify reality. Therefore, beneficial planar effects regarding load distribution over multiple elements are not taken into account in a two-dimensional model. This limitation leads to a higher stresses in the elements of the system. In addition, loads can only be applied to the fastener to prevent deformation of the top element. This is different from the load application in the Euler-Bernoulli beam theory used for the stresses and deflections and could cause deviations between the two models when a lower amount of fasteners are used. A last limitation regarding the verification of the equivalent layer, is that the verification is based on a fixed plate size, beam length and amount of fasteners. The influence of the plate size in relation to the beam length has only been considered for one other option (Section 5.4). This demonstrates that using a larger plate length in relation to the beam length, has a conservative effect when using the equations. This implies that the equations may produce more positive results than in reality when using a small plate length in relation to the beam length. In addition, using more fasteners decreases the implication regarding a smaller plate length.

For the case study (Chapter 7), the strengthening layer was applied to an existing floor in the Prinsenhof Museum in Delft. The intermediate layer was considered not to contribute to the stiffness of the section and has a negative effect on the slip modulus between the beam and equivalent layer. This negative effect is extrapolated as a factor from experiments of Roensmaens et al. (2020). The negative effect of an intermediate layer up to 100 mm on a fastener under 45 degrees can be estimated with some accuracy. However, when applying fasteners under a different angle or an intermediate layer larger than 100 mm, the negative effect of the intermediate layer contains uncertainty. The reduction factor used in this thesis is a conservative value which could result in an underestimated effective stiffness of the system.

8.4. Implication

This thesis has one main implication: the indirect sound paths (flanking). Improving the acoustics sound insulation through strengthening and additional acoustic measures might cause the indirect acoustic paths (flanking) to become more dominant.

9

Conclusion and recommendations

Timber floors have two main challenges: a low stiffness which results in a low load-bearing capacity and a low surface mass which results in a low acoustic sound insulation. This thesis aims to offer structural engineers, to make a factual choice in an early design stage for using a reversible strengthening technique on a monumental timber floor preserving its original appearance. This strengthening technique is verified for strength, stiffness and acoustics, both airborne and structure-borne sound transmission. First, a general conclusion in given on the main research question, after which all sub-questions will be briefly answered.

9.1. Main research question

For convenience, the research question is repeated here:

"What is the influence on the strength, stiffness and acoustic properties of monumental timber floors by strengthening them with multiple layers of plates fastened on top of the existing floor?"

Monumental timber floors can consist of three components: planks, joists and beams. Timber components with smaller spans and small centre-to-centre distances are normative for concentrated loads, while timber components with larger spans and large centre-to-centre distances are normative for distributed loads. Therefore, the load case determines which of these three components should be considered normative and thus strengthened. The planks are often the most significant because of their small cross-section. However, the case study demonstrated that applying additional layers of timber plates in the direction of the joist or beams provide considerate strengthening of the planks. The strengthening layer ensures a continuous layer in its applied direction, which absorbs parts of the tensile or compressive stresses. This effectively reduces the stresses in the reinforced components.

Whereas the non-strengthened monumental timber floor used to be normative on bending stresses and deflection, the reinforced floor becomes normative on the connection (between the additional layers and the reinforced component) and the deflection. A significant limitation of this strengthening technique is the finite number of fasteners that can be applied in an existing element due to the minimum distances between fasteners and edge distance. Furthermore, it is important to limit deflections by supporting and propping the floor during the reinforcement process.

Reinforcing the floor with multiple layers of timber plates fastened on top of the existing floor increases the mass and stiffness. While a doubling of mass results in a doubling of stresses and deflections, this doubling only provides a +6dB improvement in airborne sound insulation and a -4dB improvement in structure-borne sound transmitted. Furthermore, a doubling of stiffness results in a halving of stresses and deflections, but only provides a +2dB improvement in airborne sound insulation and a -1.5dB improvement in structure-borne sound transmitted. Consequently, strengthening a monumental timber floor does not significantly improve its acoustic properties. If acoustic requirements are to be met, additional measures must be applied. For monumental timber floors, this will often be a dry floating floor because of its reversibility. However, dry floating floors only add mass and do not increase stiffness, which will reduce the maximum load on the floor.

9.2. Sub-questions

9.2.1. Key parameters and their influence

Sub-question 1: *"What are the key parameters for structural assessment of monumental timber floors and how do they influence the structural assessment?"*

Structural assessment of monumental timber floors is reliable on three fixed parameters: dimension, grade and load. The dimensions of each component result in bending stiffness and stress distribution. Due to different spans and centre-to-centre distances, different loads (concentrated or distributed) are normative. Strengthening by applying additional timber layers is more effective for smaller cross-section due to its relative axial stiffness. The grade of the timber determines the magnitude of stresses the component can sustain. Higher strength classes allow for a higher maximum stress. The load which is applied to the floor, results in the magnitude of stresses which the components should bear.

Sub-question 2: *"What are the important parameters for sound transmission through monumental timber floors and how do they influence the sound insulation?"*

Sound transmission through floors is defined by four categories: airborne sounds, structure-borne sounds, flanking sounds and sound leaks. Flanking sounds and sound leaks where excluded in this thesis. Airborne as well as structure-borne sounds are influenced by three important parameters: mass, cross-sectional dimensions (stiffness) and room dimensions.

Airborne sounds are influenced by the mass law, coincidence frequency, radiation factor and internal damping. The higher the mass, the bigger the insulation from the mass law which results in a greater airborne sound insulation. The coincidence frequency is the region where the airborne sound is not insulated. When the mass increases, the coincidence frequency increases and when the stiffness increases, the coincidence frequency decreases. The coincidence frequency could be negative or positive, depending on the created coincidence frequency, because the sound is not insulated at that region. The radiation factor is influenced by the coincidence frequency and determines is sounds are radiated. The internal damping is influenced by the mass. The higher the mass, the higher the internal damping which results in a higher airborne sound insulation.

Structure-borne sounds are influenced by mass law, radiation factor, driving-point mobility and reverberation time. The higher the mass, the bigger the insulation from the mass law which results in a lower structure-borne sound transmission. The higher the mass and the higher the stiffness, the lower the driving-point mobility which results in a lower structure-borne sound transmission. The bigger the room dimensions, the higher the reverberation time which results in a higher structure-borne sound transmission.

Sub-question 4: *"What are the key parameter that influence the strengthening configuration and how do they influence the strength, stiffness and sound transmission properties of monumental timber floors?"*

The strengthening configuration has two key parameters which influence the strength, stiffness and sound transmission properties of monumental timber floors: plates and fasteners. The additional timber plates bear a part of the stresses from the reinforced components. The more layers and/or thicker the plates, the higher the effective stiffness of the system and the lower the stresses in the individual components. However, more layers and/or thicker plates result in a larger deflection of the structure of self-weight. This deflection is reduced when the additional strengthening layers are applied on a propped structure. More layers and/or thicker plates result in a higher mass and a higher stiffness. Both increase the airborne sound insulation and decrease the structure-borne sound transmitted.

The connection between the reinforced components and the additional timber plates is of great importance. This connection determines the cooperation between the individual components. A stiff connection results in a high cooperation and reduces stresses in the reinforced components. However, the forces on a stiffer connection are higher and thus its limits are reached sooner. A stiffer connection is created with more fasteners and/or more inclined fasteners which increases the stiffness of the system, therefore increasing the airborne sound insulation and decreasing the structure-borne sound transmission.

9.2.2. Calculations with additional timber layers

Sub-question 3: *"How can multiple layers of separate timber plates which are fastened on top of the existing beam, be incorporated into the stiffness calculations and how can this be validated?"*

In order to incorporate the separate timber plates in the effective stiffness calculation (γ-method), these plates should be translated to an equivalent layer. Equations 9.1, 9.2 and 9.3 calculate the deformation of a segment of plates on which the axial stiffness of the equivalent layer is based. These equations are based on the distribution of forces between the plates and connections, but exclude their relative stiffness. Since the fasteners are relatively not rigid compared to the plates, they account for practically all of the deformation in these equations (the first part). The equations have been verified by 2D-framework software (MatrixFrame).

The stresses, strains and deflections are determined by using the ordinary differential equation (ODE) of the Euler-Bernoulli beam theory. These stresses are verified by MatrixFrame with a complete model of a beam strengthened with separate timber plates. The verification showed deviations of $\pm 4\%$ between the deflection calculated with the ODE's and MatrixFrame. These deviations are generally acceptable because the variation in material properties of timber components is of the same order of magnitude which validates the equivalent layer. Furthermore, the equivalent modulus of elasticity correctly reflect the reduction in stresses in the beam which validates their stresses and strains. Therefore, the method with an equivalent modulus of elasticity is used for the calculation with an equivalent layer.

$$\Delta L_{total,2,plates} = \frac{2F}{n_{fpp} n_y K} + \frac{(n_{fpp} + 1)FL}{n_p n_{fpp} E A_{plate}} \tag{9.1}$$

$$\Delta L_{total,3,plates} = \frac{3F}{4 n_{fpp} n_y K} + \frac{(3n_{fpp} + 1)FL}{2 n_p n_{fpp} E A_{plate}} \tag{9.2}$$

$$\Delta L_{total,4,plates} = \frac{4F}{9 n_{fpp} n_y K} + \frac{(8n_{fpp} + 3)FL}{6 n_p n_{fpp} E A_{plate}} \tag{9.3}$$

9.2.3. Application on a monumental timber floor

Sub-question 5: *"Which aspects should be taken into account when this strengthening technique is to be applied on a monumental timber floor?"*

When using this strengthening technique, the following three aspects must be considered: the direction of the strengthening layer, the fasteners which become normative and the thickness of the non-cooperating intermediate layer. This strengthening technique only reinforces a component in one direction. A floor with two components (joists and beams) must be reinforced in both directions to obtain an effective strengthening. Otherwise, it will not lead to an increase in load-bearing capacity of the floor because the non-reinforced component only gains mass and just a little stiffness. The connection between the equivalent layer and beam will become normative on sections where the shear force is high. This is normative due to the finite amount of fasteners. The non-cooperating intermediate layer has a negative effect on the slip modulus of the fastener. A thicker intermediate layer will decrease the slip modulus and this effect is larger for fasteners which are applied at a smaller angle. This negative effect is counteracted by the increase in distance between the neutral axis of the equivalent layer and the central point of gravity of the system.

9.3. Recommendations

For further research the following is recommended:

- **Non-cooperating intermediate layer**
  This thesis suggested to use a factor, determined from Roensmaens' research, to convert the multiple shear planes into a single shear plane. Roensmaens et al. (2020) As a result, the slip modulus for this shear plane is reduced. This assumption is based on only three experimental values. It may therefore be useful to further investigate the influence of a non-cooperating intermediate layer on the slip modulus and whether applying a factor for substituting multiple shear planes with one shear plane is correct.

- **Equivalent layer**
  There are two limitations to the equivalent layer method that are interesting for further research: the effective number of fasteners in width direction and the relative stiffness between joint and plate. Both limitations could lead to a higher or lower equivalent stiffness which tend to lead to an over- or underestimation of the strength, stiffness and acoustic properties. A three-dimensional model is suggested to further investigate these limitations.

- **Bi-directional overlapping of plates**
  The strengthening technique is only aimed in one direction. It can therefore be meaningful to investigate further into placing the plates overlapping each other in two directions. In order to get a deeper knowledge in the planar effect.

- **Comparison to other strengthening techniques**
  For this study, only one type of reinforcement technique was considered. Further investigation into different strengthening techniques comparing them on effectiveness, reversibility, costs and sustainability would assist the structural engineer, in making a factual choice in an early design stage.

- **Flanking and leaks**
  If the floor is reinforced and acoustically improved, the flanking paths will become more dominant. Thus, it is important to investigate the influence of the strengthening technique on the flanking paths. These flanking paths will play a major role for airborne sound insulation. Structure-borne sound transmission due to flanking paths could be avoided by isolating the floating floor towards the wall.

Bibliography

Arêde, A. and Varum, H. (2008). *Strengthening and Retrofitting of Existing Structures*. Springer.

Bejtka, I. and Blaß, H. J. (2002). Joints with inclined screws. In *Proceedings of: meeting thirty-five of the international council for building research studies and documentation, CIB, Working Commission W18–Timber Structure*.

Blaß, H. J. and Bejtka, I. (2001). Screws with continuous threads in timber connections. In *RILEM Proceedings PRO*, volume 22, pages 193–202.

Blaß, H. J. and Bejtka, I. (2003). Verbindungen mit geneigt angeordneten schrauben. *Bauen mit Holz*, 105(10):68–85.

Blaß, H. J. and Steige, Y. (2019). *Steifigkeit axial beanspruchter Vollgewindeschrauben*, volume 34. KIT Scientific Publishing.

Bujoreanu, C. and Benchea, M. (2016). Experimental study on hvac sound parameters. In *IOP Conference Series: Materials Science and Engineering*, volume 147, page 012051. IOP Publishing.

Caniato, M., Bettarello, F., Fausti, P., Ferluga, A., Marsich, L., and Schmid, C. (2017). Impact sound of timber floors in sustainable buildings. *Building and Environment*, 120:110 – 122.

Cemfloor (2018). Installation of Cemfloor Screed. [Online; accessed 10-Februari-2022].

Cointe, A., Castéra, P., Morlier, P., and Galimard, P. (2007). Diagnosis and monitoring of timber buildings of cultural heritage. *Structural Safety*, 29(4):337 – 348. Probabilistic Concepts in the Design of Timber Structures.

Corradi, M., Osofero, A. I., and Borri, A. (2019). Repair and reinforcement of historic timber structures with stainless steel—a review. *Metals*, 9(1):106.

Cremer, L., Heckl, M., and Ungar, E. (1974). *Structure-borne sound*. Springer.

de Vries, P. D. I. D. (2020). Central Government Real Estate Agency. private communication.

DPA microphones (n.d.). Facts about speech intellligibility. [Online; accessed 16-August-2021].

Drs. W.F. Gard (2018). Engineered wood products. [Brightspace; accessed 26-April-2021].

Engineering & Consulting P.C., X. (2017). Bolted connections are not as simple as they seem. [Online; accessed 28-Oktober-2021].

Fermacell (2012). Plaques de sol en plâtre armé de fibres fermacell - catalogue pour éléments de construction. [Online; accessed 10-Februari-2022].

Franke, S., Franke, B., and Harte, A. M. (2015). Failure modes and reinforcement techniques for timber beams–state of the art. *Construction and Building Materials*, 97:2–13.

Frese, M. and Blaß, H. J. (2011a). Schadensanalyse von hallentragwerken aus holz. *DIBt Mitteilungen*, 42(1):25–25.

Frese, M. and Blaß, H. J. (2011b). Statistics of damages to timber structures in germany. *Engineering Structures*, 33(11):2969–2977.

Hopkins, C. (2020). *Sound insulation*. Routledge.

Hyper Physics (n.d.). Equal Loudness Curves. [Online; accessed 20-August-2021].

Ir. C.J. Janssen (2019). Building Acoustics. [Brightspace; accessed 28-April-2021].

ISSO-24 (2018). Installatiegeluid. *ISSO Kennisinstituut Bouw- en Installatietechniek*.

Joachim Blaß, H. and Sandhaas, C. (2017). *Timber Engineering - Principles for Design*. KIT Scientific Publishing, Place of publication not identified.

Jong, M. (2018). Bachelor Eindwerk Mechanisch verbonden liggers modelleren in MatrixFrame. Technische Universiteit Delft.

Joostdevree.nl (n.d.). Zwevende dekvloer; zwevende vloer. [Online; accessed 10-Februari-2022].

Kevarinmäki, A. (2002). Joints with inclined screws. cib-w18. Technical report, paper 35-7-3, Kyoto, Japan.

Kouroussis, G., Ben Fekih, L., and Descamps, T. (2017). Assessment of timber element mechanical properties using experimental modal analysis. *Construction and Building Materials*, 134:254 – 261.

Linville, J. D. et al. (2012). *Timber construction manual*. John Wiley & Sons.

Ljunggren, F., Simmons, C., and Hagberg, K. (2014). Correlation between sound insulation and occupants' perception – proposal of alternative single number rating of impact sound. *Applied Acoustics*, 85:57 – 68.

Martins, C., Santos, P., Almeida, P., Godinho, L., and Dias, A. (2015). Acoustic performance of timber and timber-concrete floors. *Construction and Building Materials*, 101:684 – 691.

Mestawood (2015). Metsä Wood structural birch plywood (PF). [Online; accessed 10-Janurai-2022].

Möhler, K. (1956). Über das tragverhalten von biegeträgern und druckstäben mit zusammengesetzten querschnitten und nachgiebigen verbindungsmitteln.

Mulder, M. (2019). Bachelor Eindwerk Verificatieregels mechanisch verbonden ligger met meer dan 3 delen. Technische Universiteit Delft.

Museum Prinsenhof Delft (n.d.). Historie van het gebouw. [Online; accessed 31-May-2021].

NEN 1070 (1999). Noise control in buildings – Specification and rating of quality. *CEN, Brussels, Belgium*.

NEN 8700 (2020). Assessment of existing structures in case of reconstruction and disapproval - Basic rules. *CEN, Brussels, Belgium*.

NEN-EN 14081-1 (2016). Timber structures - Strength graded structural timber with rectangular cross section - Part 1: General requirements. *CEN, Brussels, Belgium*.

NEN-EN 1990 (2002). Eurocode: Basis of structural design. *CEN, Brussels, Belgium*.

NEN-EN 1995-1-1 (2011). Eurocode 5: Design of timber structures - Part 1-1: General - Common rules and rules for buildings. *CEN, Brussels, Belgium*.

NEN-EN 384 (2018). Structural timber - Determination of characteristic values of mechanical properties and density. *CEN, Brussels, Belgium*.

NEN-EN-ISO 12354-1 (2017). Building acoustics - Estimation of acoustic performance of buildings from the performance of elements - Part 1: Airborne sound insulation between rooms. *CEN, Brussels, Belgium*.

NEN-EN-ISO 12354-2 (2017). Building acoustics - Estimation of acoustic performance of buildings from the performance of elements - Part 2: Impact sound insulation between rooms. *CEN, Brussels, Belgium*.

NEN-EN-ISO 338 (2016). Structural timber - Strength classes. *CEN, Brussels, Belgium*.

NEN-EN-ISO 717-1 (2020). Acoustics - Rating of sound insulation in buildings and of building elements - Part 1: Airborne sound insulation. *CEN, Brussels, Belgium*.

NEN-EN-ISO 717-2 (2020). Acoustics - Rating of sound insulation in buildings and of building elements - Part 2: Impact sound insulation. *CEN, Brussels, Belgium*.

Plyterra Group (n.d.). Sizes and number of layers. [Online; accessed 10-Janurai-2022].

Roensmaens, B., Avez, C., Parys, L. V., and Descamps, T. (2020). Refurbishment of timber floors with screwed clt panels: Tests on floor elements and connections. *International Journal of Architectural Heritage*, 0(0):1–15.

Roensmaens, B., Parys, L. V., Carpentier, O., and Descamps, T. (2018). Refurbishment of existing timber floors with screwed clt panels. *International Journal of Architectural Heritage*, 12(4):622–631.

Roonasi, P. (2003). *Sound quality evaluation of floor impact noise generated by walking*. Lulea University of Technology.

Rothoblaas (n.d.). Full threaded screw with cylindrical head: Vgz. [Online; accessed 10-Janurai-2022].

Schelling, W. (1982). Zur berechnung nachgiebig zusammengesetzter biegeträger aus beliebig vielen einzelquerschnitten. *Ingenieurholzbau in Forschung und Praxis. Karlsruhe: Bruderverlag*.

Schlotzhauer, P., Wilhelms, F., Lux, C., and Bollmus, S. (2018). Comparison of three systems for automatic grain angle determination on european hardwood for construction use. *European journal of wood and wood products*, 76(3):911–923.

Schmid, J., König, J., and Köhler, J. (2010). Fire-exposed cross-laminated timber–modelling and tests. In *World Conference on Timber Engineering*.

Sewell, E. (1970). Transmission of reverberant sound through a single-leaf partition surrounded by an infinite rigid baffle. *Journal of Sound and Vibration*, 12(1):21–32.

The Engineering Toolbox (n.d.a). NC - Noise Criterion. [Online; accessed 23-August-2021].

The Engineering Toolbox (n.d.b). RC - Room Criteria. [Online; accessed 24-August-2021].

The Engineering Toolbox (n.d.c). Wood, panel and structural timber products - mechanical properties. [Online; accessed 01-September-2021].

Tomasi, R., Crosatti, A., and Piazza, M. (2010). Theoretical and experimental analysis of timber-to-timber joints connected with inclined screws. *Construction and building materials*, 24(9):1560–1571.

Vigran, T. (2008). Room acoustics. *Building acoustics. Taylor & Francis*, pages 103–151.

Whale, L. and Smith, I. (1986). *Mechanical timber joints*. TRADA High Wycombe, UK.

Wikimedia Commons (2005). File:Fraxinus excelsior crosssection.jpg. [Online; accessed 17-Januari-2022].

Wikimedia Commons (2020). File:Deck beam dry rot.jpg. [Online; accessed 17-Januari-2022].

Wikipedia, The Free Encyclopedia (2005). A-weighting. [Online; accessed 4-May-2021].

Wikipedia, The Free Encyclopedia (n.d.). Monumentenzorg. [Online; accessed 12-December-2021].

Zeeuwse Jongens architecten (2019). Museum Prinsenhof - Delft. [Online; accessed 31-May-2021].

Österreichisches Institut für Bautechnik (2012). ETA-12/0062 SFS self-tapping screws WR. [Online; accessed 10-Janurai-2022].

List of Figures

List of Tables

V

Appendices

A

Extra equations

Equations used for strength and stiffness calculations

Bending moment

$$M_{yd} = \frac{1}{8} \cdot q_{ed} \cdot l^2$$
$$\sigma_{md} = \frac{M_{yd} \cdot 0.5h}{I_y}$$
$$f_{md} = \frac{k_{mod} \cdot k_h \cdot f_{mk}}{\gamma_m}$$
$$UC_{bending} = \frac{\sigma_{md}}{f_{md}}$$

Shear

$$V_{yd} = \frac{1}{2} \cdot q_{ed} \cdot l$$
$$\tau_{md} = \frac{2 \cdot V_{yd}}{3 \cdot A}$$
$$f_{vd} = \frac{k_{mod} \cdot f_{vk}}{\gamma_m}$$
$$UC_{shear} = \frac{\tau_{md}}{f_{vd}}$$

Compression perpendicular to the grain

$$\sigma_{c,90,md} = \frac{V_{yd}}{A_{ef}}$$
$$f_{c,90,d} = \frac{k_{mod} \cdot k_{c,90} \cdot f_{c,90,k}}{\gamma_m}$$
$$UC_{shear} = \frac{\sigma_{c,90,md}}{f_{c,90,d}}$$

Deflection

$$w_{Permanent} = \frac{5 \cdot G_k \cdot L^4}{384 \cdot E \cdot I_y}$$

$$w_{Variable} = \frac{5(Q_1 + \sum Q_i \cdot \psi_{0,i})L^4}{384 \cdot E \cdot I_y}$$

$$w_{Creep} = \frac{5 \cdot k_{def}(G_k + \sum Q_i \cdot \psi_{2,i})L^4}{384 \cdot E \cdot I_y}$$

$$w_{First} = w_{Variable} + w_{Creep}$$

$$w_{End} = w_{First} + w_{Permanent}$$

$$UC_{First} = \frac{w_{First}}{0.003 \cdot L}$$

$$UC_{End} = \frac{w_{End}}{0.004 \cdot L}$$

Equation for two and four hinged supports systems

The floors supported on masonry walls can be schematised as a beam with hinged supports see the left system in Figure A.1 and floors which have corbel pieces as a continuous beam on four supports see the right system in Figure A.1

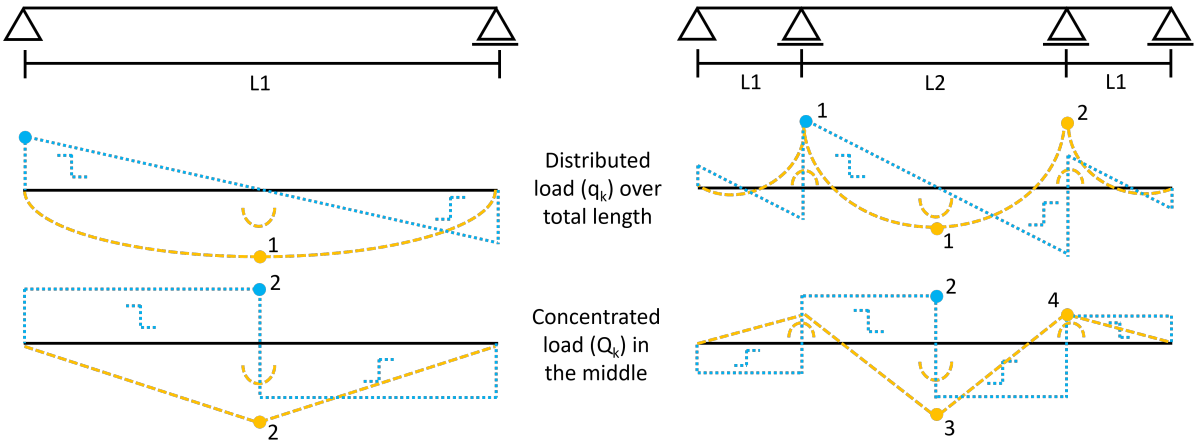

Figure A.1: Schematization for (Left) a simply supported system and (Right) a continuous system on four supports

These systems are loaded by self-weight and can be additionally loaded by a distributed or a concentrated load. To determine the maximum moment and shear force of the system the following Equations can be used if the total floor is loaded with a distributed load (DL) or a concentrated load (DL) is present in the middle of the system.

Equations for a simply supported (SS) system (q_k over the whole system; Q_k on $0.5L_1$):

$$V_{1-(SS,DL)} = 0.5 q_k L_1 \tag{A.1}$$

$$M_{1-(SS,DL)} = 0.125 q_k L_1^2 \tag{A.2}$$

$$V_{2-(SS,CL)} = 0.5 Q_k \tag{A.3}$$

$$M_{2-(SS,CL)} = 0.25 Q_k L_1 \tag{A.4}$$

Equations for a continuous system (CS) on four supports (q_k over the whole system; Q_k on $0.5L_2$):

$$V_{1-(CS,DL)} = 0.5 q_k L_2 \tag{A.5}$$

$$M_{1-(CS,DL)} = \frac{-q_k(L_1^3 - L_1 L_2^2 - 0.5L_2^3)}{8L_1 + 12L_2} \; and \; M_{2-(CS,DL)} = \frac{-q_k(L_1^3 + L_2^3)}{8L_1 + 12L_2} \tag{A.6}$$

$$V_{2-(CS,CL)} = 0.5Q_k \tag{A.7}$$

$$M_{3-(CS,CL)} = \frac{(L_1L_2 - 0.5L_1L_2 + 0.75L_2^2 - 0.375L_2^2)Q_k}{2L_1 + 3L_2} \; and \; M_{4-(CS,CL)} = \frac{-3Q_kL_2^2}{16L_1 + 24L_2} \tag{A.8}$$

Where:

V	Shear force	kN
M	Moment	kNm
L_1	Length between supports	m
L_2	Length between supports	m
q_k	distributed load	kN/m
Q_k	concentrated load	kN

B

Non-cooperating intermediate layer

Experiments from Roensmaens et al. (2020) are used to determine the influence of a non-cooperating intermediate layer.

Factor according to the push-out tests

The push-out tests demonstrated in Figure B.1, resulted in the mean slip modulus values shown in Table B.1. The factor determined in Table B.1 for the increasing height of the gap, is curve fitted as seen in Figure 2.18. Between the points, the exponential and parabolic curve are representative. But after the 100 mm gap, the exact effect cannot be guaranteed with certainty.

	Mean slip modulus $[kN/mm]$	**Factor** $\frac{Configuration_i}{Configuration_1}$ **[–]**
Configuration 1	43.25	1.00
Configuration 2	29.98	0.69
Configuration 3	24.61	0.57

Table B.1: Push-out tests from Roensmaens et al. (2020)

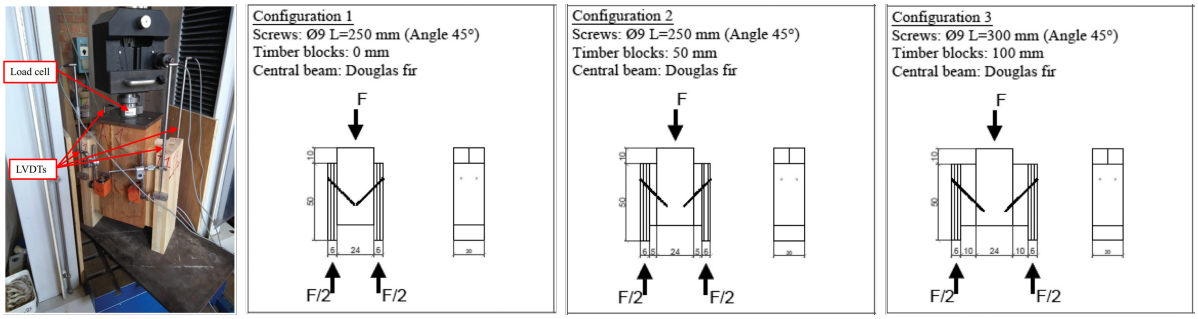

Figure B.1: Push-out tests from Roensmaens et al. (2020)

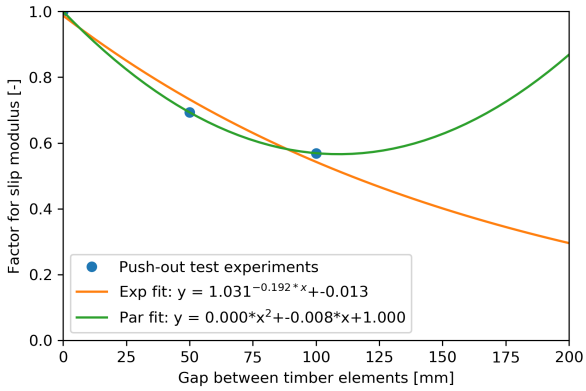

Figure B.2: Factor for slip modulus for increasing gap, from push-out tests from Roensmaens et al. (2020)

Factor according to the bending tests

The bending tests demonstrated in Figure B.3, resulted in the mean apparent bending stiffness shown in Table B.1. With the γ-method, using one- or two shear-planes, the mean slip modulus can be determined.

	Mean maximum load [kN]	**Mean apparent bending stiffness [kNm^2]**
Configuration 1	84.99	932.49
Configuration 2	91.65	1198.31
Configuration 3	119.57	1980.47

Table B.2: Bending tests from Roensmaens et al. (2020)

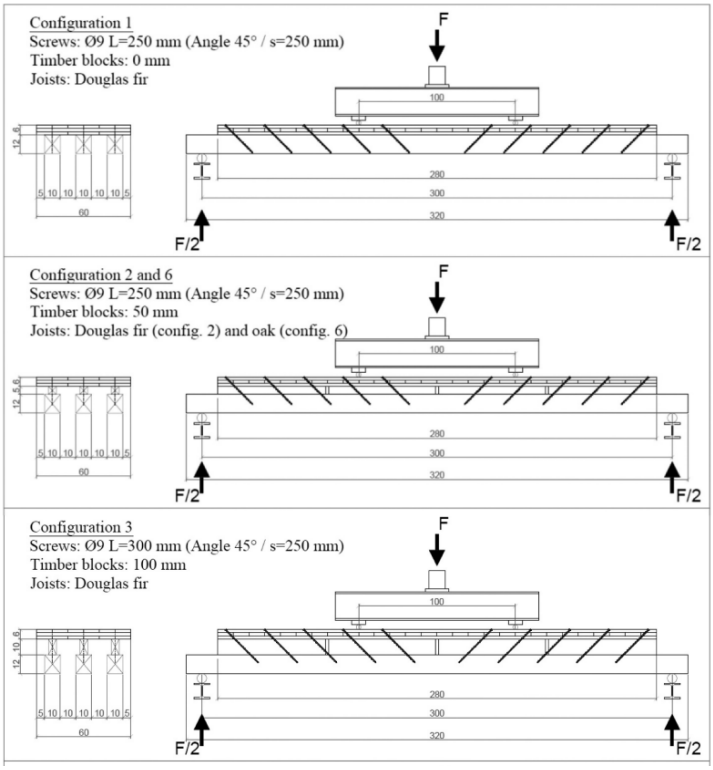

Figure B.3: Bending tests set-up from Roensmaens et al. (2020)

One shear-plane

One shear-plane can be used for the determination of the slip modulus of configuration 1 with certainty. For configuration 2 and 3 the decrease in slip modulus is expected. The Maple script of Figure B.4 is used to calculate the mean slip modulus of Table B.3.

	Mean slip modulus $[kN/mm]$	**Factor** $\frac{Configuration_i}{Configuration_1}$ **[–]**
Configuration 1	8.24	1.00
Configuration 2	*4.46*	*0.54*
Configuration 3	*5.29*	*0.64*

Table B.3: Mean slip modulus for one shear-plane

```
restart;
bclt := 200 : hclt := 60 : bbeam := 100 : hbeam := 120 : Eclt := 7400 : Ebeam := 9236 : L := 3000 : s := 250 :
gap := 50 :
Iclt := 1/12 · bclt · hclt^3;
Ibeam := 1/12 · bbeam · hbeam^3;
Aclt := bclt · hclt;
Abeam := bbeam · hbeam;
gamma1 := 1 / (1 + Eclt · Aclt · s · Pi^2 / (K · L^2)); evalf(gamma1);
gamma2 := 1 :
a2 := (gamma1 · Eclt · Aclt · (0.5 · (hclt + hbeam) + gap)) / (gamma1 · Eclt · Aclt + gamma2 · Ebeam · Abeam); evalf(a2);
a1 := (0.5 · (hclt + hbeam) + gap) − a2; evalf(a1);
K := solve(3 · (Eclt · Iclt + gamma1 · Eclt · Aclt · a1^2 + Ebeam · Ibeam + gamma2 · Ebeam · Abeam · a2^2) = 1198.31 · 10^9);
```

Figure B.4: Maple script for solving the slip modulus for one shear-plane

With the equations for the slip modulus explained in Sub-subsection 2.3.2, the slip modulus can be determined. Using the maple script shown in Figure B.5 gets a slip modulus of 7.3 kN/mm for the fastener under 45 degrees on one shear-plane. Due to assumptions which could differ from the experiment this value could be lower than the mean slip modulus of configuration 1 as demonstrated in Table B.3.

```
restart;
bclt := 200 : hclt := 60 : bbeam := 100 : hbeam := 120 : gap := 0 : Eclt := 7400 : Ebeam := 9236 : L := 3000 : s := 250 :
Iclt := 1/12 · bclt · hclt^3;
Ibeam := 1/12 · bbeam · hbeam^3;
rhoclt := 420 : rhobeam := 490 : d := 9 : angle := 45 :
ld := 250 :
ldclt := evalf(hclt / cos(angle · Pi / 180));
ldbeam := ld − ldclt - evalf(gap / cos(angle · Pi / 180));
Kv := ((rhoclt · rhobeam)^0.5)^1.5 · d / 23;
Kaxclt := 2 · d^0.6 · ldclt^0.6 · rhoclt^0.9;
Kaxbeam := 2 · d^0.6 · ldbeam^0.6 · rhobeam^0.9;
Kax := 1 / (1/Kaxclt + 1/Kaxbeam);
Ksertot := (Kv · cos(angle · Pi / 180)) · (cos(angle · Pi / 180) − 0.25 · sin(angle · Pi / 180)) + Kax · sin(angle · Pi / 180) · (sin(angle · Pi / 180) − 0.25 · cos(angle · Pi / 180));
```

Figure B.5: Maple script for solving the slip modulus for one shear-plane

Two shear-planes

Two shear-planes can only be used for configuration 2 and 3. Two shear-plane can be used for the determination of the slip modulus of configuration 2 and 3 with certainty. For configuration 1 the decrease in slip modulus is expected. The Maple script of Figure B.6 is used to calculate the mean slip modulus of Table B.4.

	Mean slip modulus [kN/mm]	Factor $\frac{Configuration_i}{Configuration_1}$ [–]
Configuration 1	*16.49*	*1.00*
Configuration 2	8.92	0.54
Configuration 3	10.58	0.64

Table B.4: Mean slip modulus for one shear-plane

```
restart;
bclt := 200 : hclt := 60 : bbeam := 100 : hbeam := 120 : Eclt := 7400 : Ebeam := 9236 : L := 3000 : s := 250 :
gap := 50 :
Iclt := 1/12 · bclt · hclt^3;
Ibeam := 1/12 · bbeam · hbeam^3;
Aclt := bclt · hclt;
Abeam := bbeam · hbeam;
gamma1 := 1 / (1 + Eclt · Aclt · s · Pi^2 / (K · L^2)) : gamma1 := evalf(gamma1);
gamma2 := 1 :
gamma3 := 1 / (1 + Ebeam · Abeam · s · Pi^2 / (K · L^2)) : gamma3 := evalf(gamma3);
a2 := (gamma1 · Eclt · Aclt · (0.5 · (hclt + gap)) − gamma3 · Ebeam · Abeam · (0.5 · (hbeam + gap))) / (gamma1 · Eclt · Aclt + gamma3 * Ebeam · Abeam) : a2 := evalf(a2);
a1 := (0.5 · (hclt + gap)) − a2 : a1 := evalf(a1);
a3 := (0.5 · (hbeam + gap)) + a2 : a3 := evalf(a3);
K := solve(3 · (Eclt · Iclt + gamma1 · Eclt · Aclt · a1^2 + Ebeam · Ibeam + gamma3 · Ebeam · Abeam · a3^2) = 1198.31 · 10^9);
```

Figure B.6: Maple script for solving the slip modulus for two shear-planes

Compare stresses and stains between one and two-shear-planes

Figures B.7 to B.12 compare the stresses and strains between one and two shear-planes for 0mm, 50mm an 100mm gap. The neutral axis is taken for that of one shear-plane. With both methods the stresses and strains match perfectly.

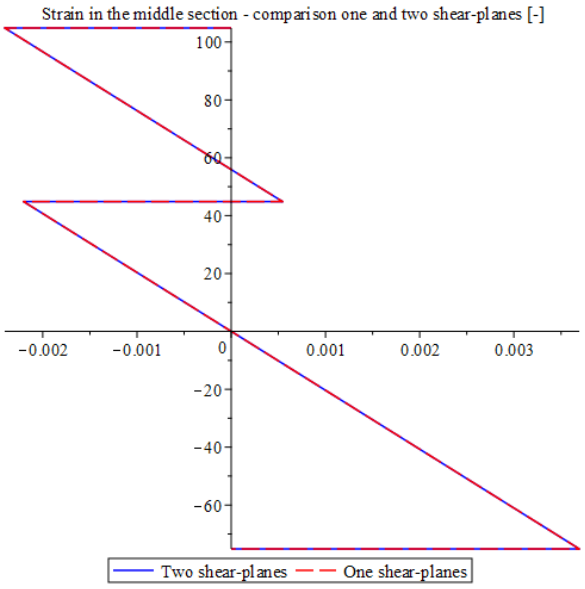

Figure B.7: Comparison of strains, 0mm gap, between one and two shear-planes

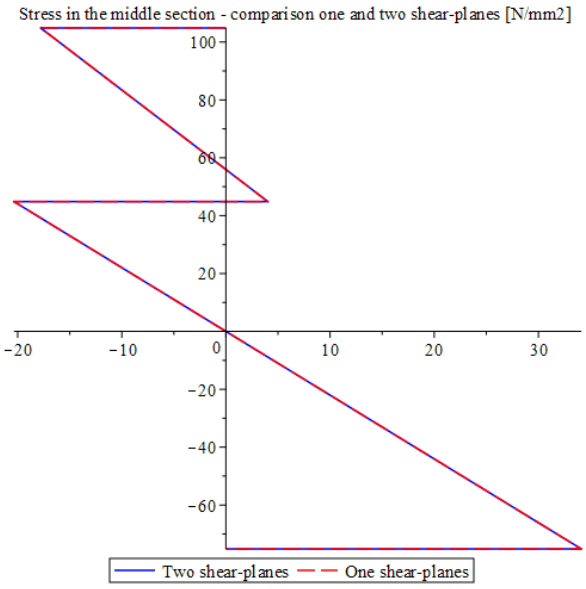

Figure B.8: Comparison of stress, 0mm gap, between one and two shear-planes

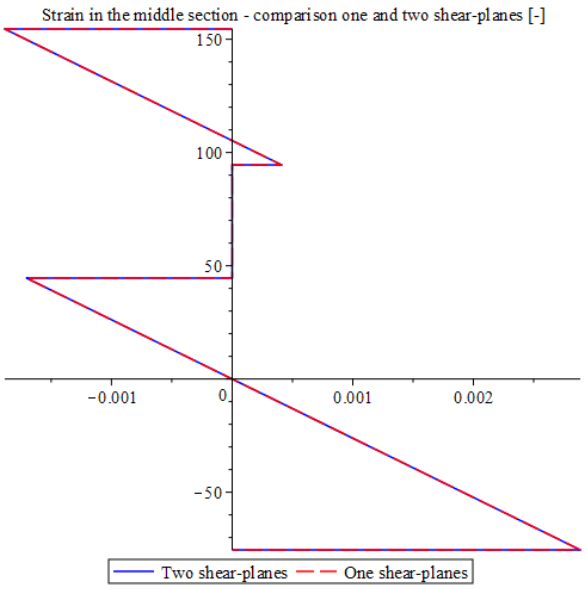

Figure B.9: Comparison of strains, 0mm gap, between one and two shear-planes

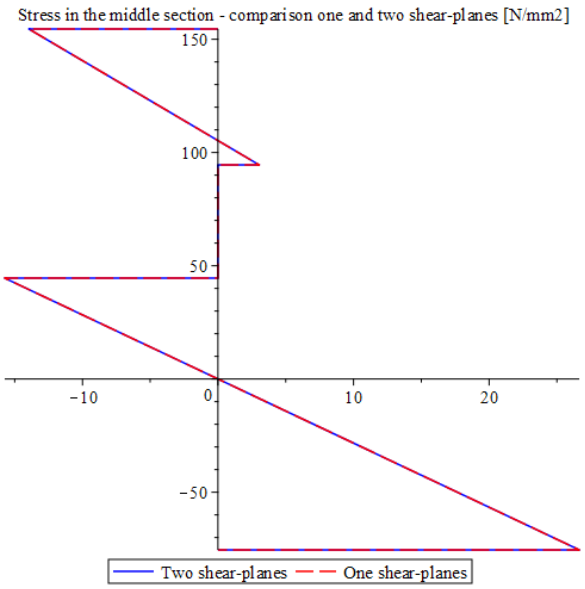

Figure B.10: Comparison of stress, 50mm gap, between one and two shear-planes

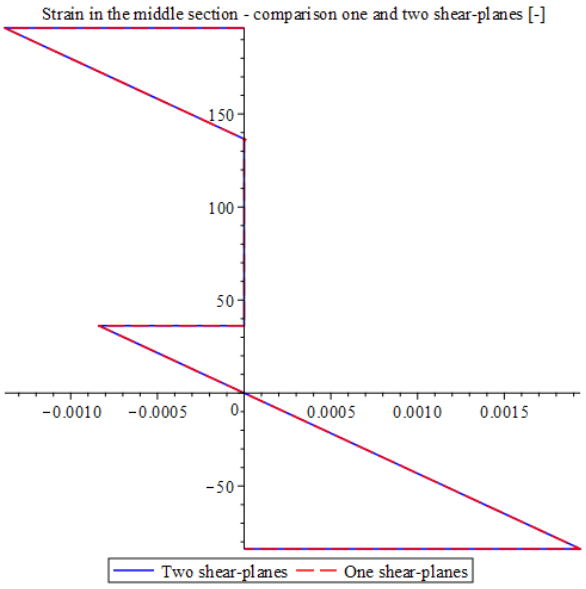

Figure B.11: Comparison of strains, 0mm gap, between one and two shear-planes

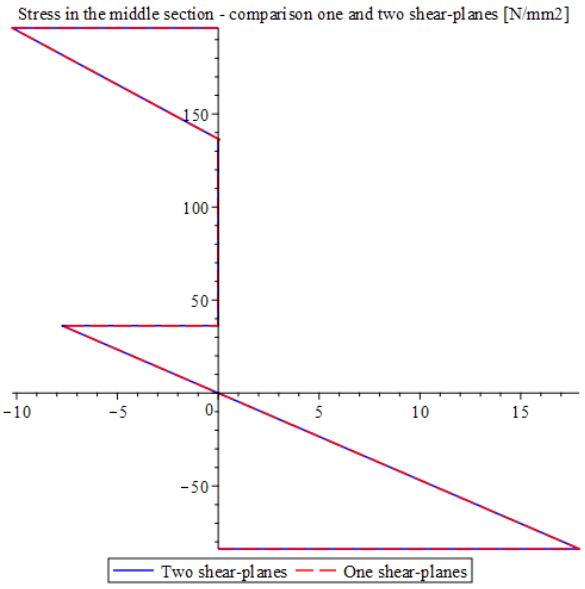

Figure B.12: Comparison of stress, 100mm gap, between one and two shear-planes

Factor

The factor determined in Tables B.3 and B.4 for the increasing height of the gap, is curve fitted as seen in Figure 2.18. Between the points, the exponential and parabolic curve are representative. But after the 100 mm gap, the exact effect cannot be guaranteed with certainty.

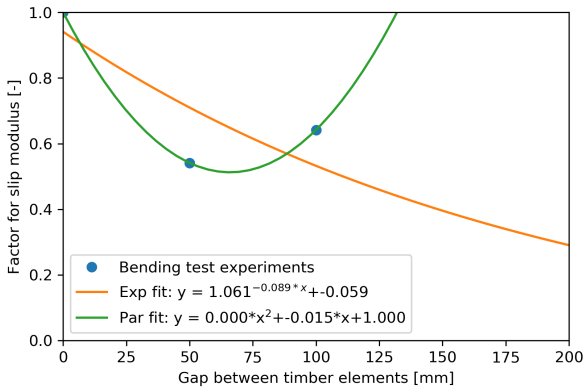

Figure B.13: Factor for slip modulus for increasing gap, from bending tests from Roensmaens et al. (2020)

Factor for the non-cooperating intermediate layer

Figure B.14 compares all the factors from the Figures B.2 and B.13. It can be concluded that the factor based on the exponential curve represents both the push-out and bending tests. If the exponential fitted factor from the bending tests is chosen a conservative value will be used.

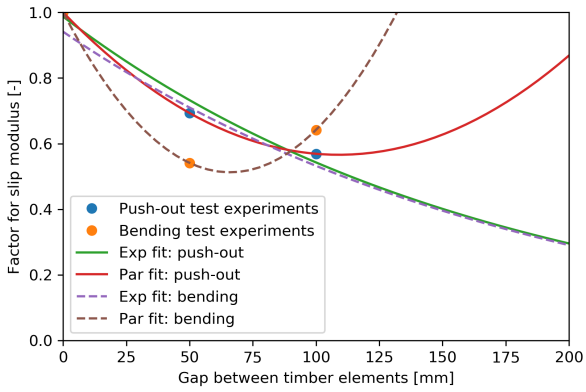

Figure B.14: Factor for slip modulus for increasing gap

C

Case study - Prinsenhof

One case study is carried out to get an answer on the first two sub-questions presented in the first chapter which deal with the current strength, stiffness and acoustic transmission properties of the timber floors. The Prinsenhof is a project of ABT which involves a monumental timber floor.

Figure C.1: Prinsenhof Delft Zeeuwse Jongens architecten (2019)

History

Museum Prinsenhof Delft is more than just a museum: it is a piece of history. One of the most dramatic incidents in Dutch history occurred in the Prinsenhof in Delft: the assassination of Prince Willem van Oranje in 1584. The bullet holes are still in the wall. Museum Prinsenhof Delft (nd)

The construction and occupation of the Prinsenhof dates back to the early 1400s. On the 30th of April 1403 a number of buildings in Delft received the status of a nunnery, named after Agatha. She was the daughter of the first matter, Alijd Buser. In the fifteenth century, the Agatha Monastery flourished. The Catholic Church's wealth, which included the Agatha Monastery, led to increasing protests and called for reforms. In 1566 the Iconoclasm broke out, however, the Agatha Monastery was well-guarded and spared. Shortly after, in 1572, the Revolt broke out and was led by Willem van Oranje who confiscated the monastery. Museum Prinsenhof Delft (nd)

Prince Willem van Oranje chose the Agatha Monastery as suitable residence. The people of Delft soon renamed the Agatha Monastery as Prinsenhof which stand for residence of the prince. The narrow

spiral staircases were not suitable for a prince and therefore a new, wider ”state staircase” was built especially for him. Tragically this staircase became the place of his assassination in 1584, see Figure C.2. Museum Prinsenhof Delft (nd)

Figure C.2: Assassination of Willem van Oranje in 1584 Museum Prinsenhof Delft (nd)

In the 17th century, the Prinsenhof was home to many trades, such as a cloth hall, homes, warehouses and a tannery. From 1795 onwards, the army claimed more and more parts of the building. However, at the end of the 19th century, a national awareness of historic monuments grew under Victor de Steurs who was widely regarded as the father of historic preservation. Wikipedia, The Free Encyclopedia (nd) Since 1925 the Prinsenhof has retained a museum function. Museum Prinsenhof Delft (nd)

Case details

The Prinsenhof has like many traditional buildings timber floor structures, see Figure C.3, which are supported on masonry walls for the first floors and supported on timber columns for the attic floors. The build-up of these floors is timber beams ”moerbalken”, joists ”kinderbinten” and planks.

Figure C.3: Guest Quarter [Bouwhistorisch onderzoek ABT, p. 140] and Dormitory [own picture]

Two floors from the Prinsenhof were chosen for this case study, see Figure C.4. The floor between the dormitory and the attic is relevant because in the new situation installations are going to be installed on the attic. And in addition, the floor between the guest quarter and the first floor, because it is imposed

on masonry walls and does not contain a concrete overlay. Which serves as a good comparison for the floor between the dormitory and the attic.

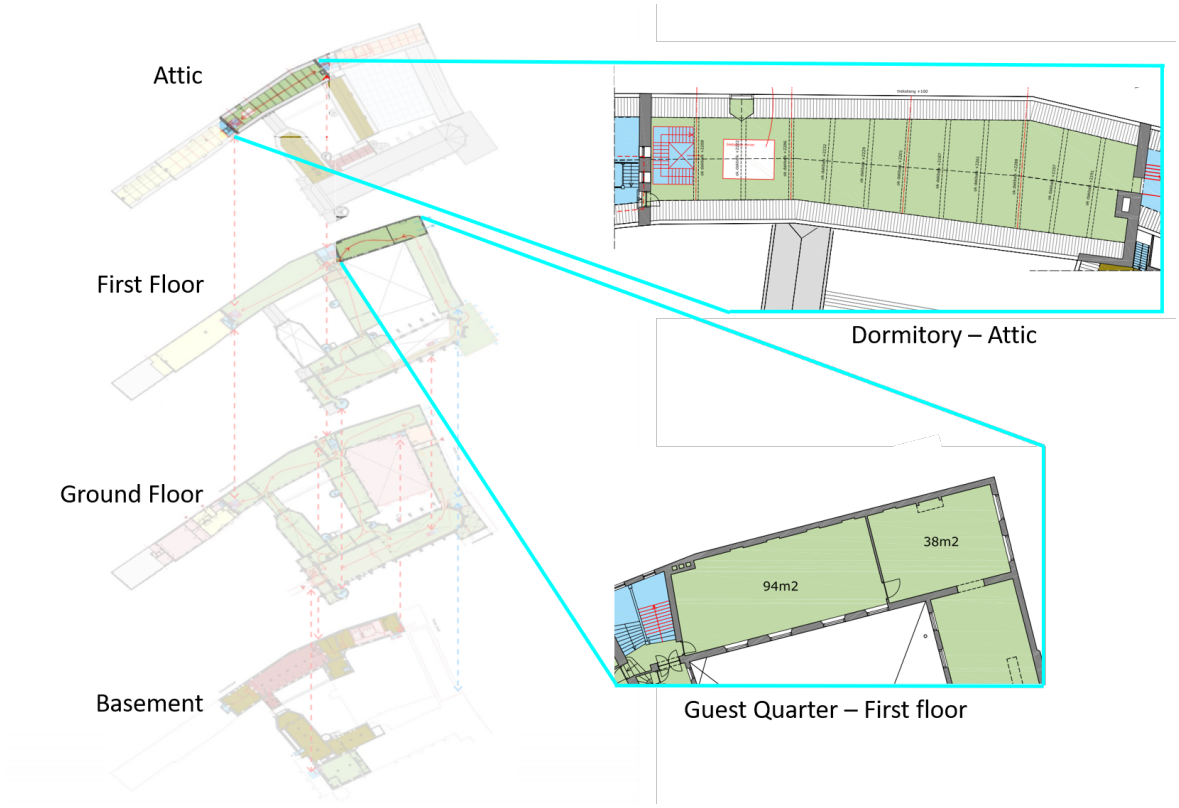

Figure C.4: Location of the two floors which are considered

The dormitory is a large room measuring approximately 30 x 8 meters (length x width) and is 9 meters wide at its largest point. In addition, the room has a height of 3.9 meters. The floor between the dormitory and the attic is supported by wooden columns and the span is ”reduced” by a corbel piece. As a result, the floor beams must carry the load of a span of maximum 7 meters.

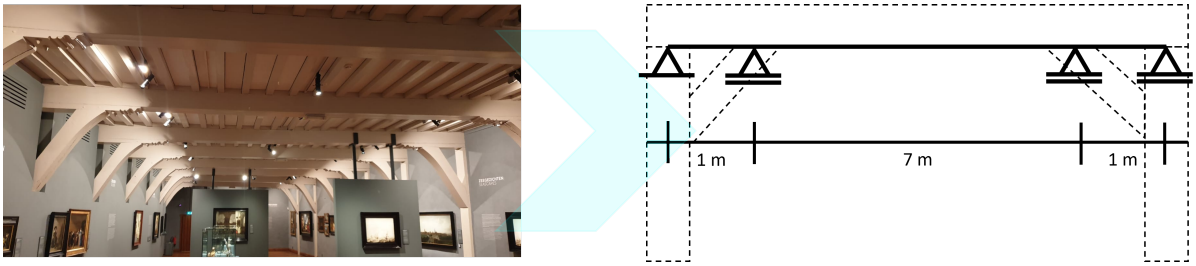

Figure C.5: Schematization of the floor between the dormitory and attic

As described before, the floor is composed of three load-bearing components: planks, joists, and beams. On top of that there is a concrete finishing layer, this is not structural in nature but was constructed around 1950 to make the separation between the attic and the dormitory waterproof. Table C.1 shows all the properties of the load-bearing parts. The strength class of these components was estimated to be the lowest grade of the species (C18 for softwood and D18 for hardwood) since it is not known, and a safe assumption must be made. The attic above the dormitory is now used for storage and has a top layer of concrete of 5 centimeters (estimated).

		Planks (C18)	Joists (C18)	Beams (D18)
Width	[mm]	200	110	300
Height	[mm]	20	110	280
Length	[mm]	380	2500	7000
$E_{m,0,mean}$	[N/mm^2]	9000	9000	9500
ρ_{mean}	[kg/m^3]	380	380	570
$f_{m,k}$	[N/mm^2]	18	18	18
$f_{v,k}$	[N/mm^2]	3.4	3.4	3.5
$f_{c,90,k}$	[N/mm^2]	2.2	2.2	4.8

Table C.1: Properties of the floor between the dormitory and attic

The guest quarter is a smaller, but higher room, measuring approximately 18 x 6 meters (length x width). In addition, the room has a height of 4.7 meters. The floor between the guest quarter and the first floor is supported by masonry walls and the maximum span of the floor here is 6 meters.

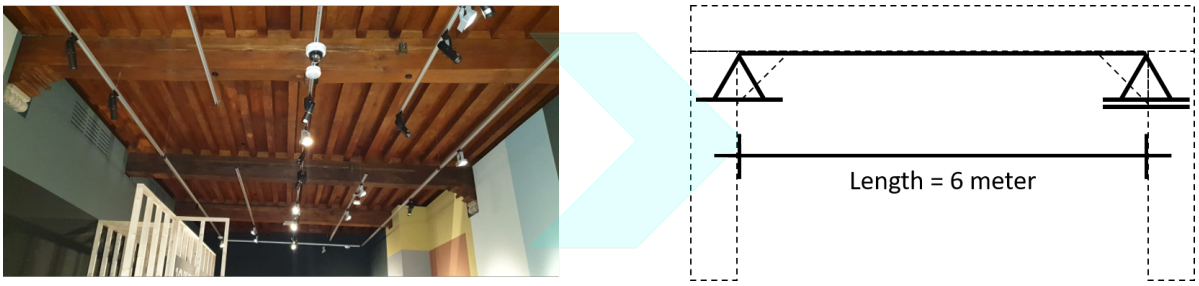

Figure C.6: Schematization of the floor between the guest quarter and first floor

The floor of the guest quarters is the same as the one before: planks, joists, and beams. However, it does not contain a concrete finishing layer. Table C.2 shows all the properties of the load-bearing parts. The strength class of these components was estimated to be the lowest grade of the species (C18 for softwood and D18 for hardwood) since it is not known, and a safe assumption must be made.

		Planks (C18)	Joists (C18)	Beams (D18)
Width	[mm]	200	100	290
Height	[mm]	20	100	340
Length	[mm]	330	3500	6000
$E_{m,0,mean}$	[N/mm^2]	9000	9000	9500
ρ_{mean}	[kg/m^3]	380	380	570
$f_{m,k}$	[N/mm^2]	18	18	18
$f_{v,k}$	[N/mm^2]	3.4	3.4	3.5
$f_{c,90,k}$	[N/mm^2]	2.2	2.2	4.8

Table C.2: Properties of the floor between the guest quarter and first floor

Load cases

Three options are considered as load case:

- Self-weight (both dormitory as guest quarter);
- Air-handling unit, which can be seen as two point loads of 4 kN with a spacing of 2 meters. For the dormitory see Figure C.7a and guest quarter Figure C.7b;
- Group of 30 people, where 30 persons over one span of 20 m^2 (guest quarter) can be seen as 1.5 kN/m^2 see Figure C.8a and over a span of 22.5 m^2 (dormitory) as 1.3 kN/m^2 see Figure C.8b.

These last two different loading situations have their own characteristic sound spectra, see Figure C.9. The spectrum for 30 persons is composed of 15 people who are simultaneously talking.

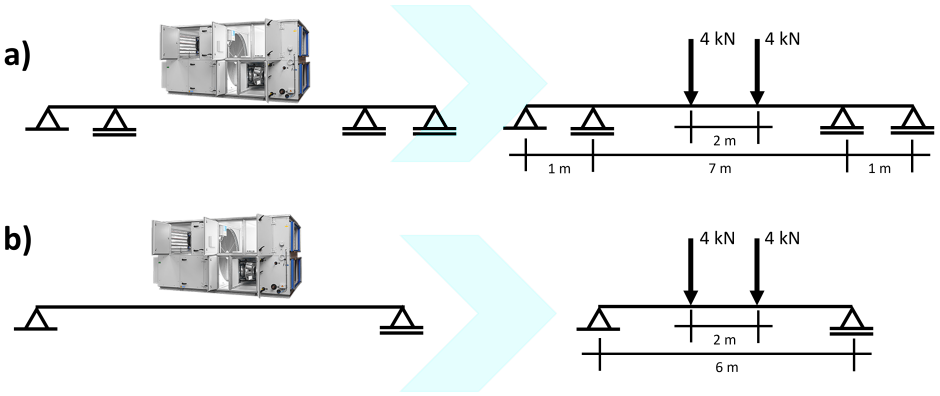

Figure C.7: Load case air-handling unit for
a) the floor between the dormitory and attic b) the floor between the guest quarter and first floor

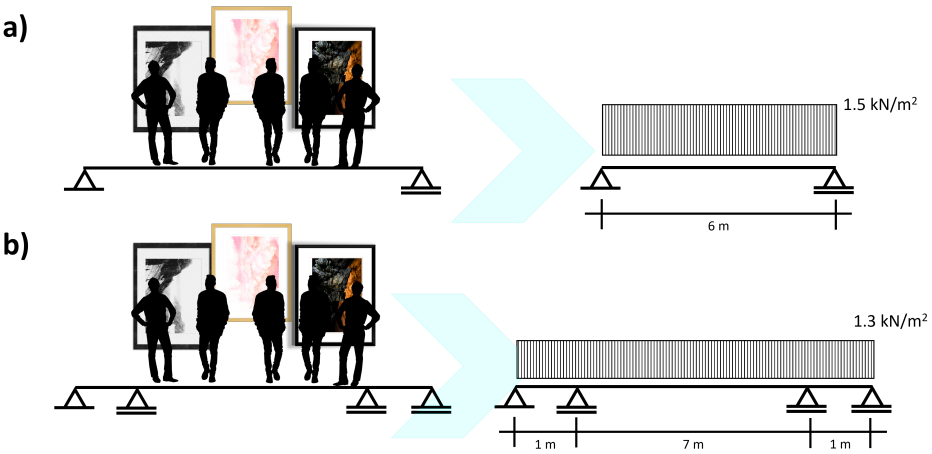

Figure C.8: Load case 30 people for
a) the floor between the guest quarter and first floor b) the floor between the dormitory and attic

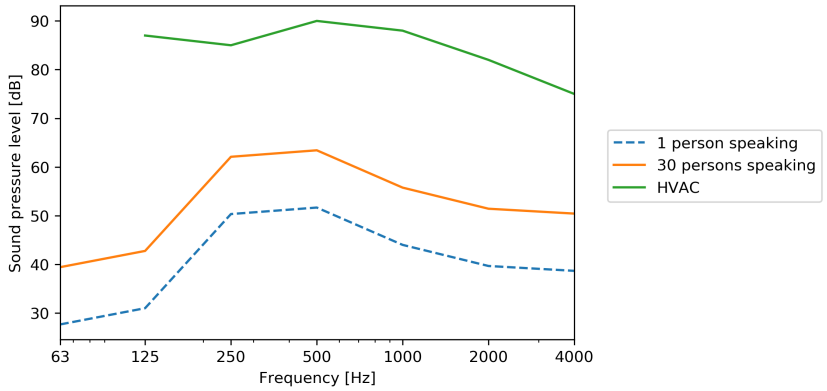

Figure C.9: Sound spectrum for 30 persons and air-handling unit

Structural calculations

For timber structures the governing load case can be determined by calculating the load combinations and dividing them by their k_{mod}. The load combinations and their safety factors can to be taken from equations 6.10a (first equation) and 6.10b (second equation) out of NEN-EN 1990 appendix A NEN-EN 1990 (2002).

$$\gamma_G G_k + \sum \gamma_Q \psi_{0,i} Q_{k,i}$$

$$\gamma_G G_k + \gamma_Q Q_{k,1} + \sum \gamma_Q \psi_{0,i} Q_{k,i}$$

Where:

γ_G	load factor for permanent loads	-
G_k	total permanent load	kN/m
γ_Q	load factor for variable loads	-
$\psi_{0,i}$	combination factor for the variable load i	-
$Q_{k,1}$	characteristic value of the leading variable load	kN/m
$Q_{k,i}$	characteristic value of variable load i	kN/m

The structure will be calculated for the renovation level according to the NEN 8700. NEN 8700 (2020) The load factors for this level can be taken as:

Renovation level 6.10a γ_G = 1.3 6.10b γ_G = 1.15 6.10ab γ_Q = 1.3

Dormitory to attic

To examine the structural performance of the load-bearing components of the floor, three aspects of the ultimate limit state were considered: bending moment (Figure C.10), shear force (Figure C.11), and compression perpendicular to the grain at the support (Figure C.12). Those aspects were examined for three situations, which are: self-weight, 30 people and an air-handling unit. In addition, the deflection in serviceability state is also calculated, see Figure C.13.

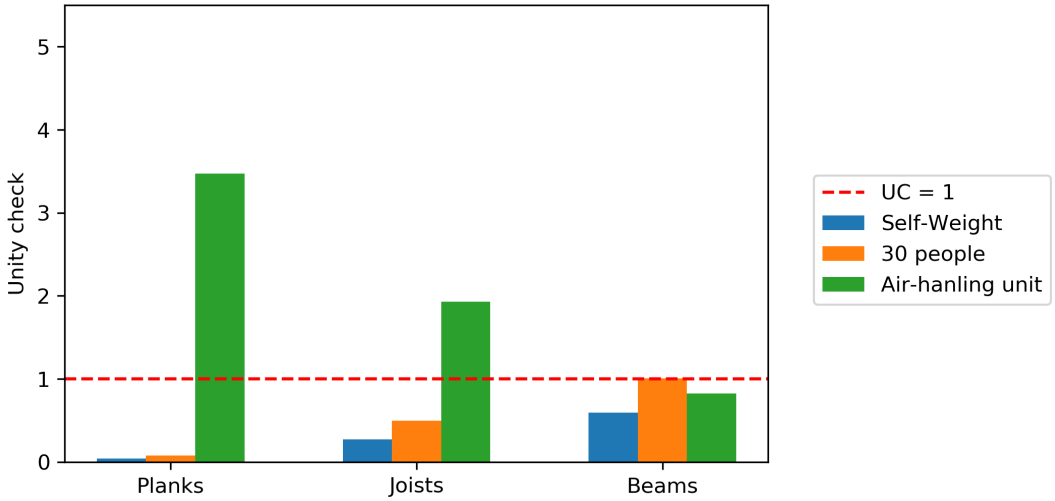

Figure C.10: Unity check for bending moment of the floor components between the dormitory and attic

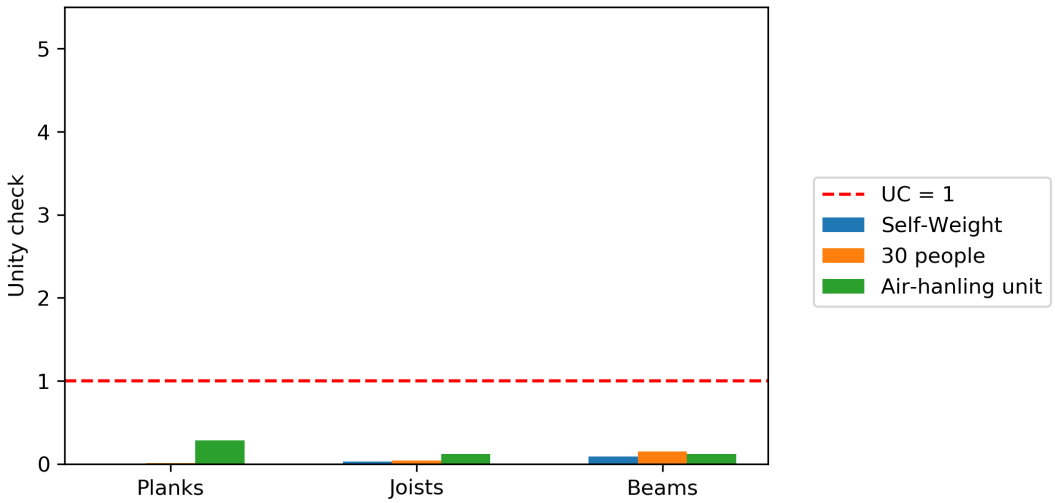

Figure C.11: Unity check for shear of the floor components between the dormitory and attic

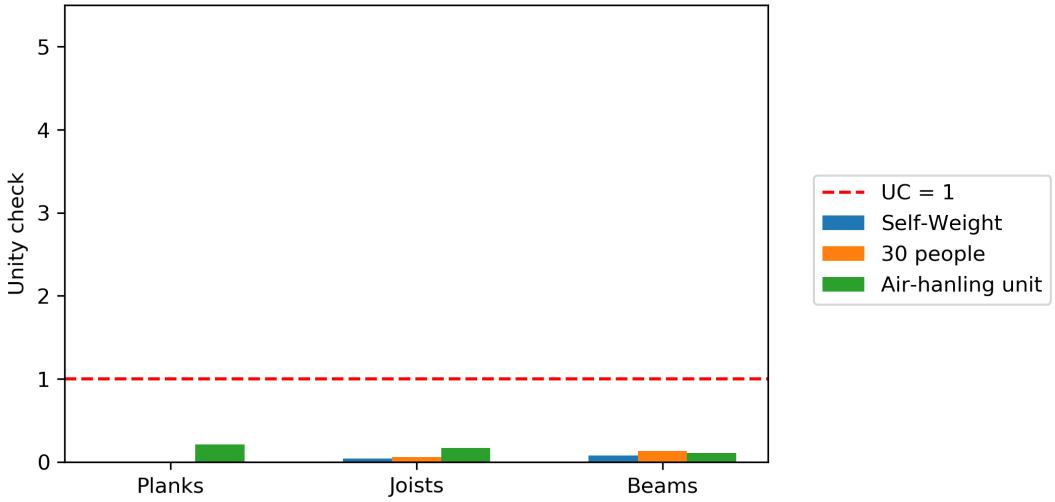

Figure C.12: Unity check for compression perpendicular to the grain of the floor components between the dormitory and attic

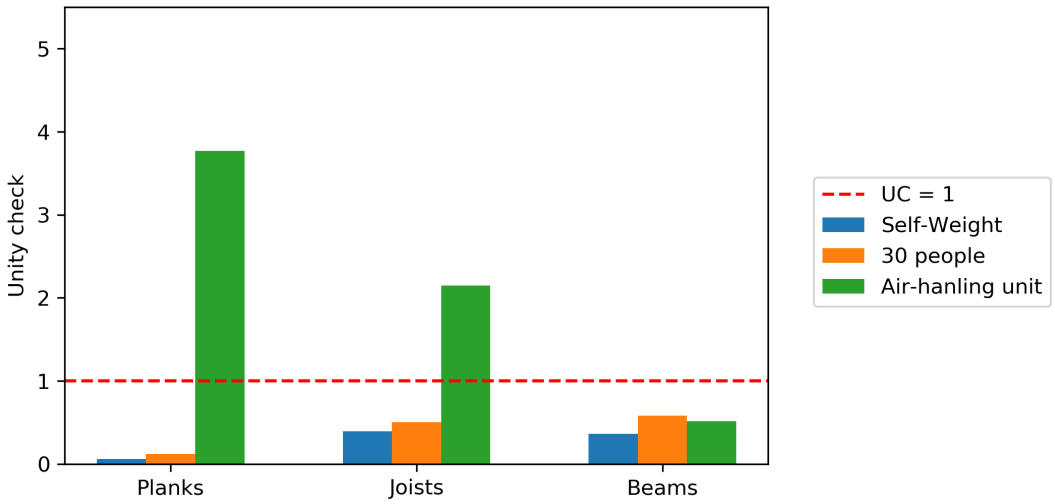

Figure C.13: Unity check for deflection of the floor components between the dormitory and attic

Guest quarter to first floor

To examine the structural performance of the load-bearing components of the floor, three aspects of the ultimate limit state were considered: bending moment, shear force, and compression perpendicular to the grain at the support. Those aspects were examined for three situations, which are: self-weight, 30 people and an air-handling unit. In addition, the deflection in serviceability state is also calculated. The full calculation can be found in Appendix C.

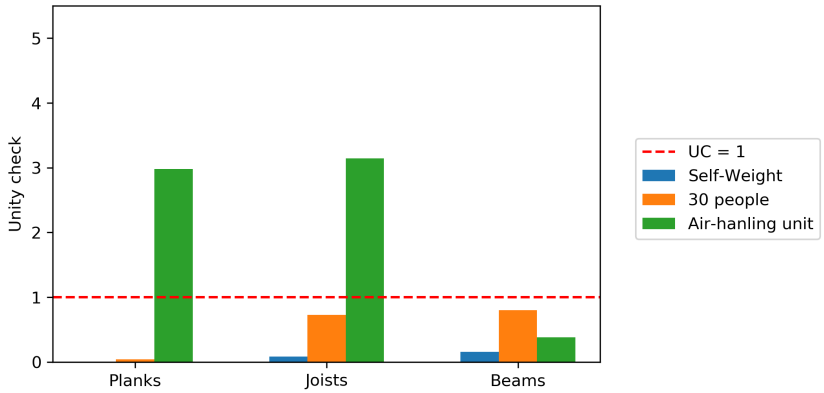

Figure C.14: Unity check for bending moment of the floor components between the guest quarter and first floor

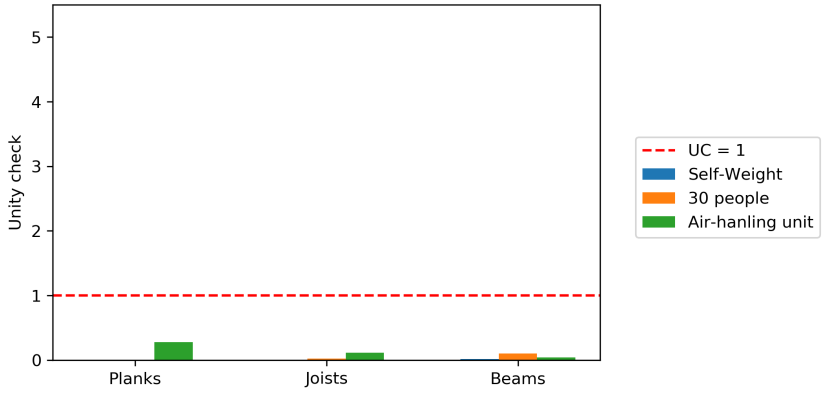

Figure C.15: Unity check for shear of the floor components between the guest quarter and first floor

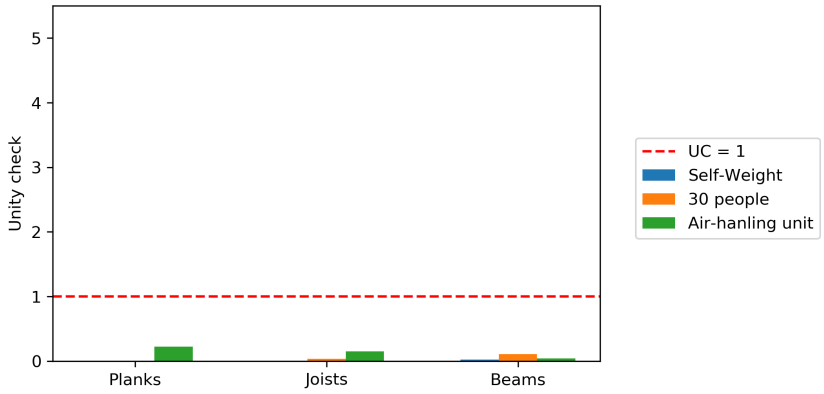

Figure C.16: Unity check for compression perpendicular to the grain of the floor components between the guest quarter and first floor

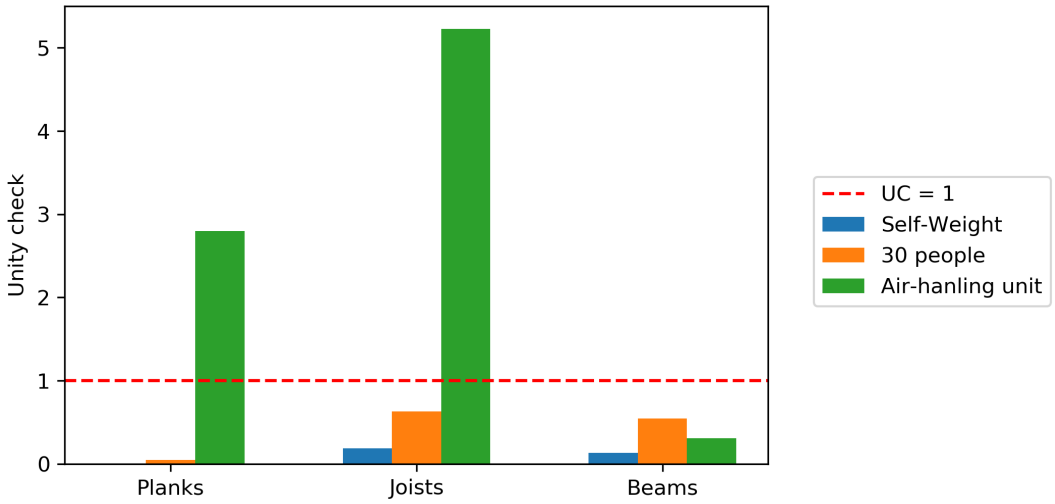

Figure C.17: Unity check for deflection of the floor components between the guest quarter and first floor

Acoustic calculations

For acoustic calculations, the size of the receiving room plays a significant role. The dimensions of the rooms can be seen in Figure C.18 for the dormitory and guest quarter. These dimensions play a role for the value of absorption materials in the room to be added and the area of the sending x receiving separation element subtracted.

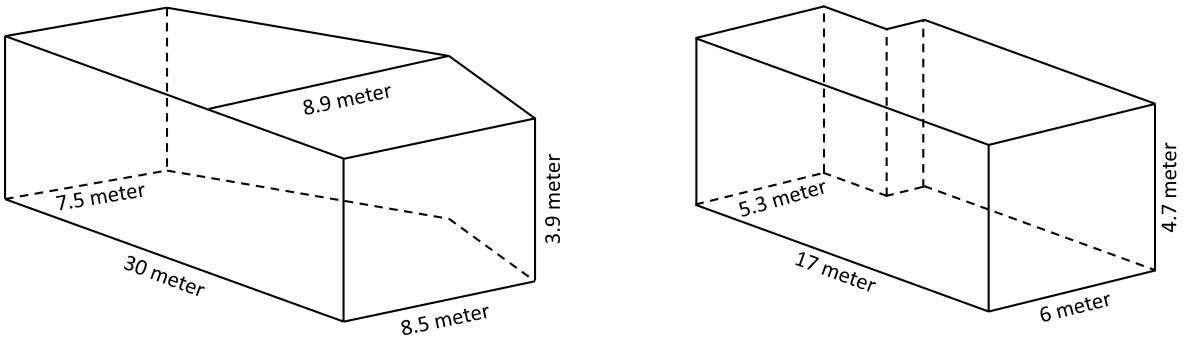

Figure C.18: Dimensions of the receiving rooms in the Prinsenhof museum. (LEFT) Dormitory and (RIGHT) Guest quarter

To examine the acoustic performance of the floor, two aspects are considered: airborne and structure-borne sounds. Both floors are tested with two methods, the RC-curves and the ISO-curves. The RC-curves are used to test 15 people who are talking and an air-handling unit which is present. The structure-borne sounds are only verified with the ISO-curve maximum L_F.

Dormitory to attic

Figures C.19 and C.20 show the ISO curve relation for airborne and structure-borne sound transmission. With R_w = 47 dB and L_{nt} = 88 dB.

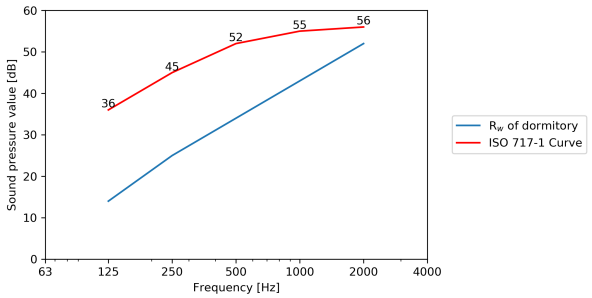

Figure C.19: ISO717-1 Airborne sound isolation between the dormitory and attic

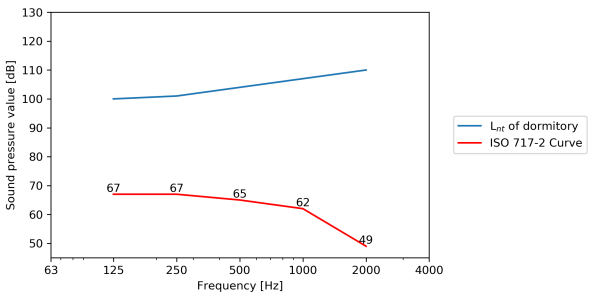

Figure C.20: ISO717-2 Structure-borne sound level between the dormitory and attic

Figure C.21 illustrates the RC curve for the two situations with airborne sound spectra. Where for the situation with 15 people talking the sound SIL = 9-R and for the air-handling unit the SIL = 36-R.

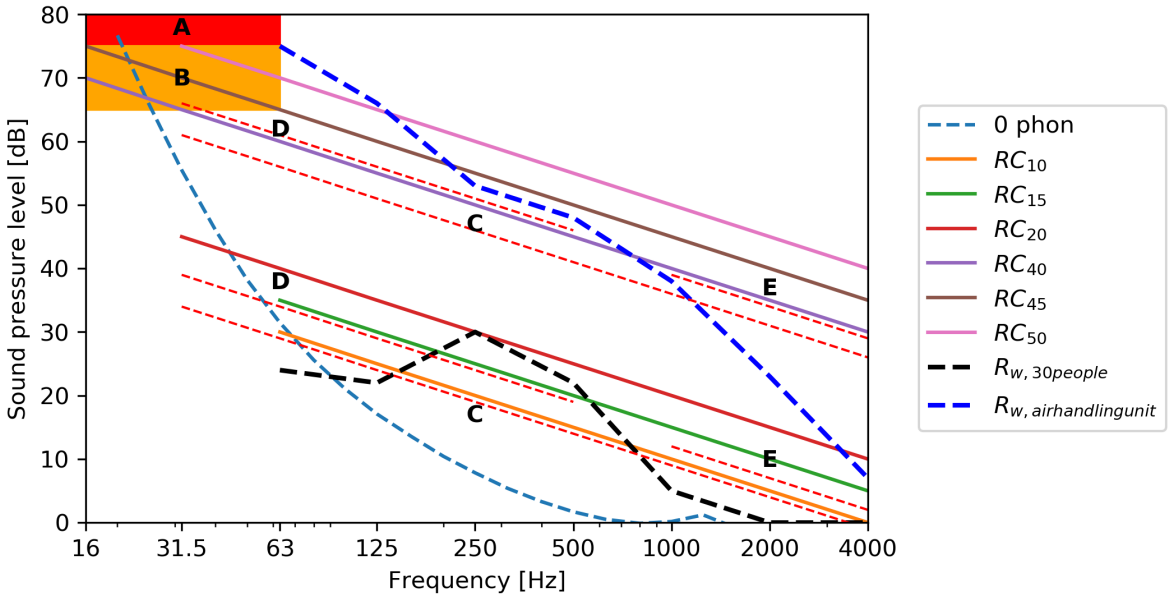

Figure C.21: RC-Curve Airborne sound isolation between the dormitory and attic

Guest quarter to first floor

Figures C.22 and C.23 show the ISO curve relation for airborne and structure-borne sound transmission. With R_w = 24 dB and $L_{n,w}$ = 1116 dB.

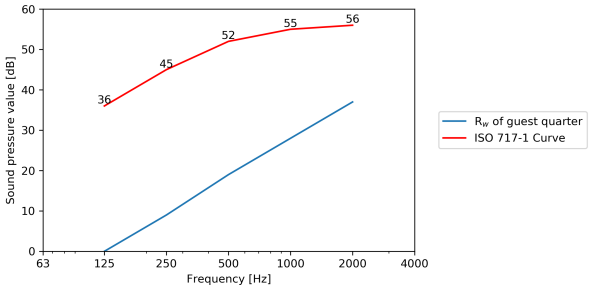

Figure C.22: ISO717-1 Airborne sound isolation between the guest quarter and first floor

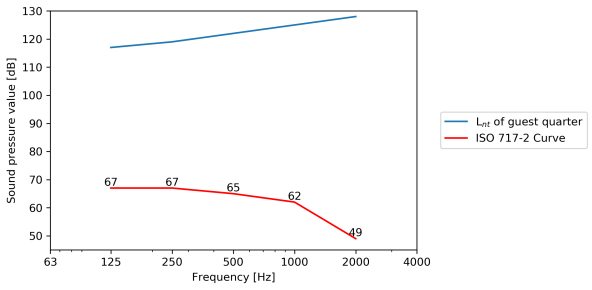

Figure C.23: ISO717-2 Structure-borne sound level between the guest quarter and first floor

Figure C.24 illustrates the RC curve for the two situations with airborne sound spectra. Where for the situation with 15 people talking the sound SIL = 29-R and for the air-handling unit the SIL = 59-R.

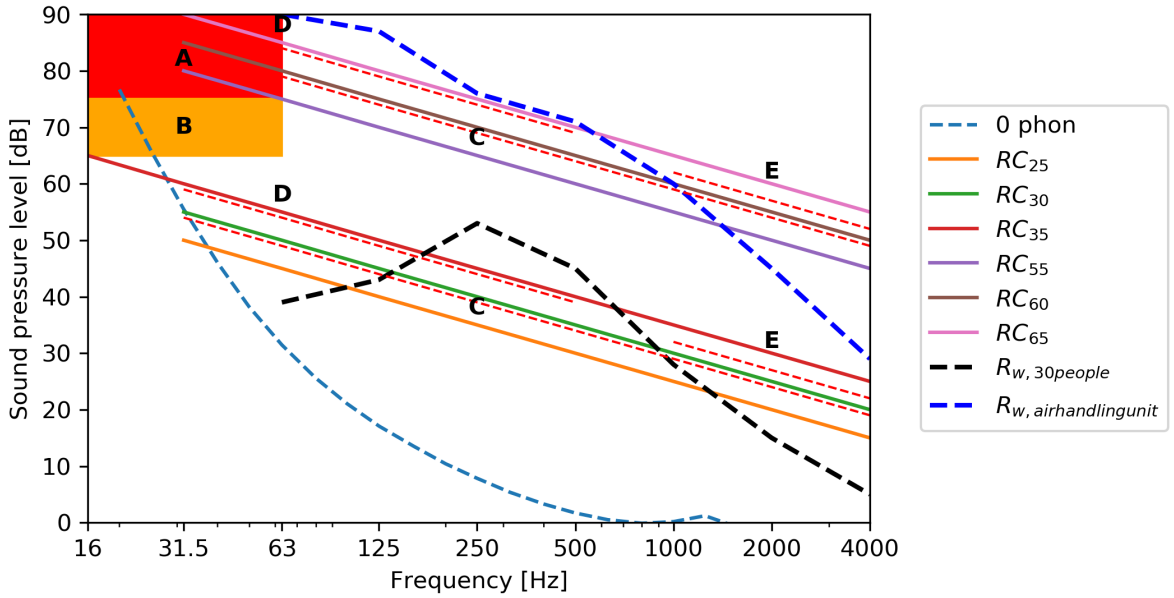

Figure C.24: RC-Curve Airborne sound isolation between the guest quarter and first floor

D

Equivalent axial stiffness for segments

For all segments, an equation for the strain of a segment can be established based on the force distribution and deformation. This has been done for two, three and four-layered plates connected by screws. These screws are always screwed through all layers and are equally distributed along the length of the layer. This spacing between joints can be seen as:

$$s = \frac{L_{pl}}{n_p n_{fpp}}$$

Where:

s	spacing between the connections	mm
L_{pl}	length of the segment (plate)	mm
n_p	layers of plates	-
n_{fpp}	number of fasteners on $1/n_p$ of the segment	-

Two layers

Two layered system, with two screws per plate, have two variants in the segments which is shown in Figure D.1.

Figure D.1: Different segments for a two layered system with two fasteners per plate

Load distribution

The load distribution of this segment can be seen in the Figures D.2, D.3 and D.4. Where the load distribution is based on a load of **10 kN**. It is noticeable that the force is evenly distributed over the number of screws between two plates.

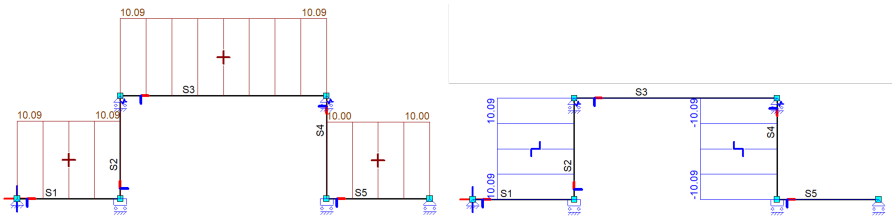

Figure D.2: Normal force and shear force distribution in a two layered system with two screws per plate

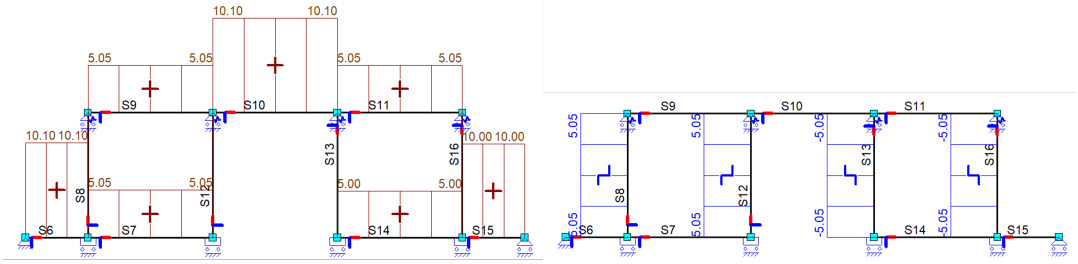

Figure D.3: Normal force and shear force distribution in a two layered system with four screws per plate

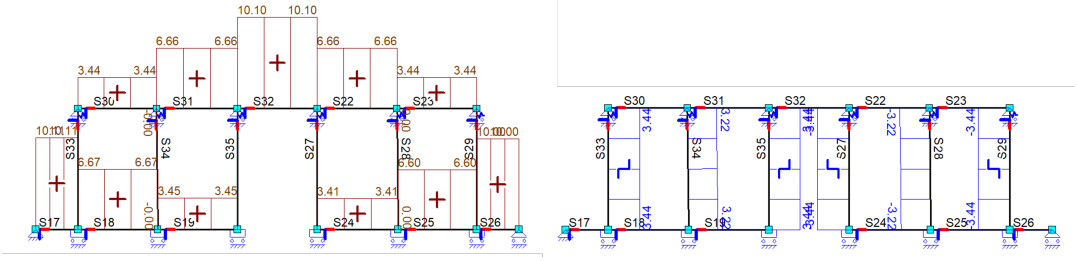

Figure D.4: Normal force and shear force distribution in a two layered system with six screws per plate

Equation

An equation can be established by taking the deformation path like shown in Figure D.5 where the deformation is composed out of that of the connections and plates.

Figure D.5: Deformation path of a two layered system

From these deformation paths a general equation can be made through checking the forces out of Figures D.2, D.3 and D.4:

Figure	n_{fpp}	Shear Force [kN]	"Factor" x $\frac{F}{n_y K}$	Tension [kN] x s [-]	"Factor" x $\frac{Fs}{EA}$
D.2	1	10 + 10	$\frac{2}{1}$	5 + 10 + 5	2
D.3	2	5 + 5	$\frac{2}{2}$	(5+5) + 10 + (5+5)	3
D.4	3	3.3 + 3.3	$\frac{2}{3}$	(5+6.7+3.3) + 10 + (3.3+6.7+5)	4
-	4	2.5 + 2.5	$\frac{2}{4}$	(5+7.5+5+2.5) + 10 + (2.5+5+7.5+5)	5

The pattern for "Factor" x $\frac{F}{n_y K}$ is given in Equation D.1 and for "Factor" x $\frac{Fs}{EA}$ in Equation D.2. And with these patterns, the general equation for the elongation of two plates can be constituted in Equation D.3.

$$\left(2, 1, \frac{2}{3}, \frac{2}{4}, \ldots\right) \; > \; "Factor" = \frac{2}{n_{fpp}} \tag{D.1}$$

$$(2, 3, 4, 5, \ldots) \; > \; "Factor" = n_{fpp} + 1 \tag{D.2}$$

$$\Delta L_{total,2,plates} = \frac{2F}{n_{fpp} n_y K} + \frac{(n_{fpp} + 1)FL}{n_p n_{fpp} E A_{plate}} \tag{D.3}$$

Elongation check

The equation created to calculate the elongation of the segments can be checked against the MatrixFrame model.

The properties of the segment for the elongation of two plates with two screws:

F	=	Force	=	10000	N
n_p	=	Number of layers	=	2	-
n_{fpp}	=	Number of screws between two distinct plates	=	1	-
n_y	=	Number of screws in effective width direction	=	1	-
K	=	Stiffness of fastener	=	100	N/mm
L	=	Length of a plate	=	4000	mm
E	=	Young's modulus	=	8000	N/mm^2
A	=	Area	=	12000	mm^2

Which result in the following elongation:

$$\Delta L_{total,2,plates} = \frac{2 \cdot 10000}{1 \cdot 1 \cdot 100} + \frac{(1+1) \cdot 10000 \cdot 4000}{2 \cdot 1 \cdot 8000 \cdot 12000} = 200.42\ mm$$

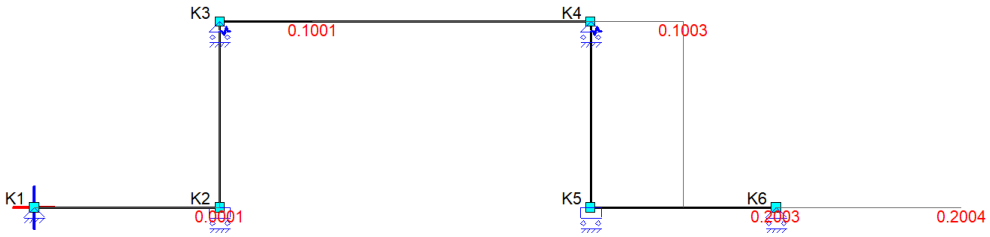

The properties of the segment for the elongation of two plates with four screws:

F	=	Force	=	10000	N
n_p	=	Number of layers	=	2	-
n_{fpp}	=	Number of screws between two distinct plates	=	2	-
n_y	=	Number of screws in effective width direction	=	1	-
K	=	Stiffness of fastener	=	100	N/mm
L	=	Length of a plate	=	4000	mm
E	=	Young's modulus	=	8000	N/mm^2
A	=	Area	=	12000	mm^2

Which result in the following elongation:

$$\Delta L_{total,2,plates} = \frac{2 \cdot 10000}{2 \cdot 1 \cdot 100} + \frac{(2+1) \cdot 10000 \cdot 4000}{2 \cdot 2 \cdot 8000 \cdot 12000} = 100.21\ mm$$

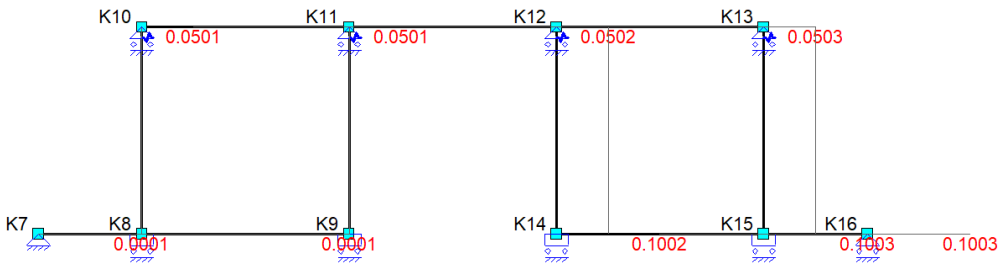

The properties of the segment for the elongation of two plates with six screws:

F	=	Force	=	10000	N
n_p	=	Number of layers	=	2	-
n_{fpp}	=	Number of screws between two distinct plates	=	3	-
n_y	=	Number of screws in effective width direction	=	1	-
K	=	Stiffness of fastener	=	100	N/mm
L	=	Length of a plate	=	4000	mm
E	=	Young's modulus	=	8000	N/mm^2
A	=	Area	=	12000	mm^2

Which result in the following elongation:

$$\Delta L_{total,2,plates} = \frac{2 \cdot 10000}{3 \cdot 1 \cdot 100} + \frac{(3+1) \cdot 10000 \cdot 4000}{2 \cdot 3 \cdot 8000 \cdot 12000} = 66.81\ mm$$

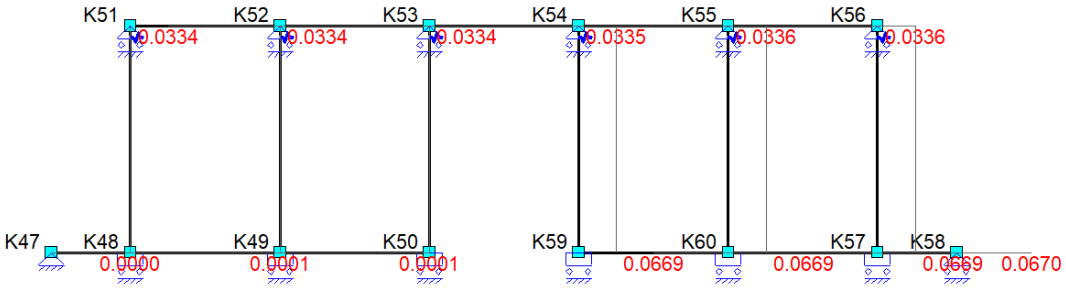

Three layers

Three layered systems, with three fasteners per plate, have six variants in the segments which are shown in Figure D.6.

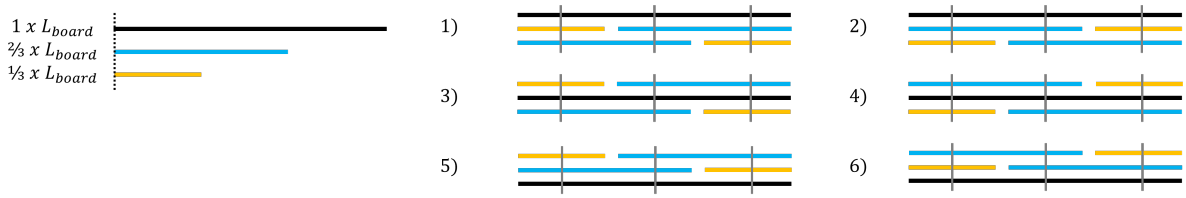

Figure D.6: Different segments for a three layered system with three fasteners per plate

Load distribution

The load distribution of three layered segments can be seen in the Figures D.7, D.8 and D.9 The load distribution is based on a load of **40 kN**.

The distribution of the load over the plates is not entirely correct, because the stiffness of the screws relative to that of the plates influences it as well. Therefore it was assumed that it has no influence, so the elongation could be calculated with the values in the Figures D.7, D.8 and D.9. Figure D.9 also shows that load induction phenomena occurs, because the model cannot be made larger since only 100 beam-elements may be used in the student version of MatrixFrame.

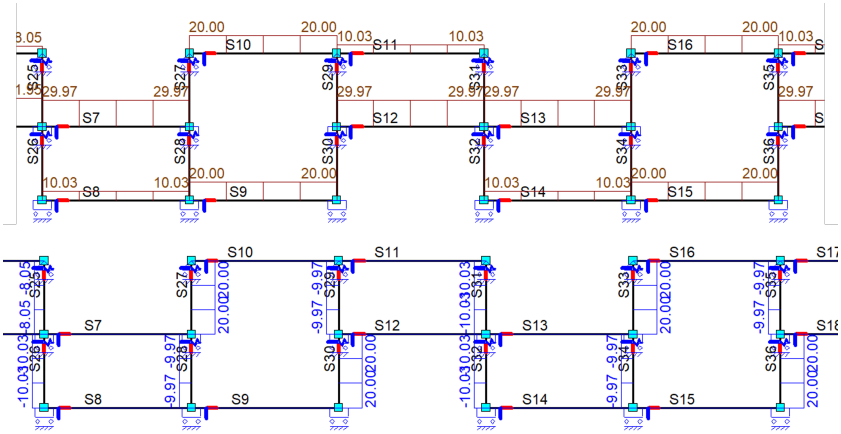

Figure D.7: Normal force and shear force distribution in a three layered segment with three screws per plate

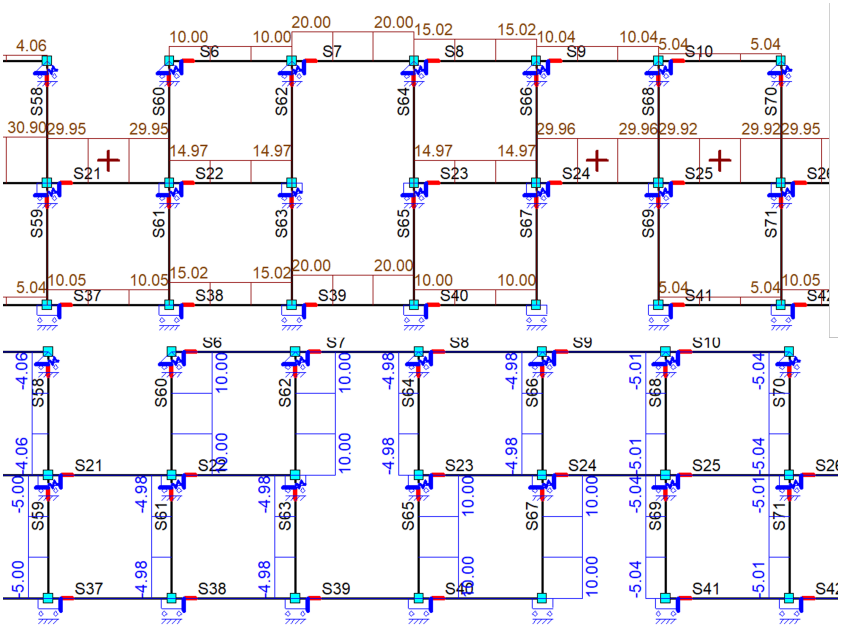

Figure D.8: Normal force and shear force distribution in a three layered segment with six screws per plate

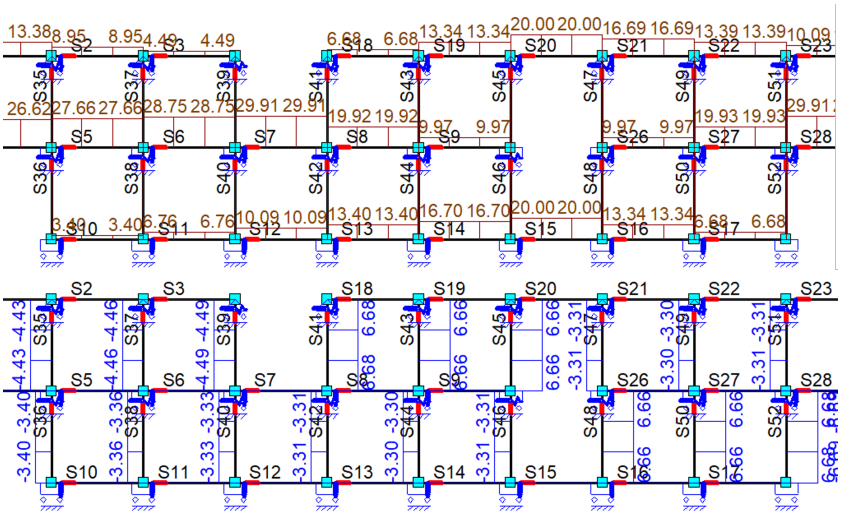

Figure D.9: Normal force and shear force distribution in a three layered segment with nine screws per plate

Equation

An equation can be established by taking the deformation path like shown in Figure D.10 where the deformation is composed out of that of the connections and plates.

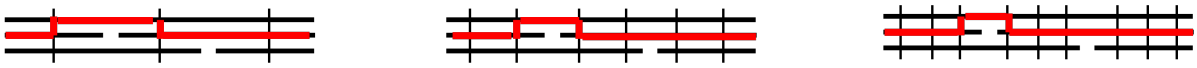

Figure D.10: Deformation path of a three layered system

From these deformation paths a general equation can be made through checking the forces out of Figures D.7, D.8 and D.9:

Figure	n_{fpp}	Shear Force [kN]	"Factor" x $\frac{F}{n_y K}$	Tension [kN] x s [-]	"Factor" x $\frac{Fs}{EA}$
D.7	1	20 + 10	$\frac{3}{4}$	15 + 20 + (30+15)	2
D.8	2	10 + 5	$\frac{3}{8}$	(15+15) + 20 + (15+30+30+15)	3.5
D.9	3	6.7 + 3.3	$\frac{3}{12}$	(15+20+10) + 20 + (10+20+30+30+30+15)	5
-	3	5 + 2.5	$\frac{3}{16}$	(15+22.5+15+7.5) + 20 + (7.5+15+22.5+30+30+30+30+15)	6.5

The pattern for "Factor" x $\frac{F}{n_y K}$ is given in Equation D.4 and for "Factor" x $\frac{Fs}{EA}$ in Equation D.5. And with these patterns, the general equation for the elongation of two plates can be constituted in Equation D.6.

$$\left(\frac{3}{4}, \frac{3}{8}, \frac{3}{12}, \frac{3}{16}, \ldots\right) > "Factor" = \frac{3}{4n_{fpp}} \tag{D.4}$$

$$(2, 3.5, 5, 6.5, \ldots) > "Factor" = \frac{3n_{fpp} + 1}{2} \tag{D.5}$$

$$\Delta L_{total,3,plates} = \frac{3F}{4n_{fpp} n_y K} + \frac{(3n_{fpp} + 1)FL}{2n_p n_{fpp} E A_{plate}} \tag{D.6}$$

Elongation check

The equation created to calculate the elongation of the segments can be checked against the MatrixFrame model. The properties of the segment for the elongation of three plates with three screws:

F	=	Force	=	40000	N
n_p	=	Number of layers	=	3	-
n_{fpp}	=	Number of screws between two distinct plates	=	1	-
n_y	=	Number of screws in effective width direction	=	1	-
K	=	Stiffness of fastener	=	100	N/mm
L	=	Length of a plate	=	5000	mm
E	=	Young's modulus	=	8000	N/mm^2
A	=	Area	=	9000	mm^2

Which result in the following elongation:

$$\Delta L_{total,3,plates} = \frac{3 \cdot 40000}{4 \cdot 1 \cdot 1 \cdot 100} + \frac{(3 \cdot 1 + 1) \cdot 40000 \cdot 5000}{2 \cdot 3 \cdot 1 \cdot 8000 \cdot 9000} = 301.85\ mm$$

The elongation in the Matrixframe model (between K10/K11 - K19/K20):

$$\Delta L_{total,3,plates} = ((0.5444 - 0.5436) - (0.2425 - 0.2416)) \cdot 1000 = 301.95\ mm$$

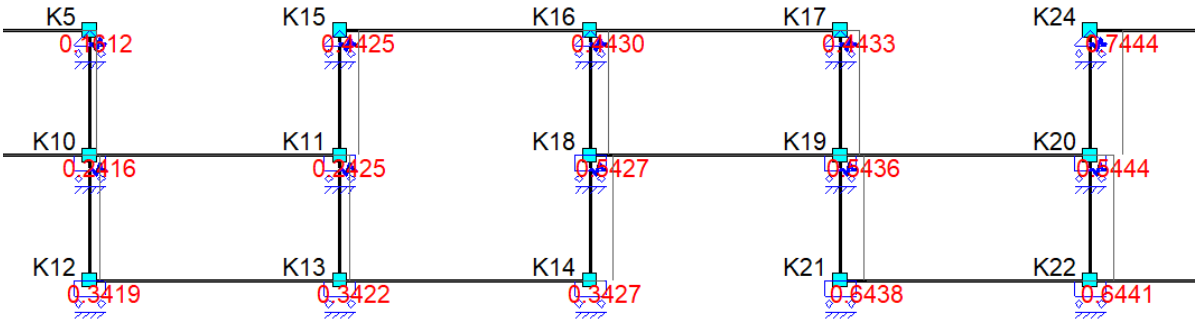

The properties of the segment for the elongation of three plates with six screws:

F	=	Force	=	40000	N
n_p	=	Number of layers	=	3	-
n_{fpp}	=	Number of screws between two distinct plates	=	2	-
n_y	=	Number of screws in effective width direction	=	1	-
K	=	Stiffness of fastener	=	100	N/mm
L	=	Length of a plate	=	6000	mm
E	=	Young's modulus	=	8000	N/mm^2
A	=	Area	=	9000	mm^2

Which result in the following elongation:

$$\Delta L_{total,3,plates} = \frac{3 \cdot 40000}{4 \cdot 2 \cdot 1 \cdot 100} + \frac{(3 \cdot 2 + 1) \cdot 40000 \cdot 6000}{2 \cdot 3 \cdot 2 \cdot 8000 \cdot 9000} = 151.94\ mm$$

The elongation in the Matrixframe model (between K7/K8 - K13/K14):

$$\Delta L_{total,3,plates} = ((0.2737 - 0.2733) - (0.1221 - 0.1216)) \cdot 1000 = 151.65\ mm$$

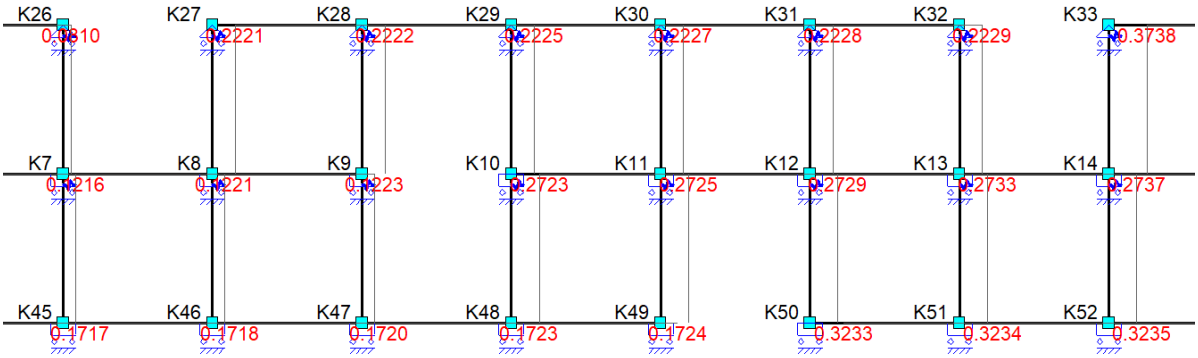

The properties of the segment for the elongation of three plates with nine screws:

F	=	Force	=	40000	N
n_p	=	Number of layers	=	3	-
n_{fpp}	=	Number of screws between two distinct plates	=	3	-
n_y	=	Number of screws in effective width direction	=	1	-
K	=	Stiffness of fastener	=	100	N/mm
L	=	Length of a plate	=	9000	mm
E	=	Young's modulus	=	8000	N/mm^2
A	=	Area	=	9000	mm^2

Which result in the following elongation:

$$\Delta L_{total,3,plates} = \frac{3 \cdot 40000}{4 \cdot 3 \cdot 1 \cdot 100} + \frac{(3 \cdot 3 + 1) \cdot 40000 \cdot 9000}{2 \cdot 3 \cdot 3 \cdot 8000 \cdot 9000} = 102.78\ mm$$

The elongation in the Matrixframe model (between K5/K6 - K32/K33):

$$\Delta L_{total,3,plates} = ((0.1478 - 0.1474) - (0.0454 - 0.0450)) \cdot 1000 = 102.4\ mm$$

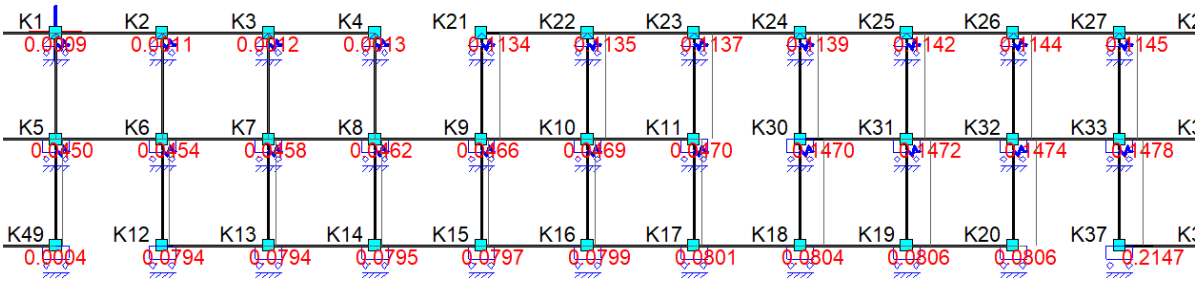

Four layers

Four layered system, with four screws per plate, have 24 variants in the segments of which a few are shown in Figure D.11.

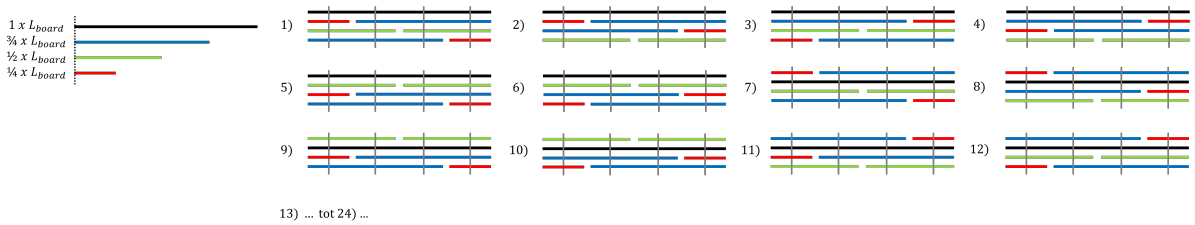

Figure D.11: Different segments for a four layered system with four fasteners per plate

Load distribution

The load distribution of four layered segments can be seen in the Figures D.12 and D.13. The load distribution is based on a load of **120 kN**.

The distribution of the load over the plates is not entirely correct, because the stiffness of the screws relative to that of the plates influences it as well. Therefore it was assumed that it has no influence, so the elongation could be calculated with the values in the Figures D.12 and D.13. Figure D.13 also shows that load induction phenomena occurs, because the model cannot be made larger since only 100 beam-elements may be used in the student version of MatrixFrame.

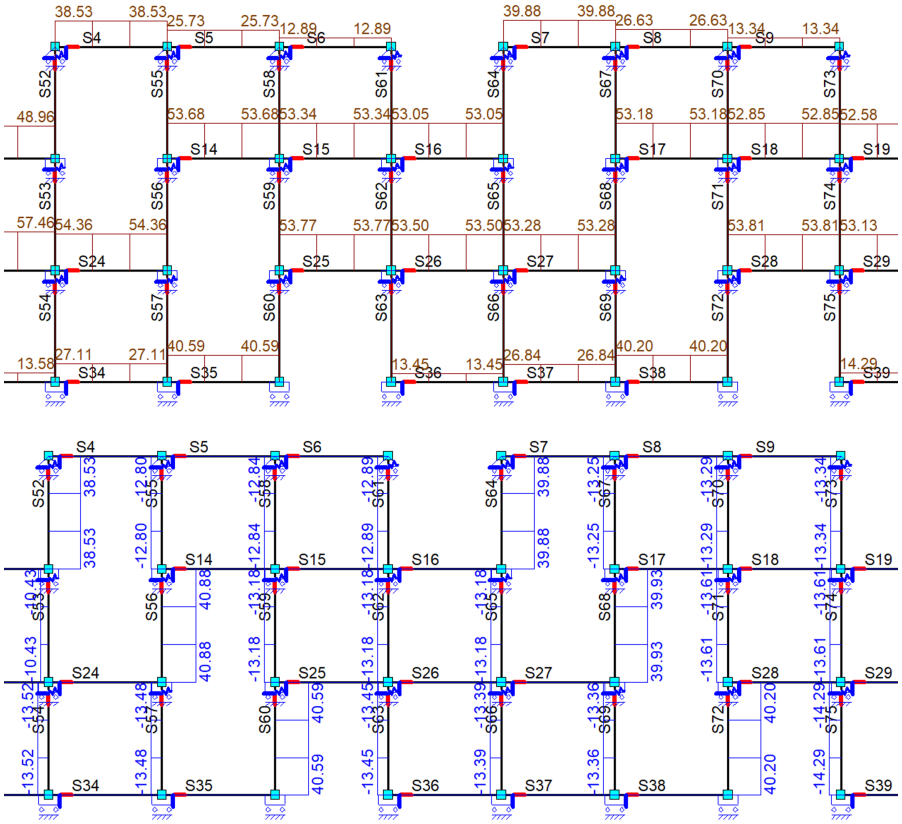

Figure D.12: Normal force and shear force distribution in a two layered system with two screws per plate

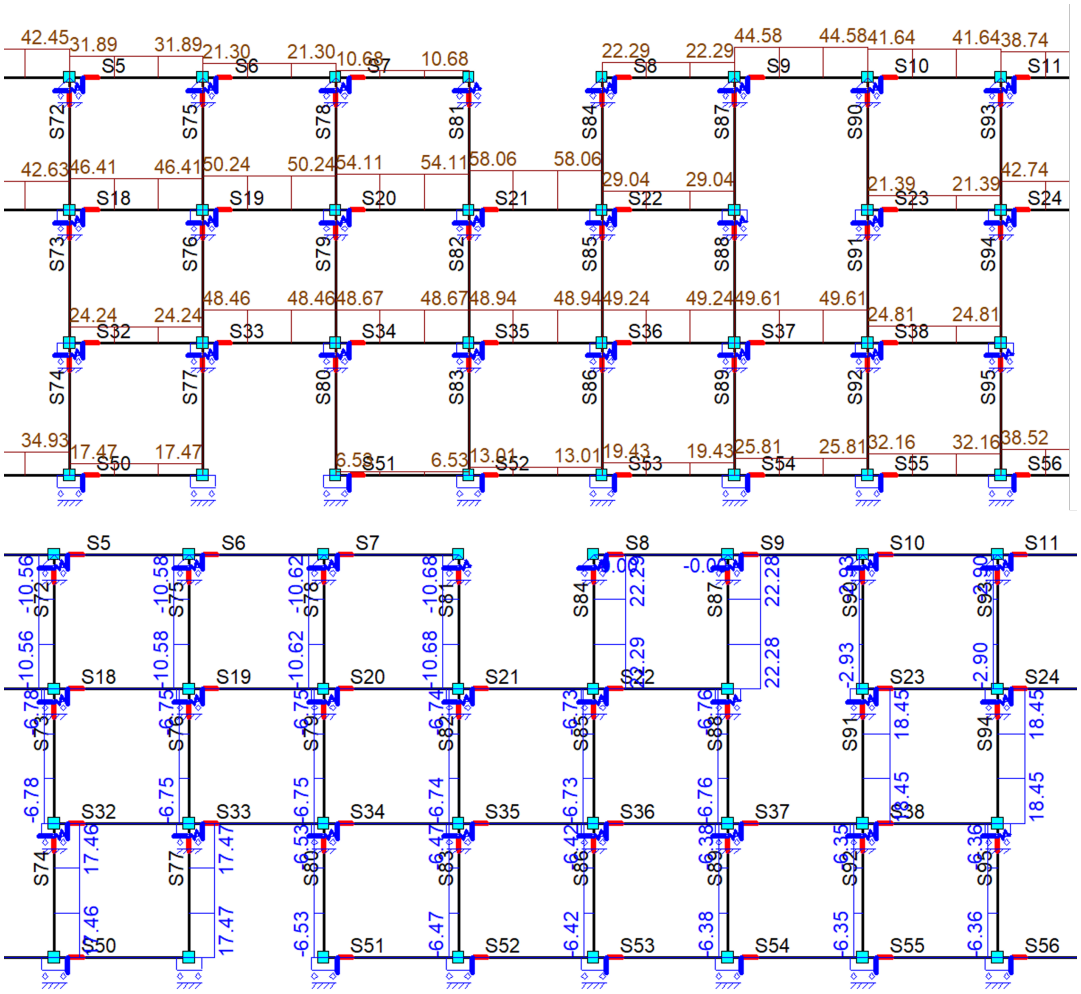

Figure D.13: Normal force and shear force distribution in a two layered system with four screws per plate

Equation

An equation can be established by taking the deformation path like shown in Figure D.14 where the deformation is composed out of that of the connections and plates.

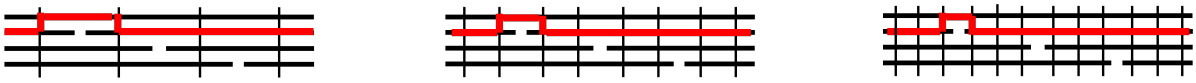

Figure D.14: Deformation path of a four layered system

From these deformation paths a general equation can be made through checking the forces out of Figures D.12 and D.13:

Figure	n_{fpp}	Shear Force [kN]	"Factor" x $\frac{F}{n_y K}$	Tension [kN] x s [-]	"Factor" x $\frac{Fs}{EA}$
D.12	1	40 + 13.3	$\frac{4}{9}$	26.7 + 40 + (53.3+53.3+26.7)	$\frac{11}{6}$
D.13	2	20 + 6.7	$\frac{4}{18}$	(26.7+26.7) + 40 + (26.7+53.3+53.3 +53.3+53.3+26.7)	$\frac{19}{6}$
-	3	13.3 + 4.4	$\frac{4}{27}$	(26.7+35.6+17.8) + 40 + (17.8+35.6+53.3+53.3+53.3 +53.3+53.3+53.3+26.7)	$\frac{27}{6}$
-	4	10 + 3.3	$\frac{4}{36}$	(26.7+40+26.7+13.3) + 40 + (13.3+26.7+40+53.3+53.3 +53.3+53.3+53.3+53.3 +53.3+53.3+26.7)	$\frac{35}{6}$

The pattern for "Factor" x $\frac{F}{n_y K}$ is given in Equation D.7 and for "Factor" x $\frac{Fs}{EA}$ in Equation D.8. And with these patterns, the general equation for the elongation of two plates can be constituted in Equation D.9.

$$\left(\frac{4}{9}, \frac{4}{18}, \frac{4}{27}, \frac{4}{36}, \ldots\right) > "Factor" = \frac{4}{9n_{fpp}} \tag{D.7}$$

$$\left(\frac{5}{3}, \frac{9}{3}, \frac{13}{3}, \frac{17}{3}, \ldots\right) > "Factor" = \frac{4n_{fpp}+1}{3} \tag{D.8}$$

$$\Delta L_{total,4,plates} = \frac{4F}{9n_{fpp}n_y K} + \frac{(4n_{fpp}+1)FL}{3n_p n_{fpp} E A_{plate}} \tag{D.9}$$

Elongation check

The equation created to calculate the elongation of the segments can be checked against the MatrixFrame model. The properties of the segment for the elongation of four plates with four screws:

F	=	Force	=	120000	N
n_p	=	Number of layers	=	4	-
n_{fpp}	=	Number of screws between two distinct plates	=	1	-
n_y	=	Number of screws in effective width direction	=	1	-
K	=	Stiffness of fastener	=	100	N/mm
L	=	Length of a plate	=	4000	mm
E	=	Young's modulus	=	8000	N/mm^2
A	=	Area	=	9000	mm^2

Which result in the following elongation:

$$\Delta L_{total,4,plates} = \frac{4 \cdot 120000}{9 \cdot 1 \cdot 1 \cdot 100} + \frac{(4 \cdot 1 + 1) \cdot 120000 \cdot 4000}{3 \cdot 4 \cdot 1 \cdot 8000 \cdot 9000} = 536.11\ mm$$

The elongation in the Matrixframe model (between K20/K21 - K24/K25):

$$\Delta L_{total,3,plates} = ((1.4509 - 1.4502) - (0.9169 - 0.9162)) \cdot 1000 = 534\ mm$$

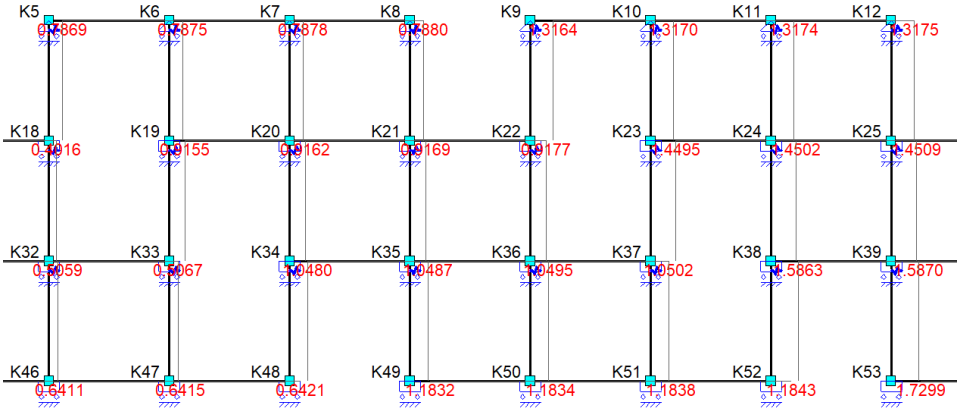

The properties of the segment for the elongation of four plates with eight screws:

F	=	Force	=	120000	N
n_p	=	Number of layers	=	4	-
n_{fpp}	=	Number of screws between two distinct plates	=	2	-
n_y	=	Number of screws in effective width direction	=	1	-
K	=	Stiffness of fastener	=	100	N/mm
L	=	Length of a plate	=	8000	mm
E	=	Young's modulus	=	8000	N/mm^2
A	=	Area	=	9000	mm^2

Which result in the following elongation:

$$\Delta L_{total,4,plates} = \frac{4 \cdot 120000}{9 \cdot 2 \cdot 1 \cdot 100} + \frac{(4 \cdot 1 + 1) \cdot 120000 \cdot 8000}{3 \cdot 4 \cdot 2 \cdot 8000 \cdot 9000} = 271.9\ mm$$

The elongation in the Matrixframe model (between K71/K72 - K81/K82):

$$\Delta L_{total,3,plates} = ((0.9124) - (0.6448)) \cdot 1000 = 267.6\ mm$$

Elongation check of all layers

Table D.1 compares the elongations of the Equation (Eq.) and MatrixFrame (M.F.) which concludes that the equations are correct.

	$n_{fpp} = 1$		$n_{fpp} = 2$		$n_{fpp} = 3$	
	Eq.	M.F.	Eq.	M.F.	Eq.	M.F.
2 layers	200.4	200.4	100.2	100.3	66.8	67.0
3 layers	301.9	302.0	151.9	151.6	102.8	102.4
4 layers	536.11	534.0	271.9	267.9	-	-

Table D.1: Elongation check of all layers